

NUCLEAR MAGNETIC RESONANCE STUDIES

NUCLEAR MAGNETIC RESONANCE STUDIES
OF
BORAX, TINCALCONITE AND FERROELECTRIC
LITHIUM HYDRAZINIUM SULPHATE

By

JOHN DAVID CUTHBERT, B.A., M.Sc.

A Thesis

Submitted to the Faculty of Graduate Studies
in Partial Fulfilment of the Requirements

for the Degree

Doctor of Philosophy

McMaster University

September 1963

DOCTOR OF PHILOSOPHY (1963)

MC MASTER UNIVERSITY,
HAMILTON, ONTARIO.

TITLE Nuclear Magnetic Resonance Studies of Borax, Tincalconite and Ferroelectric Lithium Hydrazinium Sulphate.

AUTHOR John David Cuthbert, B.A. (Oxford University 1959)

M.Sc. (University of Birmingham
1960)

SUPERVISOR Dr. H.E. Petch, Director of Research,
Mc Master University.

NUMBER OF PAGES x, 186

ABSTRACT

The quadrupole coupling tensors at the B^{11} and Na^{23} sites in borax and tincalconite, two members of the hydrated sodium tetraborate family have been completely evaluated using broadline nuclear magnetic resonance (n.m.r.) techniques. The results have enabled deductions to be made concerning the crystal chemistry of boron, the coordinations of the sodium atoms and the crystallographic symmetries.

Changes in the Li^7 n.m.r. spectrum of ferroelectric lithium hydrazinium sulphate as a function of temperature were followed in detail. A previously undetected second order phase transition leading to a high temperature polymorph is complete at $164^{\circ}C$. The quadrupole coupling tensors

at the Li^7 sites have been completely evaluated in the two phases. The second moments of the proton n.m.r. spectrum from powdered lithium hydrazinium sulphate have been determined within the temperature range -183°C to 225°C , and single crystal data on the protons have been obtained at room temperature. It is shown that the nitrogen and hydrogen atoms exist in the structure as the hydrazinium ion $\text{NH}_2\text{-NH}_3^+$. Detailed information is derived concerning the proton-proton vectors and the modes of reorientation of the NH_2 and -NH_3^+ groups at various temperatures. Mechanisms for the ferroelectric switching at room temperature and for the transition to the high temperature polymorph are proposed on the basis of the experimental evidence.

ACKNOWLEDGEMENTS

It is a pleasure to thank Dr. H.E.Petch for suggesting the excellent thesis topic, for help in interpreting the experimental results and for checking a large number of the calculations.

Thanks are also due to Dr. I.D.Brown for many valuable discussions in the field of x-ray crystallography, to Paul Cant for much information concerning dipolar interactions and to my wife who has spent many hours typing this thesis.

This research was made possible by grants-in-aid to Dr. Petch from the Defence Research Board of Canada. The author is most grateful for the tenure of a Canadian Commonwealth Scholarship throughout the period of research.

TABLE OF CONTENTS

CHAPTER I. INTRODUCTION

1. Background Survey	1
2. Factors Governing the Detection of N.M.R. Signals in Inorganic Solids	6
3. Application of N.M.R. to the Study of Hydrated Borates and Ferroelectric Crystals	10
4. Summary of the Aims of this Research	20

CHAPTER II. THEORY

1. Introduction	22
2. The Quadrupolar Hamiltonian	24
3. Matrix Elements of $\tilde{Q} \cdot (\nabla E)$	26
4. Application of Perturbation Theory	27
5. The Electric Field Gradient Tensor	29
6. Transformation Theory	30
7. The Quadrupole Coupling Tensor and Crystal Symmetry	34
8. Removal of Ambiguities in the Analysis of Data from Symmetry Related Sites	37
9. Proton Pairs in Single Crystals	38
10. Proton Pairs in Polycrystalline Samples	42
11. Equilateral Triangles of Protons	44
12. Second Moments of N.M.R. Signals Broadened by Magnetic Interactions	47
13. Linewidth Transitions in a Powdered Sample	50

CHAPTER III. APPARATUS AND EXPERIMENTAL PROCEDURE

1. The N.M.R. Spectrometer	52
2. Sample Temperature Control	57
3. Alignment of Crystals in the Applied Magnetic Field	59
4. Procedure in the Quadrupolar Interaction Studies	62

CHAPTER IV. CRYSTAL DATA

1. The Hydrated Borates, Borax and Tincalconite	65
2. Ferroelectric Lithium Hydrazinium Sulphate	69

CHAPTER V. N.M.R. STUDY OF THE B^{11} SITES IN BORAX AND

TINCALCONITE

1. Experimental Results	74
2. Discussion of Results	91
CHAPTER VI. N.M.R. STUDY OF THE Na ²³ SITES IN BORAX AND TINCALCONITE	
1. Experimental Results	99
2. Discussion of Results	111
CHAPTER VII. N.M.R. STUDY OF FERROELECTRIC LITHIUM HYDRAZINIUM SULPHATE	
1. Experimental Results	118
2. Discussion of Results	139
CHAPTER VII. SUMMARY OF RESULTS	155
APPENDIX I	159
APPENDIX II	174
TABLE OF REFERENCES	184

LIST OF FIGURES

		Page
Fig. 1	Definition of angles (α, δ, θ) which specify the orientation of a p-p vector relative to the axes, X, Y and Z.	40
Fig. 2	Theoretical and experimental n.m.r. lineshapes for p-p pairs in a powder sample.	40
Fig. 3	Energy levels for a rigid triangle of protons.	46
Fig. 4	Theoretical lineshape for a rigid equilateral array of protons in a powder, with broadening.	46
Fig. 5	Theoretical lineshape for a rotating equilateral array of protons in a powder, with broadening.	46
Fig. 6	Block diagram of n.m.r. spectrometer.	53
Fig. 7	Borax structure projected onto (100).	66
Fig. 8	A view of LiHS projected down the c-axis	71
Fig. 9	Angular dependence of the frequency difference between B^{11} satellite lines arising at the L sites in borax.	78
Fig. 10	Angular dependence of the frequency difference between the B^{11} satellite lines arising at the M sites in borax.	79
Fig. 11	Angular dependence of the frequency difference between the B^{11} satellite lines arising at the L sites in tincalconite.	80
Fig. 12	Angular dependence of the frequency difference between the B^{11} satellite lines arising at the M sites in tincalconite.	81
Fig. 13	Graphical analysis of the ambiguity for the L sites in borax.	85
Fig. 14	A projection of the borax polyion on to (010).	95

Fig. 15	Angular dependence of the frequency difference between the Na ²³ satellite lines arising at the A ₁ , A ₂ and B _{1,2} sites in borax.	103
Fig. 16	Angular dependence of the frequency difference between the Na ²³ satellite lines arising at the A ₁ , A ₂ , A ₃ , B _{1,2} and C sites in tincalconite.	104
Fig. 17	Angular dependence of the frequency separation of the Li ⁷ satellite lines from the central resonance in LiHzS at room temperature.	120
Fig. 18	Plots of Li ⁷ satellite separations at $\Theta_z = 75^\circ$ and second moments of proton resonance signal from powdered LiHzS, as a function of temperature.	124
Fig. 19	Appearance of Li ⁷ n.m.r. spectra at various temperatures.	125
Fig. 20	Angular dependence of the frequency separation of the Li ⁷ satellite lines from the central resonance in LiHzS at 205°C.	127
Fig. 21	Derivatives of the proton resonance in powdered LiHzS at various temperatures.	129
Fig. 22	Derivative of the proton resonance absorption line in a single crystal of LiHzS at orientation $\Theta_z = 35^\circ$.	135
Fig. 23	N.M.R. derivative signal showing Pake doublet believed to be from NH ₂ group.	137
Fig. 24	Separation vs angle of rotation of the separation of the members of the doublet shown in Fig. 23.	138
Fig. 25	Hydrogen bond configuration around N ₁ projected on a plane perpendicular to the N ₁ -N ₂ direction.	148
Fig. 26	The two alternative configurations of the hydrogen bonds linking the hydrazinium ions.	150

LIST OF TABLES

		Page
Table I	Fourier coefficients for the B^{11} sites in borax.	82
Table II	Fourier coefficients for the B^{11} sites in tincalconite.	83
Table III	Tensor components for the B^{11} sites in borax and tincalconite.	87
Table IV	Quadrupole coupling constants and asymmetry parameters at the B^{11} sites in borax, tincalconite and kernite.	88
Table V	Direction cosines of the principal axes of the electric field gradient tensor at the B^{11} sites in borax and tincalconite.	89
Table VI	Fourier coefficients for the Na^{23} sites in borax and tincalconite.	105
Table VII	Tensor components for the Na^{23} sites in borax and tincalconite.	108
Table VIII	Quadrupole coupling constants and asymmetry parameters at the Na^{23} sites in borax and tincalconite.	109
Table IX	Direction cosines of the principal axes of the electric field gradient tensors at the Na^{23} sites in borax and tincalconite.	110
Table X	Fourier coefficients for Li^7 sites in LiH_2S .	121
Table XI	Quadrupole coupling constants, asymmetry parameters and orientations of the electric field gradient tensors at the Li^7 sites.	122
Table XII	Table showing contributions to calculated second moment values.	141

Table XIII	N-H distances and HNH bond angles.	145
Table XIV	Direction cosines of the interatomic directions in the -NH_2 group of the hydrazinium ion.	147

CHAPTER I

INTRODUCTION

I. 1. Background Survey.

The properties of angular momentum and magnetic moment were first ascribed to a nucleus by Pauli (1924) in order to account for the hyperfine structure of atomic spectra. These concepts have since found important applications in many branches of physics, amongst which we may mention, Raman, infrared and microwave spectroscopy, hyperfine structure of electronic spin resonance, nuclear scattering, excited states of nuclei, specific heats and paramagnetism.

When an ensemble of nuclear magnets is placed in a magnetic field H_0 , their orientational energies are quantised to form the well-known Zeeman levels, whose energies are $m_I g \beta H_0$, where m_I , g and β are the magnetic quantum number, nuclear g - factor and nuclear magneton respectively. m_I can take the values $I, I-1 \dots -I$, where I is the nuclear spin. The relative populations of the Zeeman levels are given by the Maxwell-Boltzmann statistical factor, exponential $(-\Delta E/KT)$, with $\Delta E = g \beta H_0$. The nucleus couples with an applied oscillating magnetic field through its magnetic dipole mo-

-ment $\vec{\mu}$, and consideration of the matrix elements in the expression for the probability amplitudes shows immediately that all transitions are "forbidden" except when m_I changes by unity. When the Zeeman energy levels are shifted by perturbations whose magnitudes are small compared with $g\beta H_0$, the above selection rules are unaltered but the relative populations of the levels change slightly. Since we shall deal in this work with small perturbations, these population changes will be overlooked for the purposes of the following discussion.

Using the Gouy method, nuclear paramagnetism was first demonstrated by Lasarew and Schubnikow (1937) for solid hydrogen, whose diamagnetic contribution is very small. Besides giving a value of the proton magnetic moment within 10% of the presently accepted value, the experiment indicated that the nuclear magnets came to temperature equilibrium with their environment in a short time even at low temperatures.

Meanwhile atomic and molecular beam experiments, pioneered by Stern and Gerlach (1921), were used extensively during the period 1921 - 1939 to measure magnetic moments and spins. In 1939 the beam methods were enormously improved by Rabi et al (1939) by the introduction of the resonance technique, in which the particles are passed through a uniform magnetic field, H_0 , situated between the balanced inhomogen-

-eous fields, and, whilst in H_0 , are subjected to polarised electromagnetic radiation of such a frequency as to induce transitions between their quantised energy levels. A sharp change in the number of particles reaching the detector indicates that the resonance condition has been achieved. For homogeneous fields of several gauss, the resonant frequency lies in the radio frequency range, 100 kc/sec. to 100 Mc/sec and since frequencies can be very accurately measured, this technique has greatly increased the accuracy with which nuclear magnet moments can be measured.

It was realised that the resonance phenomenon should not be restricted to gaseous matter, but should also occur in condensed matter. Gorter (1936) attempted unsuccessfully to detect the absorption of radio frequency energy due to the unequally populated Zeeman levels of Li^7 in crystalline LiF and protons in crystalline potassium alum using a calorimetric method of detection. Gorter and Broer (1942) tried again using Li^7 in solid $LiCl$ and F^{19} in solid KF , this time looking for the anomalous dispersion which should accompany the absorption, but failed once more. Looking back, Gorter has pointed out the failures were registered largely because of an unfortunate choice of materials with relatively long relaxation times. However, late in 1945, successful experiments were carried out by two teams working independently, using

slightly different techniques. Purcell, Torrey and Pound (1946) detected the additional loss of energy from a tuned circuit supplying radio frequency power when the resonance conditions for protons in paraffin was attained. Bloch, Hansen and Packard (1946) used the method of nuclear induction to detect the resonance condition for protons in water. The latter method is readily understood by appealing to the semiclassical picture of the resonance process. Here we have the nuclei precessing about the applied magnetic field, H_0 , at the Larmour frequency, ν_0 , and an oscillating magnetic field H_1 circularly polarised perpendicular to H_0 . If the frequency of H_1 is altered until it reaches ν_0 , there will be a constant phase difference between the precessing nuclei and H_1 so that a simultaneous torque will be exerted on all the nuclei perpendicular to their axis of precession. Consequently there will be a uniform change in their orientation with respect to H_0 , which can be detected as an induced e.m.f. in a receiving coil wound with its axis perpendicular to the oscillator coil. Basically both experiments are the same with equal ultimate sensitivity, but Purcell's method is more convenient when only the resonance frequency ν , and the intensity $g(\nu)$ of the absorption as a function of ν are required, while the Bloch scheme has found predominant application in the study of the kinetics of the absorption process, for

instance in the study of various spin relaxation mechanisms.

For three or four years following these two experiments, investigators concentrated mainly on increasing their knowledge of the physical processes involved and measuring magnetic moments. The years following 1950, however, have seen the application of the basic resonance experiment to a large number of problems in all divisions of science and one is impressed by the number of papers still appearing.

For instance, so-called "fine line" nuclear magnetic resonance spectroscopy in the liquid state has been developed into one of the organic chemist's most useful tools of analysis, owing to the small, but easily detected "signal splittings" which are characteristic of the chemical environment of a nuclear species in the molecules. In addition, the chemist is able to follow the progress of certain chemical reactions by observing changes in the spectrum. The water content of biological materials may be estimated without affecting the tissues in any detrimental way. Aerial surveys of the earth's magnetic field can now be made easily and with the utmost precision using very recently developed methods employing n.m.r. The magnetic field produced in an electro-magnet can be stabilised by a suitable feedback circuit which derives the sense of the error signal from the slope of the absorption peak of a n.m.r. absorption signal

from a sample placed in the field and, in addition, the value of the field strength is determined. N.M.R. studies of metals lead to information about the energy states at the top of the conduction band due to an interaction between the nuclei and the electrons at the Fermi surface. Information can be derived about the short range disorder in materials, produced by nuclear radiations or cold working; nuclei in paramagnetic and antiferromagnetic crystals provide indications of the magnetic behaviour of these materials whilst changes in the n.m.r. spectrum provide a powerful tool to study phase changes in many types of material. It is the application of n.m.r. to certain structural studies of the solid state that forms the basis of this thesis.

I. 2. Factors Governing the Detection of N.M.R. Signals in Inorganic Solids.

Our experimental arrangement (described in more detail in Chapter III) was designed so that a pure n.m.r. absorption signal can be observed. This was achieved by the use of a marginal oscillator technique in which the same coil acts as a transmitter and detector of radio frequency power. When the frequency, ν , of the tank circuit satisfies the resonance condition

$$\Delta E = E_m - E_{m-1} = h\nu ,$$

where E_m is the energy of a nucleus in a perturbed Zeeman state m_I , stimulated emission and absorption takes place. If the spin system was initially in thermal equilibrium with the lattice (used here as a general term meaning extra nuclear environment), there will be a fraction $\exp(\Delta E/KT)$ more of the nuclei in the lower Zeeman state, so that when the resonance condition is reached, a correspondingly larger amount of absorption over stimulated emission takes place. However, this would persist for only a very short interval of time in the absence of a relaxation process, since the populations of the two levels would quickly become equal, a situation called radiofrequency saturation. Fortunately, however, spin-lattice interactions enable energy to be transferred from the nuclear spin system to the lattice, thereby allowing an absorption signal to be continuously observed.

The strength of the absorption signal depends upon a number of factors, some of which can be assessed before a n.m.r. experiment begins. Theory shows (Andrew 1955, for example) that the signal to noise ratio depends on the resonance frequency, the sample temperature T , the nuclear g -factor and the spin-spin and spin-lattice relaxation times T_1 and T_2 , through an expression of the form

$$\text{signal noise ratio} \sim g \left(\frac{h\nu}{kT} \right)^{2/3} \left(\frac{T_2}{T_1} \right)^{1/2}$$

Obviously, large magnetic moments and field strengths favour intense signals, as do long spin-spin relaxation times and short spin-lattice relaxation times. Before one can say that low temperatures also produce stronger signals, the temperature dependence of T_1 must be known. Large magnetic/^{dipole}and electric quadrupole moments also help by providing short spin-lattice relaxation times, due to their increased effectiveness in coupling with the random magnetic and electric fields produced by lattice vibrations. Here the lattice plays the part of a thermodynamic sink because of its high specific heat, which is some one thousand times the specific heat of the nuclear spin system. The nature of the lattice enters in a less well-defined manner through the spectrum of frequencies it produces at a given nuclear site. In general, the greater the freedom of movement permitted the atomic constituents of a material, the more effective is the coupling between lattice and spin system. Hydrogen atoms, with their large magnetic moment and large thermal motions per unit of thermal energy, are prominent in shortening spin-lattice relaxation times. Covalently bonded materials containing heavy atoms represent an opposite extreme. Here the unfavourably long spin-lattice relaxation times often encountered in such materials can usually be reduced by creating electron paramagnetic centres with the use of penetrating γ -rays. In general there is an

optimum extent to which the nuclear spin system and lattice should be coupled, since signal broadening (and consequent loss of sensitivity) is caused both through dipole-dipole interactions similar to those described in section II.9 and through the operation of the Heisenberg Uncertainty Relations, because of the lifetimes of the nuclear spin states being too greatly reduced.

The nuclei with which we are concerned, Li^7 , B^{11} , Na^{23} , and H^1 , all have large magnetic moments and, except for hydrogen, quadrupole moments. In borax and lithium hydrazinium sulphate, we know that there is extensive hydrogen bonding throughout the frameworks and that some protons are reorienting at room temperature, so that good signals were expected from these two crystals. Although the crystal structure for tincalconite is unknown, its similar density and hardness to borax leads us to expect a certain amount of hydrogen bonding in it also, but magnetic resonance work has shown the protons to be much more rigidly held than for borax (Pake 1948, Dharmatti et al 1962, Maricic et al 1962). Nevertheless signals comparable to those from borax were anticipated.

In this section the chief factors entering into the observation of the n.m.r. signals in inorganic solids have been briefly discussed, taking as examples the materials of

concern in this work. However it will not be necessary to mention these important considerations again, since they do not determine the frequencies at which the resonances are found. The theory governing the frequency distribution of the resonances is described in Chapter II, and it is from this non-kinematical aspect that we use n.m.r. to gain information about the solid state.

3. Applications of N.M.R to the Study of Hydrated Borates and Ferroelectric Crystals.

Magnetic dipole-dipole and electric quadrupole interactions are the important ways that a nucleus "feels" its environment in an inorganic solid. These interactions perturb the Zeeman levels, thereby enabling the nuclear environment to be studied. The shifts of the levels cause the absorption signal occurring at the Larmor frequency to split into components, the number of which depends on the nuclear spin, the number of unique and symmetry related sites in the crystal unit cell, and the nature, electric or magnetic, of the interaction (see Chapter II).

In quadrupolar studies, the electric quadrupole coupling tensor, (Ψ_{ij}) , is derived. It is the product of the unchanging nuclear quadrupole moment, $^{(1)} eQ$, and the electric

⁽¹⁾

The scalar quadrupole moment, Q , is defined by eq. 2.13

field gradient tensor⁽¹⁾, (ϕ_{ij}) . It is a second rank, symmetric and traceless tensor. In the principal axis system, the tensor is usually described in terms of its largest component, called the quadrupole coupling constant⁽²⁾, eQq/h , and the ratio of the difference between the smallest and intermediate components to the largest component, called the asymmetry parameter, η . The calculation from first principals of (ψ_{ij}) is a notoriously difficult problem, even when a good value of the quadrupole moment can be obtained from other sources. Although agreement between experimental and calculated values of (ψ_{ij}) have been obtained in a few simple cases, the success of such calculations has not been extended to the more complex units of interest here. In spite of the lack of a firm theoretical interpretation, (ψ_{ij}) can still yield information about the solid state through a more empirical approach, which will be exemplified in the thesis.

Because of its potential utility in semiconductors, high energy fuels and as a component of hard materials with high melting points, recent years have seen a great surge of

(1)

Also denoted as (\tilde{VE}) when no specific reference to the Cartesian representation is intended (see Chapter II).

(2)

In accordance with convention ϕ_{zz} has been replaced by q (see section 2.7)

interest in the physics and chemistry of boron. Although boron is widespread in nature, only in a limited number of localities are large deposits of boron containing materials found in nature. In the Western Hemisphere, the commercially important deposits are at Kramer and Seales Lake, where the boron containing minerals are almost exclusively borax, tincalconite and kernite. In the U.S.S.R., the borate deposits of the Inder Lakes region have been intensively mined. Here the mineral ores are a whole series of hydrated calcium and magnesium borates.

In its oxy-salts, boron rivals silicon in number and complexity. Borates ranging in composition from CaB_2O_4 to $\text{Mg}_7\text{Cl}_2\text{B}_{16}\text{O}_{30}$ may be prepared or are found as minerals. As was the case with the silicates, they were originally supposed to be derived from hypothetical acids with formulae such as $\text{H}_6\text{B}_8\text{O}_{16}$ and $\text{H}_2\text{B}_{10}\text{O}_{16}$. Later work has shown that such formulae are quite meaningless since the complex structures are characteristic of the solid state alone and break down into simpler units in solution.

Because of the late start in the intensive investigations of boron, much research has yet to be done before one can say that the chemical behavior of boron is understood as well as that of silicon, which it resembles in many ways. The chemistry of boron, however, is more complicated than that of

silicon, because it can exhibit valencies of either three or four. Amongst the many borates, the hydrated members are of central importance, to the industrialist because they are the chief source of boron, and to the scientist because of the chemical and crystallographic problems arising from their complex structures.

The structures of a number of hydrated borates have now been revealed by x-ray investigations. A study of these structures has enabled Christ (1960) and Ross and Edwards (1960) to propose a set of "rules" which seemingly govern the nature of the boron-oxygen complexes existing in the hydrated borates of known structure. Thus boron combines either with three oxygen atoms to form a BO_3 triangle or with four oxygen atoms to form a BO_4 tetrahedron. Triangles and tetrahedra may then combine together to form a variety of polyions by corner sharing of oxygen atoms, and the polyions may exist as discrete elements in the structures or they may, by sharing oxygen atoms, combine to become structural units in long chains or even three-dimensional networks. Christ (1960) then utilised his "rules", along with other available crystallographic and chemical evidence to predict the type of polyion occurring in each of some twenty hydrated borates of unknown structure.

Because of the much greater strength of the bonds within the complexes (referring here to boron-oxygen triangles,

tetrahedra and polyions) as compared to the bonds uniting the complexes to form the structure, one would expect the quadrupole coupling tensor to be determined primarily by the complex involved, rather than by the structure within which the complex finds itself. Extrapolating from symmetry considerations for the ideal unit allows one to predict that eqQ/h for a B^{11} nucleus at the centre of BO_4 tetrahedron would be very small if the tetrahedron existed in a discrete unit in the crystal and somewhat larger if the tetrahedron were bound with other tetrahedra and triangles to form a condensed polyion such as a closed ring. For a B^{11} nucleus at the centre of a BO_3 triangle, one would predict (1) that eqQ/h would be considerably larger than in the case of a tetrahedron (2) that the value of η would be very small and (3) that the z-principal axis of the tensor would be nearly perpendicular to the plane containing the triangle. Using materials whose structures are known, these considerations have been verified for discrete BO_4 tetrahedra in teepelite (Ross and Edwards 1959) and for two tetrahedra and a triangle in a closed ring in colemanite (Holuj and Petch 1960). The characteristic values of eqQ/h are unambiguous, falling at about 100, 500 and 2500 kc/sec for discrete tetrahedra, tetrahedra in closed ring polyions and triangles respectively.

These considerations have enabled the utilization

of n.m.r. as a tool to check Christ's (1960) postulates as to type of polyions to be found in many of the hydrated borates of unknown structures. As an example, the n.m.r. investigations of B¹¹ sites in single crystals of inderite and lesserite by Pennington and Petch (1960,62) indicated that both these minerals contained two BO₄ tetrahedra and one BO₃ triangle in the form of a closed ring polyion, in complete accordance with Christ's predictions for the colemanite-inoite series.

The series of hydrated sodium tetraborates, borax, tincalconite and kernite, whose chemical compositions are Na₂B₄O₇xH₂O with x = 10, 5, and 4, respectively, have attracted the attention of a number of researchers. However a literature survey showed that the firmly established structural data on these compounds was rather scant while the data derived from x-ray and n.m.r. studies were sometimes found to be conflicting. The basic crystallographic features of the minerals is well known, (Palanche et al 1951) being reported in Chapter IV. One interesting point is that the spacegroup of tincalconite is not uniquely determined by x-ray methods.

The first reported structural investigation was performed on kernite, for which Portoles (1945, 47, 48) proposed a structure. However the work of Waterman and Volkoff (1955) discredited it. These workers made a detailed single

crystal study of the B^{11} sites and derived the complete quadrupole coupling tensors for the four unique B^{11} sites. The chief object of their work was to analyse the complex radio frequency absorption spectrum in terms of the number of unique B^{11} sites and the crystal symmetry, so that no attempt was made to interpret the results from the bonding aspect. However, it should be remembered that at the time, the ideas concerning the interpretation of quadrupole coupling tensors as explained above were not formulated. Besides the B^{11} study Waterman and Volkoff also made preliminary examinations of the Na^{23} spectra at several orientations. The number of signals showed conclusively that Portoles' structure was incorrect, since he proposed three unique Na^{23} sites whereas the n.m.r. results indicated only two.

A year later, a structure for borax was reported by Morimoto (1956). He found that the boron atoms were contained in a tightly bound boron-oxygen polyion which is composed of two BO_3 triangles and two BO_4 tetrahedra linked together by corner sharing of oxygen atoms, with the sodium atoms octahedrally coordinated to the oxygen atoms of water molecules. The structure is described in more detail in Chapter IV.

The remaining experimental work of a structural nature has been concerned with n.m.r. studies of polycrystalline samples. The n.m.r. work on the protons, mentioned in section 12

will not be discussed since it has no relevance to the present topic. Bray et al (1961) have included borax and tincalconite in a range of powdered borates whose B^{11} n.m.r. spectra they have studied. They interpreted their data as showing that both tetrahedrally and trigonally bonded boron was present, but were unable to say anything concerning the number of unique sites of either type. Dharmatti et al (1962) performed a similar investigation that also included the Na^{23} sites. Their conclusions on the B^{11} sites were the same as those of Bray. For the Na^{23} investigations they reported, in contradiction to Morimoto's structure for borax, that the two sodium atoms in the asymmetric unit occupy equivalent sites with the quadrupole coupling constant having an upper limit of 750 kc/sec. They interpreted their results for tincalconite as indicating the existence of sodium atoms in two quite different sites with the Na^{23} quadrupole coupling constant having an upper limit of 630 kc/sec at one site and a value of 1360 kc/sec at the other. Because of the possible overlap of signals from sites possessing very similar quadrupole coupling tensors, it can be misleading to draw such conclusions from data obtained from powder samples alone, particularly for crystals with structures as complicated as the tetraborates.

A research program connected with this series of

borates now presents itself. The primary aim is the accurate determination of the quadrupole coupling tensors at all the B^{11} and Na^{23} sites for borax and tincalconite using single crystal techniques. These data will enable the conclusions derived from the powder work described above to be critically appraised, and allow the evaluation of the space-group of tincalconite. This done, Christ's prediction that the borax type polyion occurs also in tincalconite and kernite can be tested. For the latter crystal, Waterman and Volkoff's data on the B^{11} sites will be used. By comparing the values of eqQ/h at the Na^{23} sites in tincalconite and borax, the coordinations of the Na^{23} atoms in tincalconite may be inferred.

Another application of n.m.r. is to the study of ferroelectricity in crystals. Although the phenomenon of ferroelectricity has been extensively studied in recent years, much remains to be understood on an atomic scale about its nature. X-ray and neutron diffraction studies of ferroelectric crystals are most helpful in improving this situation but n.m.r. techniques can make important contributions. The resonance signal of a nucleus in a crystal depends strongly upon the particular state of the crystal and therefore may be used to detect and study the progress of phase transitions even when the actual atomic displacements are exceedingly small. Furthermore, in hydrogen bonded crystals, where the

interproton distances are not too much greater than the distances over which proton motion occurs, n.m.r. may clarify the role of the hydrogen atoms in the ferroelectric transition.

Lithium hydrazinium sulphate, $\text{Li}(\text{N}_2\text{H}_5)\text{SO}_4$ (abbreviated to LiHzS), is a material in which one might expect protons to play an important role in its ferroelectric behavior. Pepinsky et al (1958) who discovered its ferroelectric property, reported that it gave a good ferroelectric hysteresis loop over the temperature range from below -15°C to above 80°C . No dielectric anomalies were detected between -196°C and 140°C . Excessive conductivity interfered with both measurements at higher temperatures. Specific heat measurements over the range -120° to 205° also failed to indicate a phase transition. These results suggest that the substance remains ferroelectric up to 205°C . LiHzS is amenable to a n.m.r. study because the Li^7 nuclei act as probes which are sensitive to changes in the framework of the crystal, while the protons provide information on the N-H bonds and the status of the hydrogen bonds linking the nitrogen atoms to the framework. It was decided to examine the Li^7 and proton signals in detail at room temperature and to use selected signals to follow changes that occurred as the crystal temperature was altered. It should be possible to correlate changes in the Li^7 spectrum with those in the proton spectrum, culminating in a postulate of

the mechanism for the ferroelectric transition, if such a transition occurs below the decomposition temperature. The mechanism of the ferroelectric switching process may also be elucidated if sufficient information on the positions of the protons can be obtained from single crystal studies of the proton spectra at room temperature.

I. 4. Summary of the Aims of this Research.

A. The hydrated borates.

The room temperature n.m.r. investigations of the hydrated borates, borax and tincalconite were undertaken with the following purposes in mind:

(a) to evaluate the quadrupole coupling tensors at all the B^{11} and Na^{23} sites.

(b) to obtain an independent check on the correctness of Morimoto's (1956) proposed structure of borax, the validity of which has been recently questioned.

(c) to determine the correct space group for tincalconite from amongst the three possibilities allowed by x-rays.

(d) to correlate, as far as possible, the orientation and magnitude of the quadrupole coupling tensor at each B^{11} site with the nuclear environment, to test Christ's postulates for the borax series and to determine the orientation of the polyion in tincalconite.

(e) to infer the coordination of the Na^{23} sites in tincalconite.

B. Ferroelectric Lithium Hydrazinium Sulphate.

The main purpose of this work was to examine the n.m.r. spectra as a function of temperature to:

(a) detect and study the transition between the low and high temperature phases, if such occurs below the decomposition temperature of 285°C .

(b) obtain quantitative data for the quadrupole coupling tensors at the Li^7 sites at room temperature and in the high temperature phase.

(c) obtain information about the motions of the protons in the high and low temperature phases of LiHzS , with a view to relating them to a possible mechanism for the ferroelectric transition.

CHAPTER II

THEORY

II. 1. Introduction.

The total interaction energy of the nucleus with a static electromagnetic field is described by a summation of products involving the multipole electric and magnetic moments and the appropriate field derivatives. However, on account of parity and symmetry considerations, the possible nuclear moments are restricted to electric monopoles, quadrupoles, hexadecapoles, etc and magnetic dipoles, octopoles ...etc. Since we shall only be concerned with the orientational-dependent components of the Hamiltonian, the energy contribution entering through the monopole moment may be disregarded, and because octopole and higher moments are so small, they too may be neglected. The only important contributions, therefore, arise through the nuclear magnetic moment, $\vec{\mu}$, and the electric quadrupole moment, Q , which interact with the total magnetic field and electric field gradients respectively, at the nucleus.

Ideally there are no unpaired electrons in the substances which are discussed in this work, so that the main magnetic interaction at a nuclear site arises from the

coupling of the nuclear magnetic moment with the sum of the applied magnetic field and the small magnetic fields produced by neighbouring nuclear magnetic moments. The small diamagnetic effect in the crystals is taken into account by considering the magnetic field values at a nuclear site.

The Hamiltonian operator for the interaction of a nucleus at a given site with the static electromagnetic fields may therefore be written:

$$\hat{H} = -\hat{\vec{\mu}} \cdot \vec{H}_0 + \hat{Q} \cdot (\vec{\nabla} E) - \sum_i \hat{\vec{\mu}} \cdot \vec{H}_i, \quad (2.1)$$

where H_0 is the large applied field,

H_i is the small magnetic field produced by the neighbouring nucleus "i",

$\vec{\nabla} E$ is the electric field gradient^{tensor}/evaluated in the laboratory axes x', y', z' , with z' along H_0 .

These fields are evaluated at the nuclear site under consideration.

The eigenvalue problem which has to be solved is

$$\hat{H} \psi(I, m) = E_{I, m} \psi(I, m), \quad (2.2)$$

where $\psi(I, m)$ represents the wavefunction of the nucleus in the perturbed Zeeman state m . Analytical solutions of high accuracy may be obtained by applying the methods of perturbation theory. For the crystals of interest in this work it will become apparent that the interactions in eq 2.1, namely, $\vec{\mu} \cdot \vec{H}_0$, $\hat{Q} \cdot (\vec{\nabla} E)$ and $\vec{\mu} \cdot \vec{H}_i$ have the following approximate energies

in units of Plank's constant: 10 Mc/sec, 0.025 to 2.5 Mc/sec and 100 Kc/sec, respectively. The second and third terms are therefore regarded as perturbations on the magnetic interaction $\vec{\mu} \cdot \vec{H}_0$ so that one can use as basic eigenfunctions the set $|Im\rangle$ which describes the $(2I+1)$ Zeeman energy states of an isolated nucleus of spin I in a magnetic field.

It will be found convenient to treat the magnetic and electric splittings separately. This simplifies application of the theory to the experimental data, without reducing its generality. The convenience arises because the Li^7 , B^{11} and Na^{23} nuclei all have nearest neighbours consisting of O^{16} whose nucleus possesses no dipole moment. Since the magnetic dipole field falls off as r^{-3} , the next nearest neighbours produce fields at the Li^7 , B^{11} and Na^{23} sites which are weak and merely produce slight broadening of a satellite signal. Conversely, in the proton magnetic resonance studies quadrupolar effects are completely absent because the proton has no observable quadrupole moment. Quadrupole perturbations will be treated in sections 2 to 8 and magnetic perturbations in sections 9 to 13.

II. 2. The Quadrupolar Hamiltonian.

Classical Potential theory shows that the electromagnetic energy of a nucleus in a crystal is

$$\iint \frac{\rho_e(\vec{r}_e) \rho_n(\vec{r}_n) dv_e dv_n}{|\vec{r}_e - \vec{r}_n|}, \quad (2.3)$$

where the vector origin is the nuclear centre and \vec{r}_e , \vec{r}_n are the vectors locating the interacting elements of electronic charge $\rho_e(\vec{r}_e) dv_e$, and nuclear charge $\rho_n(\vec{r}_n) dv_n$.

From the definition of the Legendre Polynomials,

$$\frac{1}{|\vec{r}_e - \vec{r}_n|} = \frac{1}{r_e} \sum_{k=0}^{\infty} \left(\frac{r_n}{r_e}\right)^k P_k(\cos \theta_{en}), \quad (r_n \ll r_e) \quad (2.4)$$

where θ_{en} is defined by $\cos^{-1}(\vec{r}_e \cdot \vec{r}_n) / |\vec{r}_e| |\vec{r}_n|$. In polar coordinates $\vec{r}_i = (r_i, \theta_i, \phi_i)$ so that the Spherical Harmonic Addition Theorem gives

$$P_k(\cos \theta_{en}) = Y_k^0(\theta_{en}, \phi) = \sum_{q=-k}^{+k} \sqrt{\frac{4\pi}{2k+1}} Y_k^q(\theta_e, \phi_e) Y_k^{-q}(\theta_n, \phi_n) \quad (2.5)$$

Using eqs 4 and 5, eq 3 becomes

$$\iint \frac{\rho_e(\vec{r}_e) \rho_n(\vec{r}_n)}{r_e} \sum_{k=0}^{\infty} \sum_{q=-k}^{+k} \left(\frac{r_n}{r_e}\right)^k \frac{4\pi}{2k+1} Y_k^{-q}(\theta_n, \phi_n) Y_k^q(\theta_e, \phi_e) dv_e dv_n \quad (2.6)$$

Neglecting all moments except the quadrupole moment, in accordance with section II.1, the quadrupolar interaction becomes

$$\left(\frac{4\pi}{5}\right) \iint \frac{\rho_e(\vec{r}_e) \rho_n(\vec{r}_n)}{r_e} \sum_{q=-2}^2 \left(\frac{r_n}{r_e}\right)^2 Y_2^{-q} Y_2^q dv_e dv_n. \quad (2.7)$$

In tensor notation,

26

$$\tilde{Q} \cdot (\tilde{\nabla E}) = \sum_{q=-2}^{+2} (-1)^q Q_{2,q} (\nabla E)_{2,-q} \quad (2.8)$$

where

$$Q_{2,q} = \sqrt{\frac{4\pi}{5}} \int \rho_n r_n^2 Y_2^q(\theta_n, \phi_n) dv_n \quad (2.9)$$

and

$$(\nabla E)_{2,-q} = \sqrt{\frac{4\pi}{5}} \int \frac{\rho_e}{r_e^3} Y_2^{-q}(\theta_e, \phi_e) dv_e \quad (2.10)$$

II. 3. Matrix Elements of $\hat{Q} \cdot (\hat{\nabla E})$

In eqs. 9 and 10, if we regard the position variables as operators, the quantum mechanical quadrupolar Hamiltonian operator $\hat{Q} \cdot (\hat{\nabla E})$ is obtained, whose matrix elements with respect to the eigenfunctions $|I, m\rangle$ are required. Since $(\tilde{\nabla E})_{2,q}$ contains only electronic operator variables it is diagonal in the nuclear wavefunction, ^{representation} so that

$$\langle I, m' | \hat{Q}_{2,q} \cdot (\hat{\nabla E})_{2,-q} | I, m \rangle = \langle I, m' | \hat{Q}_{2,q} | I, m \rangle (\tilde{\nabla E})_{2,-q} \quad (2.11)$$

Eq. 9 shows that $Q_{2,q}$ transforms in the same way as a spherical harmonic, and is therefore an irreducible tensor of rank two. The integration in eq. 9 does not affect the definition because of the linear manner that tensors add so that we may apply the Wigner-Eckart Theorem. The following matrix elements are finite

$$\begin{aligned} \langle I, m | \hat{Q}_{2,0} | I, m \rangle &= \langle I, 2, m, 0 | I, 2, I, m \rangle \langle I || \hat{Q}_2 || I \rangle \\ \langle I, m \pm 1 | \hat{Q}_{2, \mp 1} | I, m \rangle &= \langle I, 2, m \pm 1, \mp 1 | I, 2, I, m \rangle \langle I || \hat{Q}_2 || I \rangle \\ \langle I, m \pm 2 | \hat{Q}_{2, \mp 2} | I, m \rangle &= \langle I, 2, m \pm 2, \mp 2 | I, 2, I, m \rangle \langle I || \hat{Q}_2 || I \rangle \end{aligned} \quad (2.12)$$

The measured value of the quadrupole moment of the nucleus is

$$eQ = \langle I, I | \hat{Q}_2, 0 | I, I \rangle = \langle I, 2, I, 0 | I, 2, I, 0 \rangle \langle I || \hat{Q}_2 || I \rangle \quad (2.13)$$

Tables for the evaluation of the Clebsch-Gordon coefficients may be found in the book by Condon and Shortly (1935), for instance, enabling eqs 12 and 13 to be expressed in terms of I, m and Q , thus:

$$\begin{aligned} \langle I, m | \hat{Q}_2, 0 | I, m \rangle &= A [3m^2 - I(I+1)] (\tilde{\nabla}E)_0 \\ \langle I, m | \hat{Q}_2, 0 | I, m \pm 1 \rangle &= \mp \frac{\sqrt{6}}{2} A (2m \pm 1) [(I \mp m + 1)(I \mp m)]^{1/2} (\tilde{\nabla}E)_{\pm 1} \\ \langle I, m | \hat{Q}_2, 0 | I, m \pm 2 \rangle &= \frac{\sqrt{6}}{2} A [(I \mp m)(I \mp m - 1)(I \mp m + 1)(I \mp m + 2)]^{1/2} (\tilde{\nabla}E)_{\pm 2} \end{aligned}$$

where $A = \frac{eQ}{2I(2I-1)} \quad (2.14)$

II. 4. Application of Perturbation Theory.

Perturbation theory gives the following correction terms to the energy E_m^0 of an unperturbed system in the Zeeman state characterised by the magnetic quantum number m :

first order,

$$E_m^1 = \langle I, m | \hat{Q}_2, 0 | I, m \rangle \quad (2.15)$$

second order,

$$E_m^2 = \sum_{m'}' \frac{\langle I, m | \hat{Q}_2, 0 | I, m' \rangle \langle I, m' | \hat{Q}_2, 0 | I, m \rangle}{E_m^0 - E_{m'}^0} \quad (2.16)$$

where the prime on the summation indicates that $m'=m$ is not included in the summation. The total energy E_m becomes

$$E_m = E_m^0 + E_m^1 + E_m^2 \dots \quad (2.17)$$

Using eqs 14, 15 and 16, eq 17 gives

$$E_m = mg\beta H_0 + A [3m^2 - I(I+1)] (\tilde{\nabla}E)_0$$

$$\begin{aligned}
& + \frac{3A^2 (\tilde{\nu}E)_1 (\tilde{\nu}E)_{-1}^m [4I(I+1) - 1 - 8m^2]}{g\beta H_0} \\
& + \frac{3A^2 (\tilde{\nu}E)_2 (\tilde{\nu}E)_{-2}^m [2I(I+1) - 1 - 2m^2]}{g\beta H_0} \quad (2.18)
\end{aligned}$$

Allowed transitions (in which $|\Delta m| = 1$) between the perturbed energy levels give rise to the n.m.r. spectrum. For a nucleus with a half integral spin I , the spectrum of resonance signals consists of a central component at ν_c , from transitions between the $|m| = \frac{1}{2}$ levels, and $(I - \frac{1}{2})$ pairs of "satellites" at ν_m'' and ν_m' from transitions $m \leftrightarrow m-1$, and $-(m-1) \leftrightarrow -m$ with $I \gg m \gg \frac{1}{2}$. In the case of integral spin I , there is no central component but there are I pairs of satellites. Eq. 18 gives the following relationships between ν_m'' , ν_m' , ν_c and $\bar{\nu}$, worked to the second order correction:

$$\Delta\nu = \nu_m'' - \nu_m' = \frac{3(2m-1)}{2I(2I-1)} \frac{eQ}{h} (\tilde{\nu}E)_0 \quad (2.19)$$

$$\begin{aligned}
\bar{\nu} - \nu_0 &= \frac{\nu_m'' + \nu_m'}{2} = \left(\frac{eQ}{h}\right)^2 \frac{1}{2\nu_0} \frac{1}{2I(2I-1)} \times \\
& \times \left\{ \left[2I(I+1) - 1 - 2(3m^2 - 3m + 1) \right] (\tilde{\nu}E)_{\pm 2}^2 \right. \\
& \quad \left. - \left[4I(I+1) - 1 - 8(3m^2 - 3m + 1) \right] (\tilde{\nu}E)_{\pm 1}^2 \right\} \quad (2.20)
\end{aligned}$$

$$\begin{aligned}
\nu_c - \nu_0 &= 2\nu_0 \frac{1}{[2I(2I+1)]^2} \left(\frac{eQ}{h}\right)^2 \left\{ \left[2I(2I+1) - 3/2 \right] (\tilde{\nu}E)_{\pm 2}^2 \right. \\
& \quad \left. - \left[4I(I+1) - 3 \right] (\tilde{\nu}E)_{\pm 1}^2 \right\} \quad (2.21)
\end{aligned}$$

$\nu_0 = \frac{g\beta H_0}{h}$ is called the resonance frequency of the unperturbed system and $\frac{\nu_m'' + \nu_m'}{2}$ is the centroid of the satellite pair ν_m'' and ν_m' .

II. 5. The Electric Field Gradient Tensor.

The electric field gradient tensor ($\widetilde{\nabla E}$) is defined by eq 10 in the polar coordinate system with z' parallel to H_0 . Since fields at the nucleus arising from charges external to that volume are being considered, Maxwell's equations show that

$$\vec{\nabla} \cdot \vec{E} = 0 \quad (2.22a)$$

and
$$\vec{\nabla} \wedge \vec{E} = 0. \quad (2.22b)$$

Whatever form the tensor takes, these equations must be implicit. In the non-irreducible Cartesian form, a component of the electric field gradient tensor is $\phi_{ij} = \frac{d^2\phi}{dx_i dx_j}$.

Therefore, from eq 22a

$$\sum_i \phi_{ii} = 0 \quad (2.23a)$$

and from eq 22b

$$\phi_{ij} = \phi_{ji} \quad (2.23b)$$

Hence the tensor is traceless and symmetric. For the purpose of setting up the following theory, the irreducible Cartesian tensor is required, as follows,

$$\begin{aligned} (\widetilde{\nabla E})_{0}^{x'y'z'} &= \frac{1}{2} \phi_{z'z'} \\ (\widetilde{\nabla E})_{\pm 1}^{x'y'z'} &= \pm \frac{1}{\sqrt{6}} (\phi_{z'x'} \pm \phi_{y'z'}) \\ (\widetilde{\nabla E})_{\pm 2}^{x'y'z'} &= \frac{1}{2\sqrt{6}} (\phi_{x'x'} - \phi_{y'y'} \pm 2i\phi_{x'y'}) \end{aligned} \quad (2.24)$$

II. 6. Transformation Theory.

It is necessary to describe the crystalline electric fields at a nuclear site with respect to orthogonal axes X,Y,Z, which are chosen to coincide as far as possible with the natural crystallographic vectors a,b,c. Therefore the field gradient tensor components in the x',y',z' system are to be related to the components in the X,Y,Z system. The initial orientation of the crystal is chosen so that X,Y,Z coincide with y',z',x' and anticlockwise rotations through angles $+\theta_x$ are considered. Formally the transformation is achieved by means of the $D^{(j)}$ rotation matrices, thus

$$(\tilde{\nabla}E)_q^{x'y'z'} = \sum_{q'=-2}^{+2} D_{qq'}^{(2)} (\tilde{\nabla}E)_{q'}^{XYZ} \quad (2.25)$$

In our case

$$D_{qq'}^{(2)}(\alpha, \beta, \gamma) = D_{qq'}^{(2)}(0, \beta, \pi/2)$$

where

$$\beta = -(\theta_x + 90^\circ)$$

Formulae given by Rose (1957) for the $d^{(j)}$ coefficients are readily adapted to determine the matrix elements $D_{qq'}^{(j)}$ and using eqs 24 in conjunction with eq 25, the following relations are obtained upon substitution:

$$\begin{aligned} (\tilde{\nabla}E)_0 &= 1/4(\phi_{YY} + \phi_{ZZ}) + 1/4(\phi_{YY} - \phi_{ZZ})\cos 2\theta_x - \frac{1}{2}\phi_{YZ}\sin 2\theta_x \\ (\tilde{\nabla}E)_{\pm 1} &= 1/\sqrt{6} \left[\mp \left\{ \phi_{YZ}\cos 2\theta_x + \frac{1}{2}(\phi_{YX} - \phi_{ZZ})\sin 2\theta_x \right\} \right. \\ &\quad \left. - i \left\{ \phi_{XY}\cos 2\theta_x - \phi_{ZX}\sin 2\theta_x \right\} \right] \end{aligned}$$

$$(\tilde{\nabla}E)_{\pm 2} = 1/(\sqrt{6}) \left[3/2(\phi_{YY} + \phi_{ZZ}) - 1/2(\phi_{YX} - \phi_{ZZ}) \cos 2\theta_X + \phi_{YZ} \sin 2\theta_X \right. \\ \left. \pm 2i(\theta_{ZX} \cos 2\theta_X + \phi_{XY} \sin 2\theta_X) \right] \quad (2.26)$$

Direct substitution of eq 26 into eqs 19, 20 and 21 yields the following important relations:

$$\Delta \nu = \frac{1}{2}(2m-1) \{ a_X + b_X \cos 2\theta_X + c_X \sin 2\theta_X \} \quad (2.27)$$

where

$$a_X = K(\Psi_{YY} + \Psi_{ZZ}) \quad (2.28a)$$

$$b_X = K(\Psi_{YY} - \Psi_{ZZ}) \quad (2.28b)$$

$$c_X = -2K \Psi_{YZ} \quad (2.28c)$$

where

$$K = 3/2I(2I-1), \quad \Psi_{ij} = \frac{eQ}{h} \cdot \phi_{ij} \quad (2.28d)$$

and

$$\nu_c - \nu_o = n_X + p_X \cos 2\theta_X + r_X \sin 2\theta_X + u_X \cos 4\theta_X + v_X \sin 4\theta_X \quad (2.29)$$

Where

$$n_X = 1/96 \nu_o \{ 18a_X^2 - 7(b_X^2 + c_X^2) - 4(c_Y^2 + c_Z^2) \}$$

$$p_X = 1/8 \nu_o \{ (-a_X b_X - c_Y^2 - c_Z^2) \}$$

$$r_X = 1/8 \nu_o \{ (a_X c_X + 2c_Y c_Z) \}$$

$$u_X = 3/32 \nu_o \{ (b_X^2 - c_X^2) \}$$

$$v_X = 3/16 \nu_o (b_X c_X)$$

and

$$\bar{\nu} - \nu_o = \bar{n}_X + \bar{p}_X \cos 2\theta_X + \bar{r}_X \sin 2\theta_X + \bar{u}_X \cos 4\theta_X + \bar{v}_X \sin 4\theta_X$$

where

$$\bar{n}_X = 1/12 \nu_o (b_X^2 + c_X^2 + c_Y^2 + c_Z^2)$$

$$\bar{p}_X = -1/12 \nu_o (c_Y^2 + c_Z^2)$$

$$\bar{r}_X = -1/6 \nu_o c_Y c_Z$$

$$\bar{u}_X = -1/12 \nu_o (b_X^2 - c_X^2)$$

$$\bar{v}_X = -1/6 \nu_o b_X c_X$$

By cyclically permuting the X,Y,Z suffixes, the corresponding expressions for the Y, and Z rotations can be obtained. The tensor is called the quadrupole coupling tensor (Q.C.T.) and Laplace's equation must hold for it also, ie. $\nabla^2\psi = 0$. Thus from eqs. 28 a and b,

$$a_X = \frac{1}{2}(b_Y - a_Y) = -\frac{1}{2}(b_Z + a_Z) \quad (2.30 a)$$

$$b_X = -\frac{1}{2}(3a_Y - b_Y) = \frac{1}{2}(3a_Z - b_Z). \quad (2.30 b)$$

Three values for each of the diagonal components ψ_{ii} of the Q.C.T. are obtained. These are averaged and with the single values of the non-diagonal components ψ_{ij} form the complete 3x3 tensor.

The Q.C.T. contains all the physical information relevant to the electric field gradient at a particular nuclear site. To obtain this tensor, the above theory shows that the crystal must be rotated about the X,Y, and Z axes successively, and the resonance spectrum scanned at suitable angular intervals. The frequency differences $\nu'' - \nu'$ between the satellites are formed, and the first order Fourier coefficients a_i, b_i, c_i , ($i = X, Y, Z$) obtained. From these, the tensor can be written down immediately. The formation of

$\frac{\nu'' + \nu'}{2} - \nu_0$ from the same data gives the second order coefficients n_i, p_i, r_i, v_i, u_i , ($i = X, Y, Z$) which may be used to resolve certain ambiguities concerning the c_i -coefficients of certain symmetry related sites.

The tensor is diagonalised by standard methods to obtain the eigenvalues γ_i and direction cosines of the principal axes with respect to the X,Y,Z system. The secular determinant may be written as

$$\gamma^3 - a\gamma - b = 0 \quad (2.31a)$$

where

$$a = \Psi_{XY}^2 + \Psi_{YZ}^2 + \Psi_{ZX}^2 - \Psi_{XX}\Psi_{YY} - \Psi_{YY}\Psi_{ZZ} - \Psi_{ZZ}\Psi_{XX}$$

$$b = \Psi_{XX}\Psi_{YY}\Psi_{ZZ} + 2\Psi_{XY}\Psi_{YZ}\Psi_{ZX} - \Psi_{XX}\Psi_{ZY}^2 - \Psi_{YY}\Psi_{ZX}^2 - \Psi_{ZZ}\Psi_{XY}^2 \quad (2.31b \& c)$$

The value of "a" is invariant under the transformation

$\Psi_{ij} \rightarrow \Psi_{ji}$, whilst "b" changes sign. The relative signs of the tensor components are chosen to make "b" positive. The roots of equation 31a are

$$\gamma_n = 2(a/3)^{\frac{1}{2}} \cos(\alpha - 2\pi n/3) \quad n=1,2,3. \quad (2.32)$$

where

$$\cos 3\alpha = b/2.(a/3)^{1.5}$$

γ_3 is positive and γ_1 and γ_2 are negative, with

$$|\gamma_3| \geq |\gamma_2| \geq |\gamma_1| \quad \text{and} \quad \sum \gamma_i = 0. \quad \text{The direction cosines}$$

λ_n, μ_n, ν_n , of the principal axes corresponding to γ_n are found from

$$\frac{\lambda_n}{D_{1n}} = \frac{\mu_n}{D_{2n}} = \frac{\nu_n}{D_{3n}} = \frac{t_1}{[D_{1n}^2 + D_{2n}^2 + D_{3n}^2]^{\frac{1}{2}}}$$

where

$$D_{1n} = \Psi_{XY}\Psi_{YZ} - \Psi_{ZX}(\Psi_{YY} - \gamma_n)$$

$$D_{2n} = \Psi_{XY}\Psi_{ZX} - \Psi_{YZ}(\Psi_{XX} - \gamma_n)$$

$$D_{3n} = (\Psi_{XX} - \gamma_n)(\Psi_{YY} - \gamma_n) - \Psi_{XY}^2$$

The relative signs of $\lambda_n, \gamma_n, \delta_n$ are fixed but not their absolute signs - characteristic of a second rank tensor. δ_3 is called the quadrupole coupling constant, expressing the magnitude of the quadrupolar interaction in units of kc/sec, and δ_2 and δ_1 , are usually combined into the "asymmetry parameter" $\eta = \frac{|\delta_1 - \delta_2|}{\delta_3}$, which is the measure of the departure of the electric fields from cylindrical symmetry.

II. 7. The Quadrupole Coupling Tensor and Crystal Symmetry.

The above discussion has shown how to evaluate the tensor components $\Psi_{ij} = K\phi_{ij}$ with $i, j = X, Y, Z$ and $K = \frac{eQ}{h}$ from the basic frequency data for a given site. Section II.6 shows that, in the principal axis system, x, y, z , the tensor may be written as

$$\left(\begin{array}{ccc} \delta_1 = \frac{-(1-\eta) e q Q}{2 h} & 0 & 0 \\ 0 & \delta_2 = \frac{-(1+\eta) e q Q}{2 h} & 0 \\ 0 & 0 & \delta_3 = \frac{e q Q}{h} \end{array} \right)$$

where the conventional substitution $q = \phi_{zz}$ has been made.

The orientation of the principal axis system x, y, z relative to X, Y, Z is described by the direction cosines matrix

Reference Axis	Principal Axis		
	x	y	z
X	λ_1	λ_2	λ_3
Y	μ_1	μ_2	μ_3
Z	ν_1	ν_2	ν_3

By definition, each unique site of an atomic species in the crystalline unit cell has a chemical environment which gives rise to specific electric field gradients at the nucleus. Evaluation of the distinct values of the quadrupole coupling constant and asymmetry parameters enables the number of unique sites to be deduced. In practice this enumeration can often be achieved immediately upon the examination of the spectra at special crystal orientations without eQ/h values being first evaluated.

Further sites are generated from the unique sites by the symmetry elements and amongst these symmetry related sites only those whose principal axes present different orientations with respect to the magnetic field will be distinguished. Sites related by translation elements or a centre of inversion can never be distinguished in the n.m.r. experiment. The signals from symmetry related sites may coalesce under certain circumstances to give a "reduced" spectrum. For instance, when a two-fold axis or the normal to a mirror plane is held perpendicular or parallel to H_0 the signals from pairs of related sites will coalesce; a three fold axis held parallel to H_0 will give a triply degenerate spectrum. In addition, the symmetry of the ν', ν'' vs θ curves must be compatible with the symmetry elements. Consequently if the number of asymmetric units per unit cell and the space group of the

crystal are known from chemical and x-ray data the n.m.r. spectrum must be consistent with this regarding the number and symmetry of the signals. Alternatively, when the space group is not uniquely determined from x-rays when the crystal structure is unknown, the information obtained from n.m.r. on the point group, in conjunction with the available x-ray evidence usually enables the space group to be determined. In the following chapters examples of both situations will be met.

For atoms in general positions the crystal symmetry imposes no restrictions on the orientation of the principal axes. When however an atom is located in a special position, the symmetry of the field gradients at the site are determined directly by the type of symmetry at the site. Thus, for an atom located on a mirror plane or on a two-fold axis, one principal axis lies along the normal or the two-fold axis respectively. Similarly the z-principal axis at an atomic site lying on a three fold axis is constrained to be along the three fold axis, and in addition $\eta = 0$. We note, however, that no constraints are imposed on the principal axis orientations of sites situated on glide planes or two-fold screw axes.

II. 8. Removal of Ambiguities in the Analysis of Data from Symmetry Related Sites.

In section II.7 we have indicated that whenever the rotation axis coincides with a two-fold axis or the normal to a mirror plane, the spectrum becomes doubly degenerate. Due to this choice of rotation axis, equivalent lines from each pair of sites related to the two-fold axis or mirror plane coalesce at each of the orientations common to two rotations resulting in an uncertainty in the lines to associate with a given nuclear site and hence in the signs of the c -coefficients. For the sites possessing large quadrupole interactions, the signs of second order perturbation coefficients " r_i " enable the correct combination of signs of the q -coefficients to be chosen directly.

This method is not available when r_i is measured to be zero within experimental error, as, for instance, in the case of the L sites described in Ch. V. Several alternative methods have been used in the past. A choice of different rotation axes X,Y,Z such that none coincide with a crystallographic two-fold axis or the normal to a mirror plane would eliminate this difficulty, but would create problems in accurate alignment of the crystal, and is consequently unpopular.

Pennington (Thesis 1961) favoured a method in which

the crystal was reoriented to several known general positions in the magnetic field, and the spectrum scanned. Knowledge of the direction cosines of the X,Y,Z system with respect to x'y'z' system enables the splitting to be calculated for the two possible combinations of signs for the coefficients, and the values compared with the observed splittings. The method is particularly advantageous when the c_i -coefficients are large and large differences in the predictions result from small arc changes. In borax, however, which was the only case where such ambiguities had to be resolved by recourse to further measurements, the differences between the predicted values was small, particularly for the small arc movements available. Another method was therefore devised whereby the satellites were "followed" from one rotation to another, thus allowing a direct association of resonances in the three rotations. The symmetry of tincalconite permitted yet another method to be used without the need of further measurements. The details of the latter two schemes are described in detail in sections V.1 and VI.1, along with the quantitative data involved.

II. 9. Proton Pairs in Single Crystals.

The magnetic perturbation term in eq. 2 .1 will now be discussed. The fine structure of the magnetic resonance

spectrum of protons is of particular interest here since these nuclei have played an important role in the work on LiHzS. This first section is devoted to the cases of rigid and reorienting proton pairs in a single crystal.

The relative orientation of an isolated pair of interacting protons in a large magnetic field is fixed by the parameters (r, δ, θ_0) as shown in fig.1. Again the reference axes X, Y, Z bear a definite, known relation to the natural crystallographic vectors. The quantum mechanical Hamiltonian follows directly from the classical expression for the interaction energy between two magnets $\vec{\mu}_1$ and $\vec{\mu}_2$ upon substitution of $\vec{\mu}_k = \mu \hat{\sigma}_k$

$$\hat{V} = - \hat{\mu}_1 \cdot \hat{H}_2 = - \mu^2 r^{-3} [\hat{\sigma}_1 \cdot \hat{\sigma}_2 - 3(\hat{\sigma}_1 \cdot \hat{r})(\hat{\sigma}_2 \cdot \hat{r})] \quad (2.35)$$

where $\frac{1}{2}\hbar\hat{\sigma}_k$ is the intrinsic momentum operator for spin $\frac{1}{2}$ and $\mu = 2.7896$ nuclear magnetons.

Since the first order perturbation approximation is adequate, the matrix elements $\langle I, m | \hat{V} | I, m \rangle$ are required; only triplet state wavefunctions need be considered because transitions between singlet and triplet states are highly forbidden.

Following Pake(1948), the identity

$$\begin{aligned} \vec{\sigma}_1 \cdot \vec{\sigma}_2 - 3(\vec{\sigma}_1 \cdot \vec{r})(\vec{\sigma}_2 \cdot \vec{r}) \\ = \frac{1}{2}(3\cos^2\theta - 1)(\vec{\sigma}_1 \cdot \vec{\sigma}_2 - 3\sigma_{1z}\sigma_{2z}) \\ - 3/4(\sigma_{1x} + i\sigma_{1y})(\sigma_{2x} + i\sigma_{2y})\sin^2\theta \cdot e^{-2i\phi} \end{aligned}$$

Figure 1

Angles (r, δ, θ_0) used to specify the orientation of a proton-proton vector relative to the orthogonal axes X, Y, Z. θ is the angle between the p-p direction and the applied magnetic field H_0 , which lies in the XY plane.

Figure 2

The broken line shows the calculated distribution of component line centres for the proton resonance in powdered $\text{CaSO}_4 \cdot 2\text{H}_2\text{O}$, which contains proton pairs. The continuous line on the same plot is the calculated line - shape obtained by superimposing gaussians of width 1.54 gauss according to this distribution function. The dots show the experimental points obtained by Pake (1948).

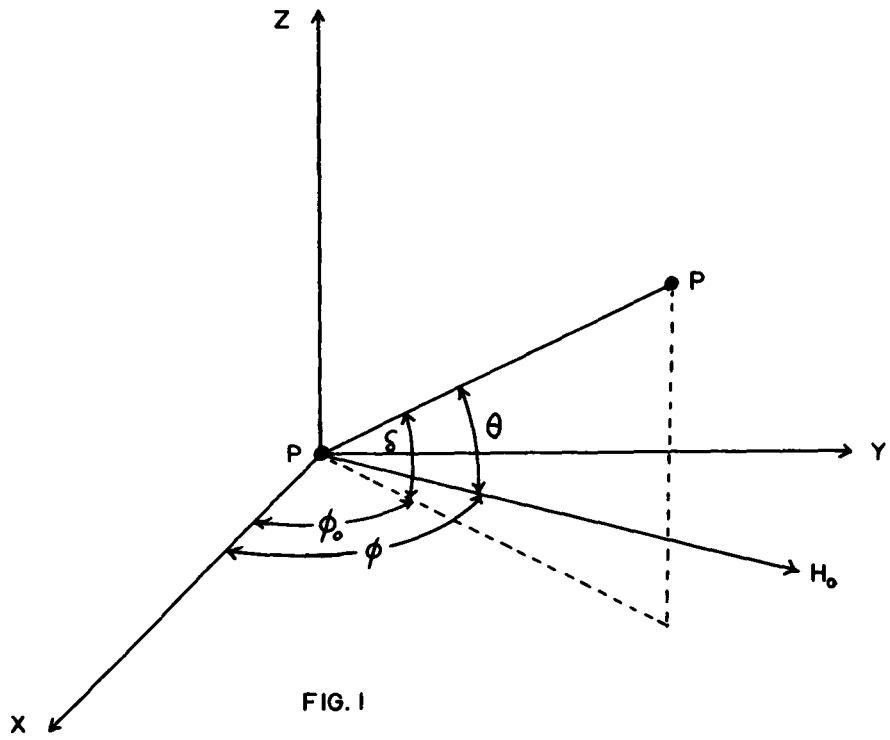


FIG. 1

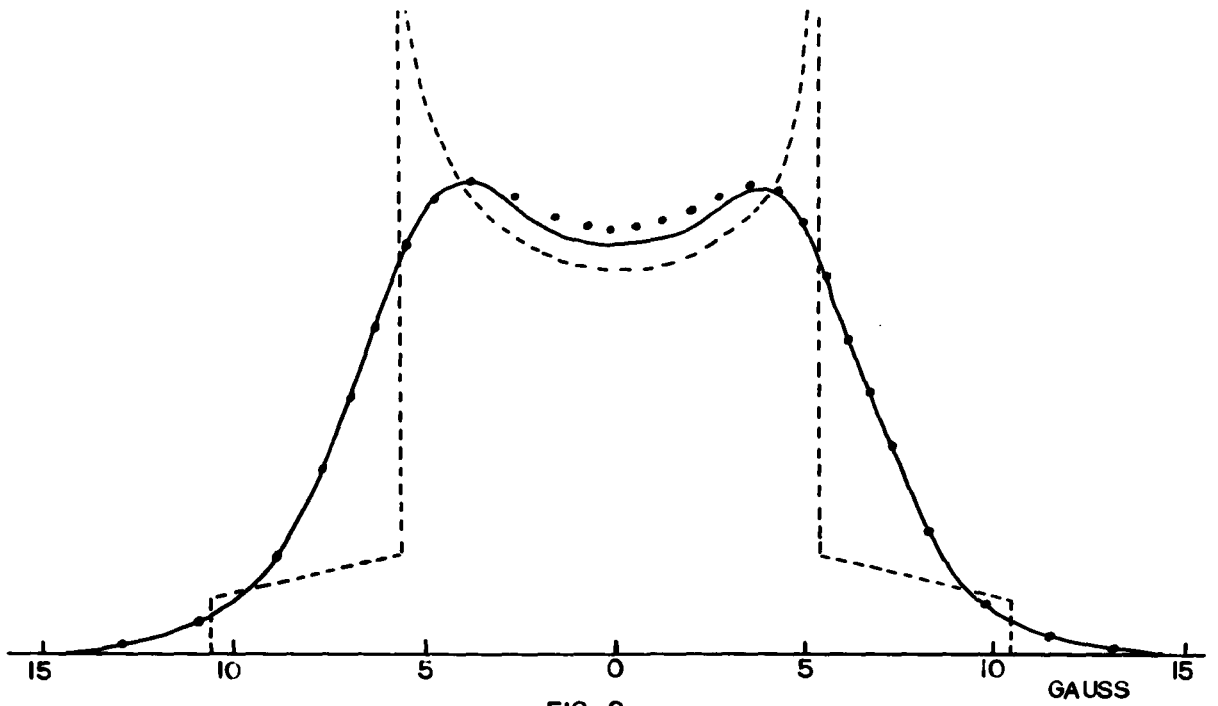


FIG. 2

$$\begin{aligned}
& -3/4(\sigma_{1x} - i\sigma_{1y})(\sigma_{2x} - i\sigma_{2y})\sin^2\theta.e^{2i\phi} \\
& -3/4 \sigma_{2z}(\sigma_{1x} + i\sigma_{1y}) + \sigma_{1z}(\sigma_{2x} + i\sigma_{2y}) \sin\theta.\cos\theta.e^{i\phi} \\
& -3/4 \sigma_{2z}(\sigma_{1x} - i\sigma_{1y}) + \sigma_{1z}(\sigma_{2x} - i\sigma_{2y}) \sin\theta.\cos\theta.e^{i\phi}
\end{aligned}$$

yields the following values for the matrix elements:

$$\begin{aligned}
\langle 1, -1 | V | 1, -1 \rangle &= -\mu^2 r^{-3} (3\cos^2\theta - 1) \\
\langle 1, 0 | V | 1, 0 \rangle &= 2\mu^2 r^{-3} (3\cos^2\theta - 1) \\
\langle 1, 1 | V | 1, 1 \rangle &= -\mu^2 r^{-3} (3\cos^2\theta - 1)
\end{aligned} \tag{2.35}$$

Therefore resonance occurs when the radio-frequency satisfies the conditions

$$\begin{aligned}
m = +1 \rightarrow m = 0 & \quad h\nu' = 2\mu H_0 + 3\mu^2 r^{-3} (3\cos^2\theta - 1) \\
m = 0 \rightarrow m = -1 & \quad h\nu' = 2\mu H_0 - 3\mu^2 r^{-3} (3\cos^2\theta - 1)
\end{aligned}$$

Hence the splitting is symmetrical about ν_0 (where $\nu_0 = 2\mu H_0/h$) and its angular dependence is

$$(\nu'' - \nu') = 6\mu^2 r^{-3} (3\cos^2\theta - 1)/h \tag{2.36}$$

In a great deal of the past work on dipole-dipole broadening, the radio-frequency was held constant, whilst the magnetic field swept through the resonance. Signal splittings are then measured in gauss and the resonance condition is written

$$H = H_0 \pm \alpha (3\cos^2\theta - 1) \tag{2.37}$$

with $\alpha = (3/2)\mu r^{-3}$ and $H = \frac{h\nu_0}{2\mu}$. This splitting can be expressed in terms of δ and ϕ_0 by the relation

$$\cos\theta = \cos\delta . \cos(\phi - \phi_0) \tag{2.38}$$

The observed widths of the absorption lines are determined chiefly by the lifetimes of the spin states (ie. on

the spin-spin relaxation time T_2) and the magnetic fields from more distant neighbours. The proton resonance from a single crystal containing p-p vectors usually consists of more than a single pair of signals. This arises, of course, through the multiplicity of orientations that the symmetry elements produce from a given p-p vector. In addition there are sometimes different chemical species of p-p vectors.

When the proton pairs are not rigid, but are reorienting about some axis at a frequency greater than the rigid lattice line width, it becomes necessary to take the time average of $\frac{1}{2}(3 \cos^2 \Theta - 1)$ over the motion. The result of this calculation shows that the resonance condition becomes

$$H = H_0 \pm \frac{1}{2} \alpha (3 \cos^2 \gamma - 1) (3 \cos^2 \Theta - 1) \quad (2.39)$$

where γ is the angle that the p-p vector makes with the axis of rotation and Θ' is the angle between the axis of rotation and the magnetic field. The fine structure still consists of two lines, but their separation is reduced by the constant factor $\frac{1}{2}(3 \cos^2 \gamma - 1)$. For the special case of the reorientation axis perpendicular to the p-p direction, the splitting is half that of the corresponding rigid lattice splitting.

II. 10. Proton Pairs in Polycrystalline Samples.

Polycrystalline samples have found much use in dipolar studies, having special merit when, for instance,

single crystals are not available, the crystal structure is unknown, or particular molecular groups thought to be present are to be identified. The shape and the value of the second moment (see section II. 12) are the important defining parameters. For a polycrystalline material containing identical proton pairs, we assume in calculating the line shape that there is an isotropic distribution of p-p vectors. Also since the Boltzmann distribution factors are essentially the same for all the triplet levels, the transition probabilities are both $\frac{1}{2}$. Then the number of transitions $m = 1 \rightarrow m = 0$ per unit time is

$$N_+ = N/2 \int_0^1 d(\cos\theta) = N/2 \int_{H_0 - \alpha}^{H_0 + 2\alpha} p_+(H) dH$$

where N is the total number of transitions per unit time and $p_+(H) dH$ is the probability that a transition from $m=1 \rightarrow m=0$ occurs in a range dH . Expressing $d(\cos\theta)$ in terms of H and dH , N_+ becomes

$$N_+ = N/2 \int (2\sqrt{3})^{-1} (\Delta H/\alpha + 1)^{-\frac{1}{2}} d(\Delta H)$$

where $\Delta H = H - H_0$. Consideration of the transition $m=0 \rightarrow m=-1$ yields $p_+(-\Delta H) = p_-(\Delta H)$ and the resultant distribution is

$$p(\Delta H) \propto (\Delta H/\alpha + 1)^{-\frac{1}{2}} \quad \text{for } +2\alpha \geq \Delta H \geq -\alpha$$

$$\propto (-\Delta H/\alpha + 1)^{-\frac{1}{2}} \quad \text{for } +\alpha \geq \Delta H \geq -2\alpha$$

The dotted line in fig.2 shows $p(\Delta H)$ plotted as a function of H with $\alpha = 5.4$ gauss, a value characteristic of water of hydration.

Now $p(\Delta H)dH$ is just the probability that the centre of a fine structure component line occurs in dH and the resultant absorption line for a powder is the superposition of bell shaped curves of finite widths weighted by the probability that their centres fall in dH_0 . If $f(H)$ is the resultant shape function, then

$$f(H) = \int_{-\infty}^{\infty} p(H' - H_0) S(H - H') dH'$$

where $S(H - H')$ is the shape of the component line. The smooth curve in Fig.2 is calculated from the above expression using α for gypsum and a Gaussian component line $S(H - H') = \exp \left[-(H - H')^2 / 2\beta^2 \right]$, with $\beta = 1.54$ gauss. β is a typical width of an isolated signal from a single crystal. In his work on gypsum, Pake (1948) found the experimental lineshape in good agreement with the theoretical one.

II 11. Equilateral Triangles of Protons.

This calculation was made by Andrew and Bersohn (1950).

The Hamiltonian for the interaction of three identical nuclei is

$$g\beta H_0 \sum_{i=1}^3 \hat{I}_{zi} + \sum_{i>j} (\hat{I}_i \cdot \hat{I}_j - 3\hat{I}_{zi} \hat{I}_{zj}) A_{ij}$$

where

$$A_{ij} = \frac{g^2 \beta^2}{2r_{ij}^3 (3\cos^2 \theta_{ij} - 1)}$$

and where θ_{ij} is the angle between \vec{r}_{ij} and \vec{H}_0 . The states of the three spin system were labelled by the eigenvalues $I_1^2, I_2^2, I_3^2, g^2, I^2$ and I_z , where $\vec{g} = \vec{I}_1 + \vec{I}_2$, $\vec{I} = \vec{g} + \vec{I}_3$ and $I_z = I_{1z} + I_{2z} + I_{3z}$

and the matrix elements of the Hamiltonian calculated. The general result is that the line whose energy was at $h\nu_0 = g\beta H_0$ is now split into a central undeviated component flanked by three pairs with energy values $\pm(3x + y)$, $\pm 2y$, and $\pm(3x - y)$ relative to the unperturbed energy. Here

$$\begin{aligned} x &= 1/4(A_{12} + A_{23} + A_{31}) & a &= \sqrt{6}/4(A_{13} + A_{23}) \\ y &= (x^2 + a^2 + b^2)^{1/2} & b &= \sqrt{2}/4(2A_{12} - A_{13} - A_{23}) \end{aligned}$$

The transition probabilities are given in the original paper. Defining Ψ as the angle between H_0 and the normal to the plane of the triangle, we obtain for the case of an equilateral triangle that

$$\begin{aligned} x &= \frac{\mu\alpha}{2}(1 - 3\cos^2\Psi) \\ y &= \mu\alpha \left[(27/4)\sin^4\Psi - 3\sin^2\Psi + 1 \right]^{1/2} \end{aligned}$$

where $\alpha = \frac{3}{2}\mu r^{-3}$, r being the length of a side of the triangle. The energy level diagram appears as in Fig.3. The line shape for a polycrystalline specimen containing rigid triangles of protons is calculated as for a p-p pair (section II.10), yielding a theoretical shape shown in Fig.4 for the case in which the broadening has been taken into account.

The interaction Hamiltonian must be modified when the nuclear pairs rotate with greater frequency than the frequency that their positions are measured in the n.m.r. experiment. Pake and Gutowsky (1950) show that for such a case the coefficients A_{ij} which contain the position coordinates must be

Figure 3

Energy levels for three nuclei of spin $\frac{1}{2}$

Figures 4 and 5

Typical lineshapes from a powder specimen containing protons at the corners of equilateral triangles. Fig. 4(a) corresponds to rigid triangles broadened by neighbours, with the derivative curve shown in Fig. 4(b). Fig. 5(a) corresponds to each triangle rotating about the normal to the plane of the triangle, with broadening by neighbours. The derivative curve is shown in Fig. 5(b).

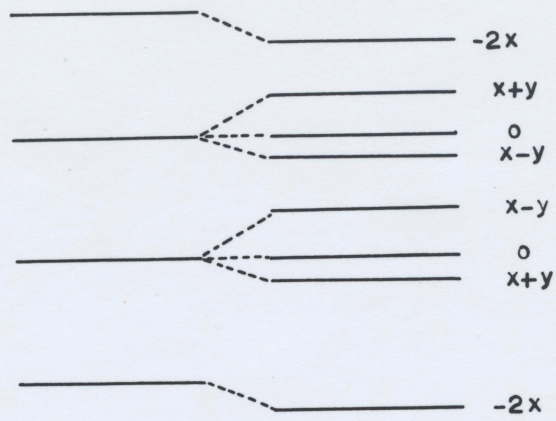


FIG. 3

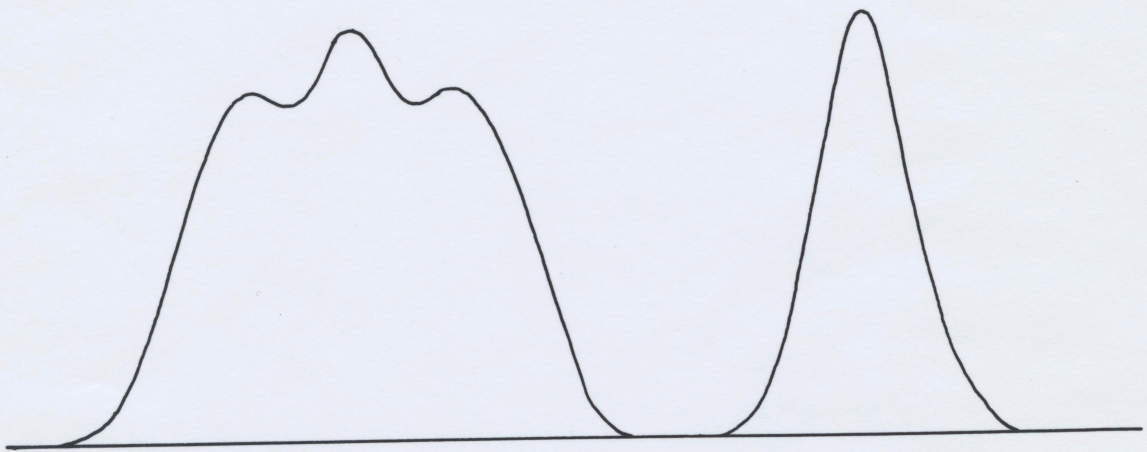


FIG. 4(a)

FIG. 5(a)

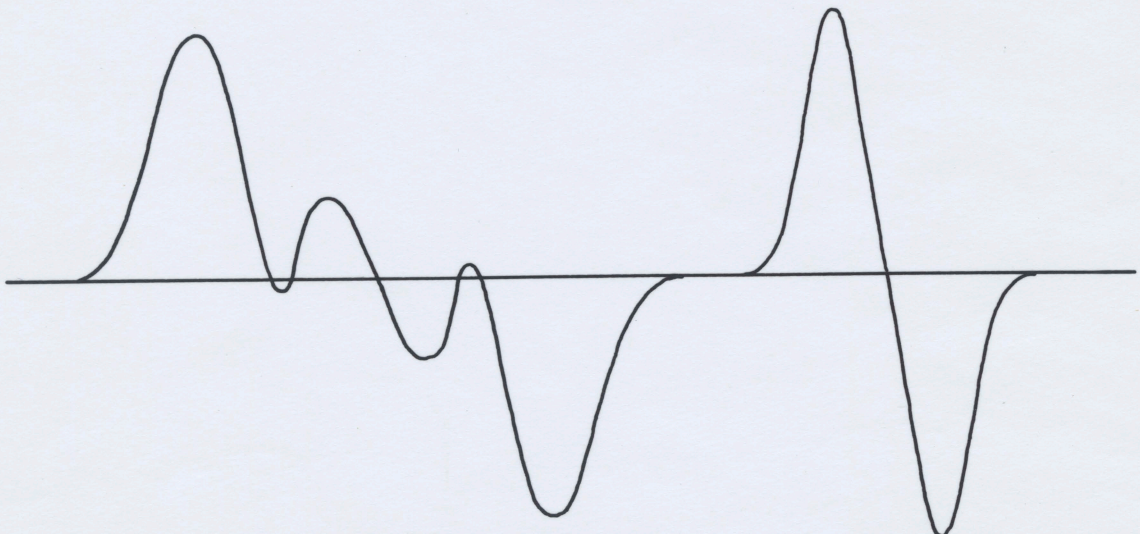


FIG. 4(b)

FIG. 5(b)

replaced by averages over the state of motion. For an equilateral triangle this replacement leads to new values of x and y , x' and y' :

$$\begin{aligned} x' &= \frac{\mu\alpha}{4}(1 - 3\cos^2\eta)(1 - 3\cos^2\epsilon) & (2.39) \\ y' &= \frac{\mu\alpha}{2}(1 - 3\cos^2\eta)\left(\frac{27\sin^4\epsilon}{4} - 3\sin^2\epsilon + 1\right)^{\frac{1}{2}} \end{aligned}$$

where ϵ and η are respectively the angles which the normal to the triangle plane and the field H_0 make with respect to the axis of rotation. In the case of a triangle rotating about the C_3 axis $\epsilon = 0$ and $x' = -y'$. Consideration of the amplitude functions show that only one pair of satellites remain each with probability $\frac{1}{4}$ flanking a central with probability $\frac{1}{2}$. The change in energy of the satellites from the unperturbed value is $\pm 4x' = \pm 2\mu\alpha(1 - 3\cos^2\eta)$ so that in gauss, the separation becomes $\pm \alpha(1 - 3\cos^2\eta)$. The functional dependence for these satellites is therefore precisely that of the normal "Pake doublet" arising from a proton pair. The typical line shape from a powder containing rotating triangles broadened by neighbours is shown in Fig. 5.

II. 12. Second Moments of n.m.r. Signals Broadened by Magnetic Interactions.

The second moment $\langle \Delta H^2 \rangle$ of an absorption signal is defined by

$$\langle \Delta H^2 \rangle = \int_{-\infty}^{+\infty} f(H) (H - H_0)^2 dH, \quad (2.40)$$

where

$$\int_{-\infty}^{+\infty} f(H) dH = 1$$

Van Vleck(1948) has deduced the following formula for $\langle \Delta H^2 \rangle$ for n.m.r. signals broadened by magnetic interactions,

$$\begin{aligned} \langle \Delta H^2 \rangle = & \frac{3}{2} \cdot I(I+1) N_s^{-1} \gamma^2 \hbar^2 \sum_{j>k} \sum_k (3\cos^2\theta_{jk} - 1)^2 r_{jk}^{-6} \\ & + \frac{1}{3} \cdot N_s^{-1} \hbar^2 \sum_j \sum_f I_f(I_f+1) \gamma_f^2 (3\cos^2\theta_{jf} - 1) r_{jf}^{-6} \end{aligned} \quad (2.41)$$

Here j,k are nuclei at resonance, and f refers to other species possessing magnetic moments. θ_{jk} is the angle the vector r_{jk} separating j and k makes with H_0 . N_s is the number of distinct nuclei at resonance.

From the standpoint of this work, a more important formula is deduced by averaging over all orientations as for a powder sample. The angular factors become

so that

$$\begin{aligned} (3\cos^2\theta_{jk} - 1)^2 \text{ average} & \rightarrow 4/5 \\ \langle \Delta H^2 \rangle = & \frac{6}{5} \cdot I(I+1) N_s^{-1} \gamma^2 \hbar^2 \sum_{j>k} \sum_k r_{jk}^{-6} \\ & + \frac{4}{15} \cdot \hbar^2 N_s^{-1} \sum_j \sum_f I_f(I_f+1) \gamma_f^2 r_{jf}^{-6} \end{aligned} \quad (2.42)$$

When the nuclei at resonance are not fixed, the second moment is reduced from the so called "rigid lattice" second moment. The value of the second moment can again be obtained from a modified form of the Van Vleck expression as follows. The spherical harmonic addition theorem yields

$$\langle P_l(\cos \theta_{jk}) \rangle_{\phi} = P_l(\cos \theta^i) P_l(\cos \gamma_{jk}) \quad (2.43)$$

where the subscript ϕ indicates an average over this variable.

For $l = 2$,

$$\langle (3\cos^2\theta_{jk} - 1) \rangle_{\phi} = \frac{1}{2} (3\cos^2\theta^i - 1) (3\cos^2\gamma_{jk} - 1) \quad (2.44)$$

The second moment for a system rotating about an axis making an angle θ' with H_0 is found by substituting eq.44 into eq. 41. For a powder, the axes are isotropically distributed, and since $(3\cos^2\theta' - 1)^2$ averaged over a sphere is $4/5$, the second moment for a powder is

$$\langle \Delta H^2 \rangle = \frac{1}{4} \left[\frac{6}{5} I(I+1) N_s^{-1} \gamma^2 h^{-2} \sum_{j>k} \sum_k (3\cos^2\gamma_{jk} - 1)^2 r_{jk}^{-6} + \frac{4}{15} N_s^{-1} h^2 \sum_j \sum_f I_f(I_f+1) \gamma_f^2 (3\cos^2\gamma_{if} - 1)^2 r_{jf}^{-6} \right] \quad (2.45)$$

Thus, to find the second moment for a powder specimen when the species at resonance is reorienting, one merely reduces the rigid lattice powder value by the factor

$$F(\gamma) = \frac{1}{4} (3\cos^2\gamma_{jk} - 1)^2 \quad (2.46)$$

For the important special cases of an NH_2 group reorienting about the axis perpendicular to the p-p vector, and an NH_3^+ group reorienting about its C_3 axis, the rigid lattice second moment is reduced by $\frac{1}{4}$ for each.

In the derivations of these expressions, the assumption was made that the pairs of nuclei move in an n-fold potential, such as $V(\theta, \phi) = (V_0/2) (1 + \cos n\phi)$ and, as the temperature is increased or the potential is altered by lattice changes, higher levels within the minima are populated. Tunneling can occur from one level to another and Bersohn (1952) has shown that for $n \gg 3$ this is indistinguishable from classical rotation for minima of closely equal depth.

II. 13. Line Width Transition in a Powder Sample.

In the previous sections on magnetic dipole broadening, we have considered either rigid lattices or lattices in which the magnetically interacting constituents are reorienting at a rate greater than the rigid lattice line width.

Bloembergen, Purcell and Pound (B.P.P.) (1948) have developed a theory to describe the so called "line-width transition".

This is the name given to the characteristic narrowing of the n.m.r. signal as reorientation sets in. B.P.P. found the width of an absorption line in terms of the Debye correlation time τ_c . Corresponding to this, a "correlation frequency" or reorientation rate, $\nu_c = (2\pi\tau_c)^{-1}$, can be defined, which one may think of as an average rate at which significant changes occur in the atomic arrangement about a given nucleus. Then B.P.P.'s eq 52 becomes

$$\delta\nu = A (2/\pi) \tan \left\{ \alpha (\delta\nu/\nu_c) \right\} \quad (2.47)$$

$\delta\nu$ is the line-width c.p.s. and α is a factor of order unity encompassing the uncertainties arising from the integration limits in B.P.P.'s eq. 35. For $\delta\nu$, Gutowsky and Pake (1950) take the separation between outermost points of maximum and minimum slope on the absorption curve of a powder sample. The constant A is the width of the absorption line for a rigid lattice ($\nu_c \rightarrow 0$)

As the reorientation rate increases and approaches the

rigid lattice width A , $\delta\nu$ decreases. Since A is typically about 100 kc/sec, the line width will be narrowed by molecular reorientations at frequencies which are very low on the thermodynamic scale.

To treat a transition from one definite line width to a narrower line characteristic of a specialised type of motion, Bersohn has shown that by introducing a separate correlation time associated with the motion eq. 52 given by B.P.P. can be written

$$(\delta\nu)^2 = B^2 + C^2(2/n)\tan^{-1}(\alpha\delta\nu/\nu_c) \quad ,$$

where $(B^2 + C^2)^{\frac{1}{2}}$ is now the rigid lattice line width. It is usual to assume that $\nu_c = \nu_0 \exp(-V/kT)$, which permits a value of the activation energy, V , to be found.

CHAPTER III

APPARATUS AND EXPERIMENTAL PROCEDURE

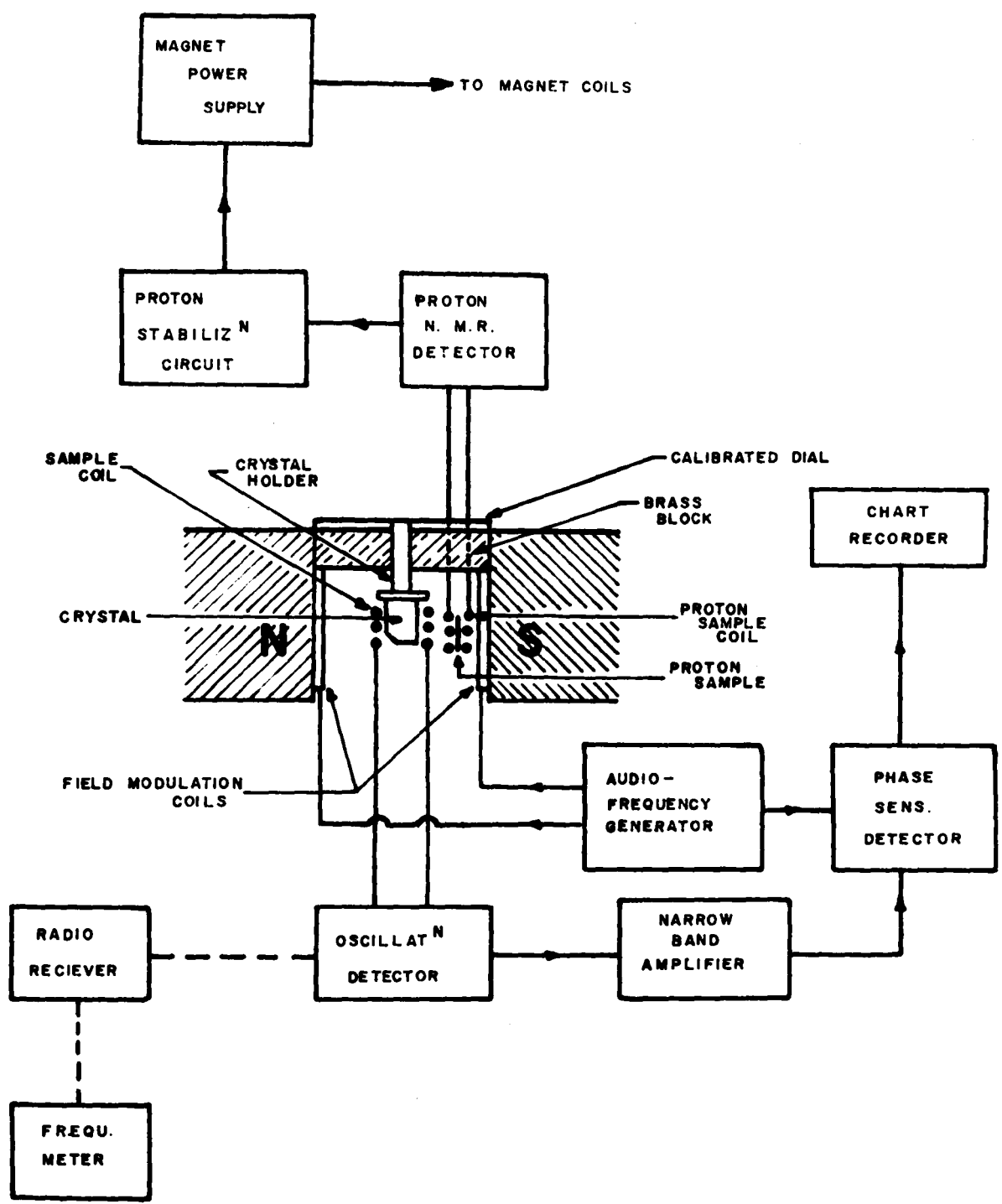
This chapter provides a brief description of the nuclear magnetic resonance spectrometer, the methods of attaining sample temperatures higher and lower than room temperature, the crystal alignment techniques, and the general form of the experiment to obtain the electric field gradient tensor. Datars (1956) gives a thorough description of the spectrometer.

III. 1. The Nuclear Magnetic Resonance Spectrometer.

A block diagram of the spectrometer is shown in Fig. 6. The large magnetic field was produced by a Varian Associates Ltd. Electromagnet with 12" diameter pole pieces and a 3" gap. Fields up to 10,000 gauss could be achieved with full magnetic current. The D.C. and A.C. stabilization of the power control circuits gave long and short term stabilities of 2:100,000 and 1:100,000 and the additional proton stabilization increased this to at least 1:250,000, the chief limitation then being the stability of the oscillator over long periods. The field inhomogeneity over the largest sample volumes used (approximately 3 cc) was such as to cause no

Figure 6

Block diagram of the nuclear magnetic resonance spectrometer.



significant broadening of the signals from the crystals. This was checked by observing the signal shape from mineral oil, whose natural line width is only a few hundred cycles/sec. It was found that the signal gave a second moment of 0.1 gauss^2 and 2 Kc/sec separating the derivative extrema. Except for the proton resonances from lithium hydrazinium sulphate at temperatures higher than 190°C , the broadening as indicated by the mineral oil signal is very small compared to the natural line widths of the n.m.r. signals obtained in this work.

The oscillating detector was of the same general design as that described by Volkoff et al (1952) and consisted of a push-pull marginal oscillator, two stages of r.f. amplification followed by detection, with d.c. feedback to the oscillator section to maintain the level of oscillation constant whilst sweeping the frequency. This was followed by a stage of audio frequency amplification and a narrow band amplifier tuned to the frequency at which the large static magnetic field was modulated. The radio frequency spectrum was scanned by slowly altering the value of the tank circuit capacitor using a clock drive followed by a gear system, permitting variable sweep rates to be used. Frequencies were measured by mixing the outputs from the marginal oscillator and a General Radio heterodyne frequency meter (Type 620 A), then

listening to the audio beat frequency with a Hallicrafters Model SX 62 A receiver and noting when this beat went to zero. With careful corrections, frequency measurements were made to within ± 0.5 kc/sec, though measurements considerably better than this (approximately ± 0.25 kc/sec) were achieved over small frequency intervals, as for instance in the proton resonance work. Considering that the centre of an absorption signal could only be located in general to within about one or two Kc/sec, due to their large breadths, the accuracy of the frequency measurement was entirely adequate.

The applied magnetic field was modulated to make the resonance condition repetitive at the modulation frequency, thereby causing the radio frequency carrier wave to be modulated at the same frequency. The depth of the modulation is proportional, for small modulations, to the slope of the absorption resonance curve. After amplification and rectification in the Schuster (1951) type phase sensitive detector, the derivative curve was recorded on a strip recorder. The major portion of the quadrupolar studies were recorded on a 6" Varian G 10 (100 mv) recording millivoltmeter. Fortunately most of the dipolar studies were done later when a superior 11" Westronics (Model D 11 A) recording milliammeter became available, enabling second moments to be evaluated with greater accuracy than with the Varian instrument.

With respect to the experimental conditions under which the resonances were sought, several points were borne in mind during these experiments. The density of r.f. electromagnetic energy in the sample determines the degree of nuclear spin saturation, and by observing the symmetry of the shape of the resonance signals and their width as a function of r.f. power, conditions were determined under which no appreciable saturation was present. The sensitivity of an oscillating detector is greatest when the r.f. power is lowest; however, the noise level due to instabilities is greater at low r.f. power, so that power levels were used between those at which saturation or excessive noise generation set in. Since the signal strength depends on the number of nuclei per unit volume of the oscillator coil, maximum sensitivity was achieved by winding the coil on the crystal whenever the shape and size of the crystal permitted and whenever the level of oscillation could be adjusted to avoid saturation. In the quadrupolar studies, modulation amplitudes approximately equal to the signal widths were used. Very much smaller modulations (about 0.6 gauss) were used for all the dipolar studies. In the latter work particularly, linearity of the detection system was essential. This was checked by inducing modulation pick up in the oscillating detector and then observing the output signal from the narrow band amplifier. Even for out-

put signals twenty times larger than those dealt with in the n.m.r. experiment, no distortion could be observed. The phase sensitive detector was thought to behave as required since the signals produced by it ^{and} another commercial model, a Princeton Applied Research Lock-In Amplifier, Type JB - 4, were indistinguishable. The linearity of the recorder was checked by standard methods. The various modulation amplitudes used in the experiments were determined by measuring the induced e.m.f. in a standard search coil placed in the sample position. For the experiments where proton signals were investigated, the magnetic field was stabilised to the fluorine resonance from teflon.

III. 2. Sample Temperature Control.

Whilst the hydrated borates were studied only at room temperature, it was found essential to obtain the Li^7 and proton signals from LiHzS over a wide temperature range. The crystal and coil assembly were contained in a cell carefully insulated with teflon. To obtain temperatures between 23°C and 225°C , a stream of air was first passed over a heated nichrome coil in a long quartz tube and then entered the cell. Temperatures in the range from below 23°C to -100°C were achieved by making use of the boil off from liquid air in a Dewar caused by an immersion heater. In both

instances, the temperature of the sample could be controlled by varying the amount of power delivered by a variac to the heater coils. The temperature of the sample was measured by a copper-constantan thermocouple which, for powder specimens was buried in the middle of the sample, and for a single crystal was placed in a small hole cut into the crystal. Fine teflon insulation was used on the copper and constantan leads and much care had to be taken to ensure that these did not vibrate in the air stream. As a further precaution against noise generation and pick up, the leads from the cell were also prevented from moving about in the large magnetic field and one point of the thermocouple circuit was at earth potential. The thermocouple e.m.f. was measured by a Croyden Precision Instrument Co. Type P4 Potentiometer. Another thermocouple monitored the temperature of the air at the outlet of the cell and equality of the temperatures at the two junctions indicated that the crystal temperature was uniform.

Observation of the spectrum at the temperature of liquid air was made more difficult, owing to the very small modulation and radiofrequency amplitude found necessary. Final measurements were obtained by immersing the coil and powder, protected in a glass test tube, in liquid air. They were entirely enclosed by a well-earthed thick brass shield with holes drilled in it. The shield greatly reduced external

pick up by the oscillator coil. At all temperatures the crystal temperature remained constant within $\pm 1^{\circ}\text{C}$ for the length of time to scan the resonance spectrum.

III. 3. Alignment of Crystals in the Applied Magnetic Field.

In order to use the Volkoff scheme to obtain the quadrupole coupling tensor, the orientation of the X,Y,Z system relative to the x',y',z' system of axes must be known, and the ultimate precision of the experiment depends to a large extent on the accuracy of the initial crystal alignment. Good accuracy has been achieved by the use of two complementary techniques, one relying on optical methods, the other using the n.m.r. spectrum itself. The crystals were mounted on a brass Unicam goniometer which itself was attached to the rotor of the sample holder, thereby enabling the crystal to be reoriented about any one of the three mutually perpendicular axes. Since all three crystals described in this thesis were artificially grown, the crystallographic faces were well developed. The x-ray studies described in Chapter IV enabled the faces to be indexed and thereby made useful in optical alignment. The optical method was normally used in the preliminary alignment but where the n.m.r. method of alignment could not be used to advantage, as in lithium hydrazinium sulphate, owing to the small angular variation of the signals,

extra care in the optical setting was taken. By coating a particular crystal face with a thin film of oil it was found possible to reflect a beam of light originating close to the telescope, from the face and back into the telescope, which was set about 12 feet from the crystal. Another portion of the beam was reflected from a plate on the crystal holder which was machined to be parallel to the rotor axis and to fit flush against the magnet pole pieces when the holder was placed in the magnetic field. Adjustment of the orientation of the crystal so that both beams were reflected simultaneously into the telescope ensured that the face was perpendicular to H_0 . The $\Theta_i = 0^\circ$ ($i = X, Y, Z$) reference orientations for the three rotations were also located by this technique, and the final orientations are believed to have been within 10 mins of arc from the desired orientation.

For borax and tincalconite the cross hairs of the travelling telescope were used to obtain orientations to within approximately 1° and $1\frac{1}{2}^\circ$ for each respectively. The lower accuracy for tincalconite resulted from the roughness of some faces. The crystals were always mounted on the arc system so that the X,Y,Z system of axes coincided as close as possible with the mutually perpendicular axes of rotation of the two goniometer arcs and the rotor shaft. The optical settings were used without further corrections in the

preliminary studies of tincalconite. For the final crystal alignment, the symmetry properties of the n.m.r. spectrum were used. In borax, the X and Z rotations were completed first followed by the Y rotation, since the optical setting corresponding to $\Theta_Y = 0^\circ$ for the Y rotation could not be checked until accurate data from the X and Z rotations had been collected. The alignment procedures in the X and Z rotations were similar, because the crystallographic two-fold axis and normal to the mirror plane lie along Y. The orientation corresponding to Y being perpendicular to H_0 was first accurately obtained, as indicated by a coalescence of the four satellite pairs to form two pairs. The rotation angle was then advanced 90° and one of the arcs adjusted to give a similar coalescence, denoting that the two-fold axis (Y) was parallel to H_0 . Since the arc movement can upset the first adjustment, this procedure was repeated until both coalescence were obtained merely by advancing by 90° . The correct orientation for the other arc was found by adjusting it so that the ν'' , ν' vs Θ curves were symmetrical about the angles corresponding to the coalescence points. For the Y rotation, the two-fold axis was adjusted to be parallel to the rotation axis by altering the arcs to give a coalescence of signals at all Θ_Y angles and the zero was found by obtaining the Θ_Y & the $\Theta_Y + 90^\circ$ angles at which the signal splittings were equal

to those for the equivalent orientations in the X and Z rotations.

For tincalconite, coalescences occur whenever one of the system of three two-fold axes is parallel or perpendicular to H_0 , with further coalescence when the three fold axis is parallel to H_0 . Hence the X and Y rotation alignments were similar to the Y and X (or Z) rotation alignments respectively for borax. In the Z rotation, the alignment was achieved by altering the arcs so that the spectrum repeated every 60° . The $\theta_i = 0^\circ$ ($i = X, Y$ or Z) orientations were determined in a straight forward manner from the angles at which coalescences occurred.

The value of the initial, quite accurate optical alignments, which permitted the preliminary n.m.r. investigations in tincalconite, can now be seen, since they enabled the crystallographic symmetry to be first evaluated and eliminated the good possibility that a large amount of time could have been wasted in taking accurate frequency measurements on a misaligned crystal.

III. 4. Procedure in the Quadrupolar Interaction Studies.

To end this chapter, a brief description of the procedure adopted in the n.m.r. experiment on quadrupole splitting studies will be made. After, the crystal was

aligned in the magnetic field and the $\theta_i = 0^\circ$ ($i = X, Y$ or Z) orientation located, the spectrum was scanned at 15° intervals from 0° to 360° . As the experiment proceeded, the resonances were plotted as a function of angle, and if, as often happened, the resonances could not be related owing to the large 15° steps, sufficient "fill in" spectra were obtained within the 15° intervals, so that all uncertainties were eliminated. This procedure was followed for the X, Y and Z rotations. For those cases where it was necessary, final experimentation consisted of "following" the satellites effectively from one rotation to another to resolve ambiguities arising from the lack of observable second order effects. The spectra were then carefully studied to obtain accurate resonance frequencies and the quantities

$$\Delta\nu = \nu'' - \nu' \text{ and } \frac{\nu'' + \nu'}{2} - \nu_0$$

formed. A twelve point Fourier analysis of this data was then performed to fit this data to eqs 2.27 and 2.29. Full advantage of the symmetry of the spectra was taken by using $\Delta\nu$'s in the Fourier analysis whose values were obtained by averaging the frequency differences over all equivalent orientations. The Fourier coefficients thus obtained permitted the quadrupole coupling tensor for each site to be written down immediately using eqs 2.28. The three values for each of the diagonal tensor components derived from the separate rotations

must for a given site, be equal within experimental error. Failure of this denotes a misalignment of the crystal in some orientation. Finally the quadrupole coupling tensor for each site was diagonalised to yield the physically important quantities $eqQ/h, \eta$ and the direction cosines of the principal axes relative to the X,Y,Z system of axes.

CHAPTER IV

CRYSTAL DATA

IV. 1. The Hydrated Borates, Borax and Tincalconite.

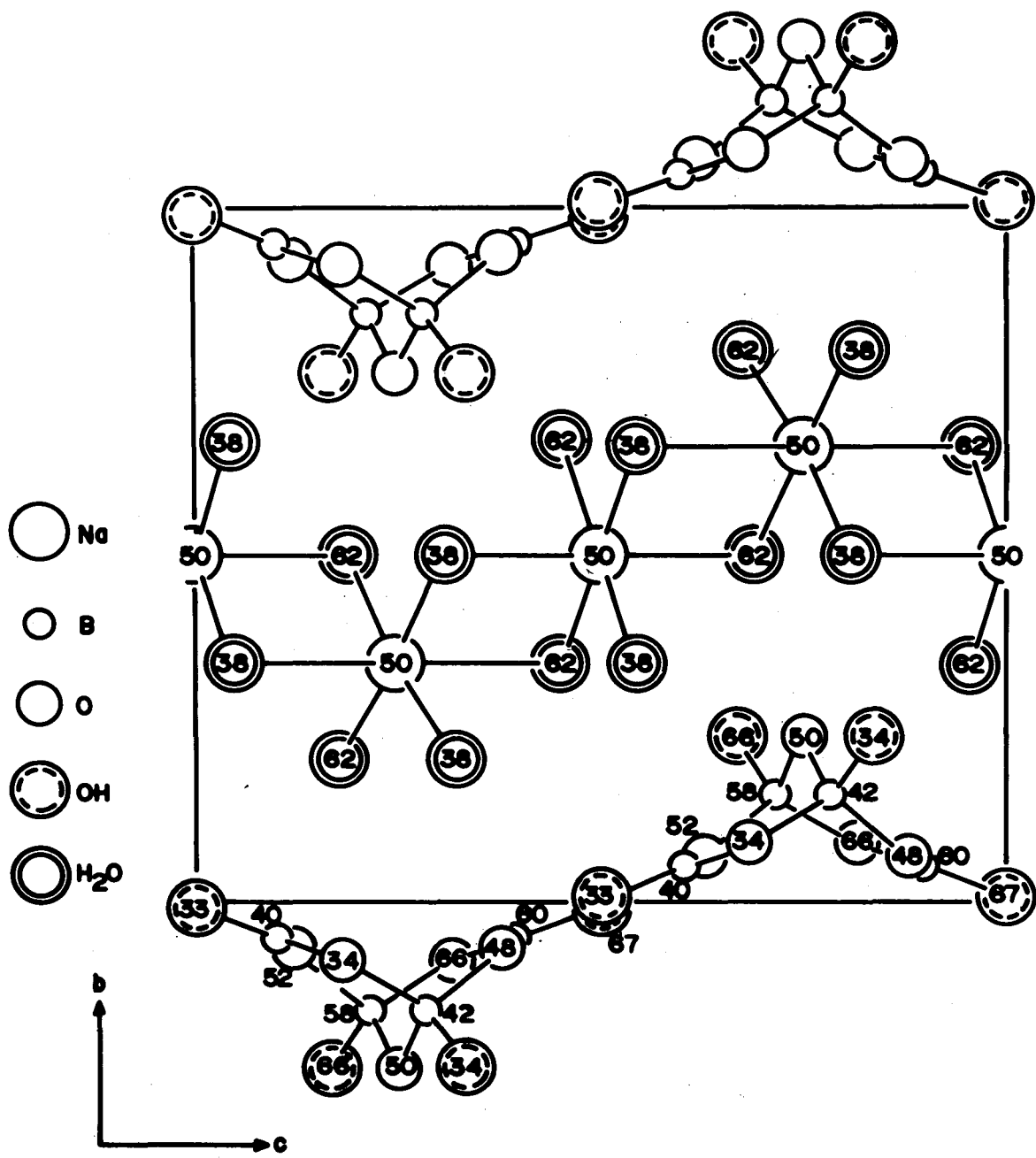
A structure has been proposed by Morimoto (1956) for borax. The crystallographic data are as follows:

monoclinic: space group $C2/c$ (C_{2h}^6)
cell dimensions: $a = 11.858 \text{ \AA}$, $b = 10.674 \text{ \AA}$
 $c = 12.197 \text{ \AA}$, $B = 106^\circ 41'$
cell contents: $4(\text{Na}_2\text{B}_4\text{O}_7 \cdot 10\text{H}_2\text{O})$

Two constituent units, chains formed by sodium atoms surrounded by water molecules and discrete boron-oxygen polyions, make up the borax structure. The chains have the composition $\text{Na}_2 \cdot 8\text{H}_2\text{O}$ and are built up of octahedra of water molecules around sodium atoms which link each other by having $\text{H}_2\text{O} - \text{H}_2\text{O}$ edges in common. The polyions are formed by two BO_3 triangles and two BO_4 tetrahedra sharing some of the oxygen atoms to form a compact group of composition $\text{B}_4\text{O}_5(\text{OH})_4$. The polyions are placed between the chains and linked to them by hydrogen bonds to form sheets parallel to (100). Within such a sheet, adjacent polyions are themselves linked by hydrogen bonds to form chains running parallel to the sodium-water molecule chains. These structural features are evident in

Figure 7

A projection of the borax structure on (100). The numbers give the height of each atom expressed as a percentage of the a-translation.



sodium tetraborate which had been purified by successive recrystallization. The borax crystals were grown by slow evaporation of a solution maintained at $+35^{\circ}\text{C}$. Crystallization occurred at numerous points on the bottom of the container but after about four months several excellent borax crystals had grown several cms above the general level of crystallization; these were carefully removed, dried and coated with oil to prevent deterioration. The crystals were colourless and tabular in habit with the approximate dimensions $1 \times 3 \times 3$ cm; the forms $\{100\}$, $\{110\}$, and $\{010\}$ were prominent. For the crystal used in the n.m.r. study, the cell dimensions derived from Precession camera photographs checked that the crystal was borax and enabled the conventional positive direction (see International Tables for x-ray Crystallography 1952) of the b crystallographic axis to be located relative to the crystal habit.

In the case of tincalconite, a seed, formed by rapid cooling of a saturated sodium tetraborate solution from 90°C to 80°C , was suspended on a fine nylon thread in a covered beaker containing a saturated solution at a temperature of 80°C . Temperature control to within $\pm 1^{\circ}$ was obtained by using an automatic device constructed by the author. Its design was similar to that described by Holuj (Thesis 1956). The temperature was lowered slowly to about 70°C when the

crystal had reached a size of about 3 x 3 x 3 cm. At this point the crystal was removed quickly from the solution and placed in an oil bath maintained at the same temperature as the solution. The temperature of the oil bath was then gradually allowed to reach room temperature so that no cracks developed in the crystal due to thermal shock. The crystal showed the same habit as the artificial crystals of tincalconite grown by Pabst and Sawyer (1948); that is, only the forms $\{10\bar{1}1\}$, $\{0001\}$ and $\{01\bar{1}2\}$ were present. To confirm that the crystal was indeed tincalconite the cell dimensions were determined from x-ray precession photographs to be $a = 11.130\text{\AA} \pm 0.016\text{\AA}$ and $c = 21.21 \pm 0.05\text{\AA}$ which are in satisfactory agreement with the values given by Minder (1935). Our x-ray data were also consistent with the space groups $R\bar{3}$, $R32$ and $R3$, and enabled the prominent faces to be indexed.

IV. 2. Ferroelectric Lithium Hydrazinium Sulphate (LiHzS)

The crystallographic data reported by Pepinsky et al. (1958) are as follows:

orthorhombic: space group $Pbn2_1$ (C_{2v}^9)

cell dimensions: $a = 8.969$, $b = 9.913$, $c = 5.178\text{\AA}$

cell contents: 4 $\text{Li}(\text{N}_2\text{H}_5)\text{SO}_4$

During the course of this work it became apparent that some of the n.m.r. data could not be fully interpreted

without a knowledge of the structure of LiHzS and so an x-ray diffraction investigation of the structure was undertaken at this University (Brown 1963). A brief description of the structure is given here.

A schematic view of the structure of LiHzS is shown in Fig. 8. The sulphur and lithium atoms are surrounded by oxygen atoms in tetrahedral arrangements and these tetrahedra are linked by corner-sharing of oxygen atoms to form a three-dimensional framework. Each oxygen atom is bonded to one lithium atom and to one sulphur atom, so that every LiO_4 tetrahedron is surrounded by four SO_4 tetrahedra and vice versa. The alternating LiO_4 and SO_4 tetrahedra thus form chains running along the two glide directions and spiralling around the screw axes. The N_2H_5^+ groups, of which only the nitrogen atoms are resolved in the x-ray analysis, are located in the large channels which run through the crystal in the direction of the c axis.

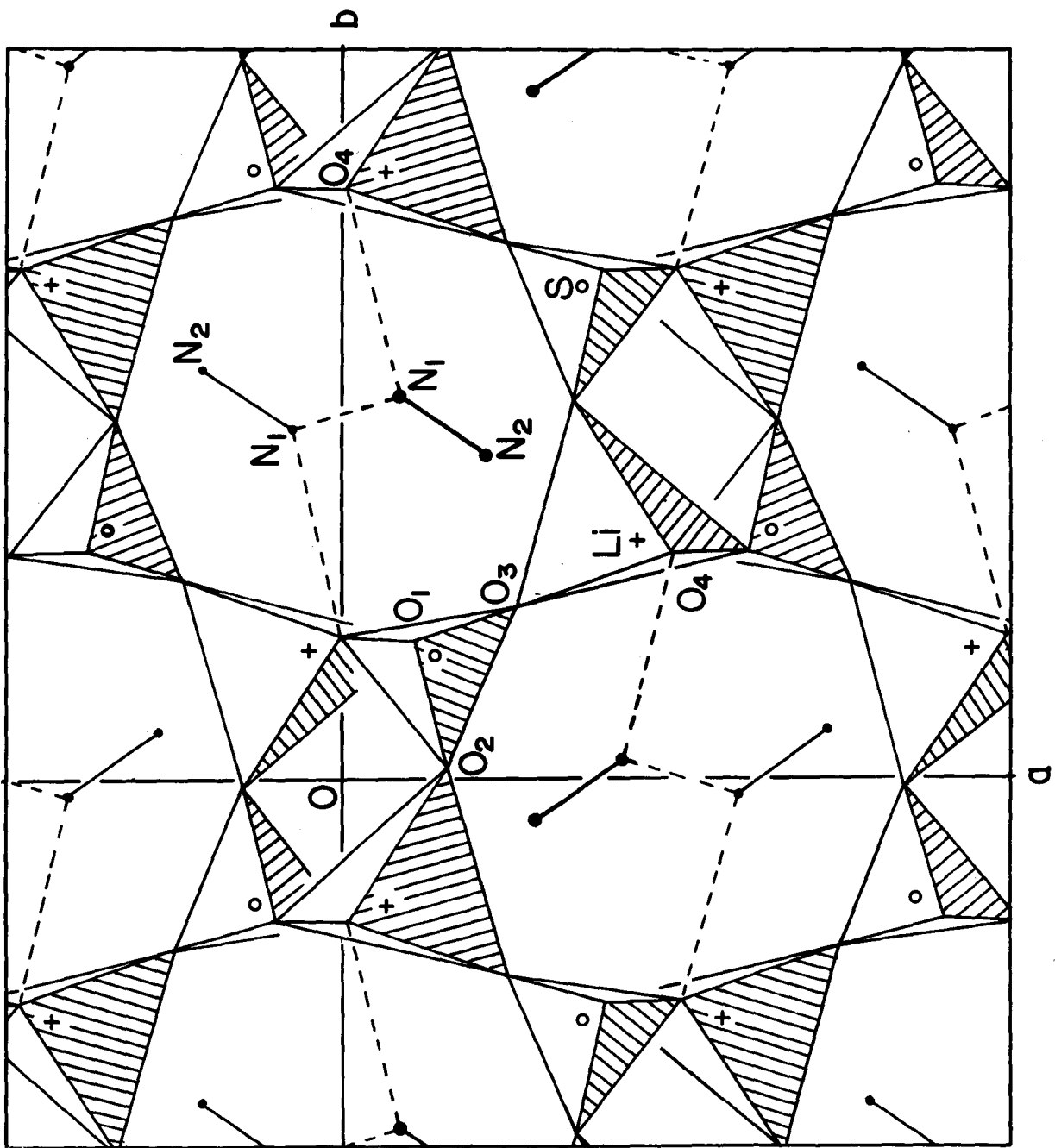
The proton resonance study to be described in Chapter VII clearly shows that the N_2H_5^+ group exists as the hydrazinium ion, $\text{NH}_2\text{-NH}_3^+$. The observed short distances between N_1 and O_4 and between the N_1 atoms related by the screw axis suggests that N_1 is part of the -NH_2 group and that it is linked by one hydrogen bond to the framework and by the other to an adjacent -NH_2 group. Thus the hydrazinium ions are

Figure 8

A view of lithium hydrazinium sulphate projected down the c axis. Except for the oxygen atoms which are at the apices of the tetrahedra, the atoms are indicated as follows:

sulphur	small open circle
lithium	cross
nitrogen	small solid circle

Hydrogen bonds involving the -NH_2 groups are indicated by dashed lines.



linked by hydrogen bonds to form infinite chains parallel to the c axis. These hydrogen bonds have been represented as dashed lines in Fig.8 . It has also been inferred from the proton resonance study that at room temperature the -NH_3^+ group is rotating about the N-N axis.

The LiHzS used in this work was prepared from reagent-grade Li_2CO_3 and $(\text{N}_2\text{H}_6)\text{SO}_4$ and purified with one cycle of recrystallization. Seed crystals are readily obtained by the slow evaporation of small amounts of aqueous solution in, for instance, a watch glass. Single crystals were grown by suspending a seed crystal in a saturated aqueous solution and then slowly lowering the temperature from about 35°C to 25°C over a period of two weeks. Another temperature control device of the same design as that used to grow tincalconite, was constructed. The chief difficulty in growing large single crystals of LiHzS was to prevent seeding on the crystal suspension and on the seed itself. Trial and error procedures showed that a very fine, straight copper suspension wire eliminated the first difficulty, whilst the second was reduced by lowering the seed and suspension for a few seconds into distilled water before it entered the LiHzS mother solution. The crystals were rotated in the mother solution at a rate of two revolutions per minute to prevent bubbles of CO_2 from forming on the seed and causing irregular growth. Large,

transparent, colourless crystals were obtained which were elongated along the c axis with prominent (100), (110) and (101) faces. The copper suspension wires were easily removed from the crystals by using an Industrial "Airbrasive" Unit, Model C. X-ray precession photographs were taken with these crystals to confirm that they were LiHzS and to index the prominent faces. The cell dimensions were found to be in excellent agreement with those determined by Pepinsky et al (1958) and the space group suggested by Pepinsky et al (1958) was confirmed.

Three LiHzS/^{crystals}were used in these experiments. They were all prepared in an identical manner, although from different batches of material. The first crystal, with the approximate dimensions 2 x 4 x 3 cm, was used for the room temperature study of the Li⁷ spectrum and in the ferroelectric switching experiments, the second, which was about 1.5 x 3 x 3 cm, was used in the search for a phase transition and for the study of the Li⁷ spectrum in the high temperature form of LiHzS, and the third, about 1.5 x 1.5 x 2.5 cm in size, was used for the proton study at room temperature. Powdered samples used in the proton study were obtained by crushing a large single crystal. The orthogonal axes X,Y,Z were chosen parallel to the a,b,c axes, respectively.

CHAPTER V

N.M.R. STUDY OF THE B^{11} SITES IN BORAX AND TINCALCONITE

The n.m.r. investigations of the B^{11} sites in the hydrated sodium tetraborates are described first, followed in Chapter VI by the study of the Na^{23} sites. We anticipate here the results of Chapter VI, which show our n.m.r. results on the Na^{23} sites in borax to be in complete agreement with Morimoto's proposed structure.

V. 1. Experimental Results.

For borax, the orthogonal axes X,Y,Z were chosen parallel, respectively, to the $\vec{b} \wedge \vec{c}$, \vec{b} and \vec{c} crystallographic directions. The B^{11} spectrum was found to consist of a total of eleven lines and was interpreted as the superposition of "simple" spectra from B^{11} nuclei at four sites. At two of these sites the quadrupole interaction was strong, so that the maximum separation of satellites was large and the central lines were displaced from ν_0 . At the other two sites, the quadrupole interaction was weak with the result that the separation of satellites was never very great and the central lines coincided at ν_0 to produce a single intense line counted as one in the eleven line spectrum. Whenever the crystal was

oriented with the Y axis either parallel or perpendicular to the magnetic field, lines related by the two-fold axis coalesced to produce a reduced spectrum of only six lines. There are thus only two unique B^{11} sites in the unit cell of borax, one at which the quadrupole interaction is strong and one at which it is weak.

For tincalconite, a thorough preliminary study was made before the final accurate measurements were taken, because of the uncertainty regarding the crystallographic space group (see section IV. 1). In the preliminary work, the Na^{23} and the B^{11} signals were scanned in three rotations about orthogonal axes X, Y and Z. Optical alignments of the crystal were made as described in section III. 3. After the results of the preliminary work had been studied and the space group evaluated, the same set of rotation axes were adopted for the final measurements, that is the X, Y, Z axes were taken parallel to the crystallographic directions \vec{a}_1 , $\vec{c} \wedge \vec{a}_1$, and \vec{c} , respectively. The knowledge gained of the orientational dependences of the satellite resonances helped in the final accurate n.m.r. alignment, performed as described in section III. 3.

The B^{11} spectrum was considerably more complex than in the case of borax as it consisted of a total of 31 lines. Again the intense line at ν_0 was counted as only one line although it consisted of six unresolved lines. The behavior

of the lines was consistent with strong quadrupole interactions at six sites and weak at the other six. In the Z-rotation all 31 lines appeared and the symmetry of the spectrum was consistent with the existence of a three fold axis parallel to the axis of rotation. Whenever the crystal was oriented with the X-axis parallel or perpendicular to the magnetic field, symmetry related pairs of lines coalesced to give a reduced spectrum of 16 lines indicating that the X-axis is either parallel to a two-fold rotation axis or perpendicular to a mirror or glide plane, but etch figure evidence and the lack of systematic extinctions rule out the latter two possibilities. Furthermore, when the crystal was oriented with the X-axis perpendicular to H_0 and the Z axis simultaneously parallel to the magnetic field, additional lines coalesced to produce a reduced spectrum of only six lines which were equivalent to the superposition of simple spectra from one site at which the quadrupole interaction was strong and one site at which it was weak. Thus the six sites in both the strong and weak interaction groups are related by the point group 32 and there are only two unique B^{11} sites in the unit cell of tincalconite, just as in borax. The apparent complexity of the spectrum in tincalconite simply arises because the point group of the crystal allows all the symmetry related sites in the unit cell to be separately distinguished

in the n.m.r. experiment.

For each of the rotations about the X, Y and Z axes, the B^{11} spectra were recorded at 15° intervals from 0° to 360° and the frequencies of the equivalent lines were averaged over all equivalent angles. The rotation angles for the X, Y and Z rotations were measured from the positions at which the Y, Z and X axes, respectively, were parallel to the magnetic field direction. The resonance frequencies are tabulated in Appendix I. The average values for the $\nu_{3/2}'' - \nu_{3/2}'$ data are shown in Figs. 9 and 10 for borax and in Figs. 11 and 12 for tincalconite. The sites at which the quadrupole interaction is weak have been denoted by L_i and those at which it is strong by M_i . These data were analysed to yield the Fourier coefficients a, b, and c of eq 2.27 and are given in Tables I and II for borax and tincalconite, respectively; the combination of signs given to the c-coefficients had to be determined by the methods described in the next paragraph. In the case of the M sites the quadrupole interaction was sufficiently large to produce second order effects and the n, p, r, u and v coefficients for the shift of the centroid of the satellites are also given in Tables I and II.

The correct combination of signs of the c-coefficients associated with a given site could not be determined from the $\nu_{3/2}'' - \nu_{3/2}'$ data alone because in each crystal one of the

Figure 9

Angular dependence of the frequency difference between the B^{11} satellite lines arising at the L sites in borax for rotations about the X,Y and Z axes.

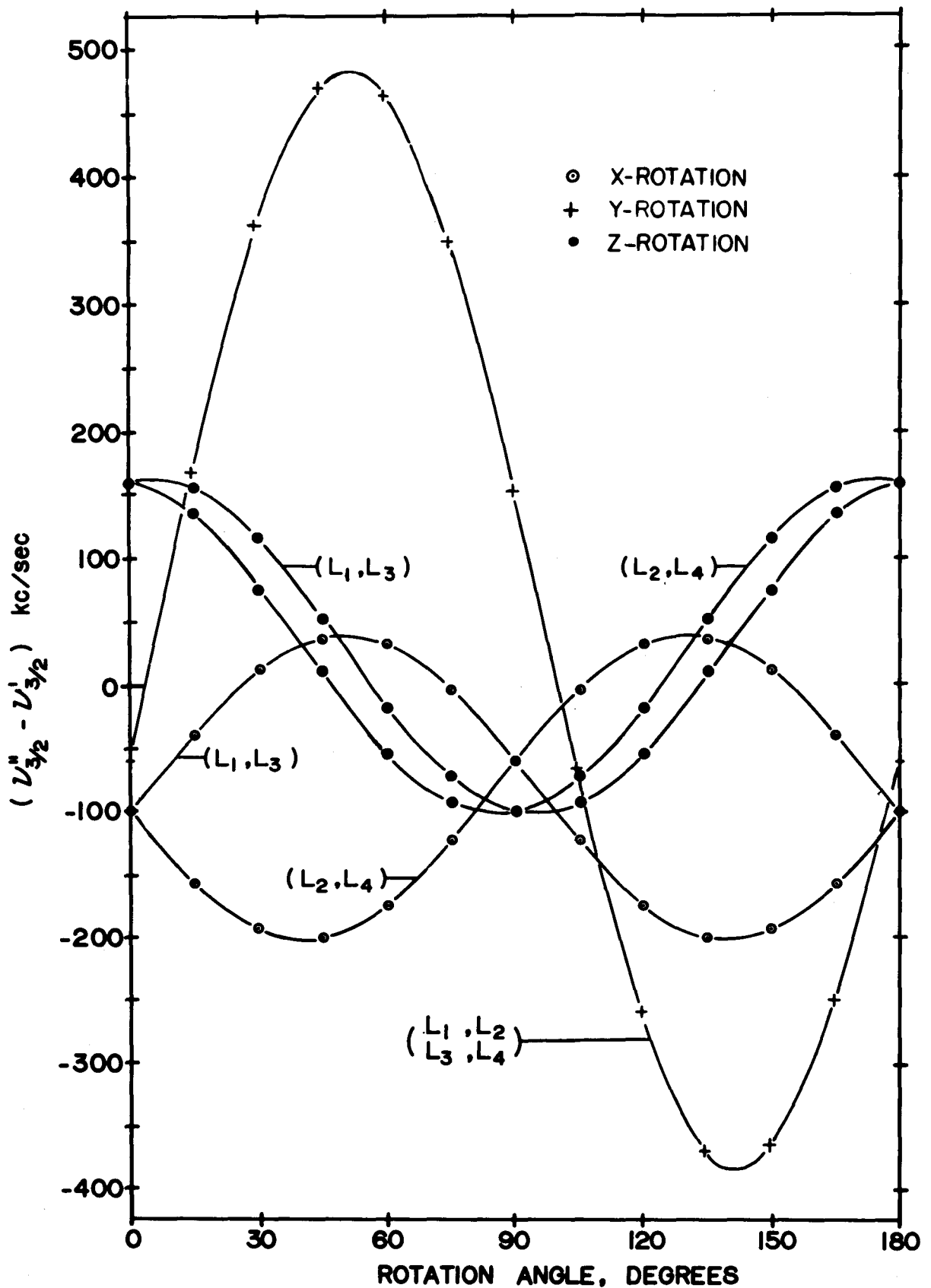


Figure 10

Angular dependence of the frequency difference between the B^{11} satellite lines arising at the M sites in borax for rotations about the X,Y and Z axes.

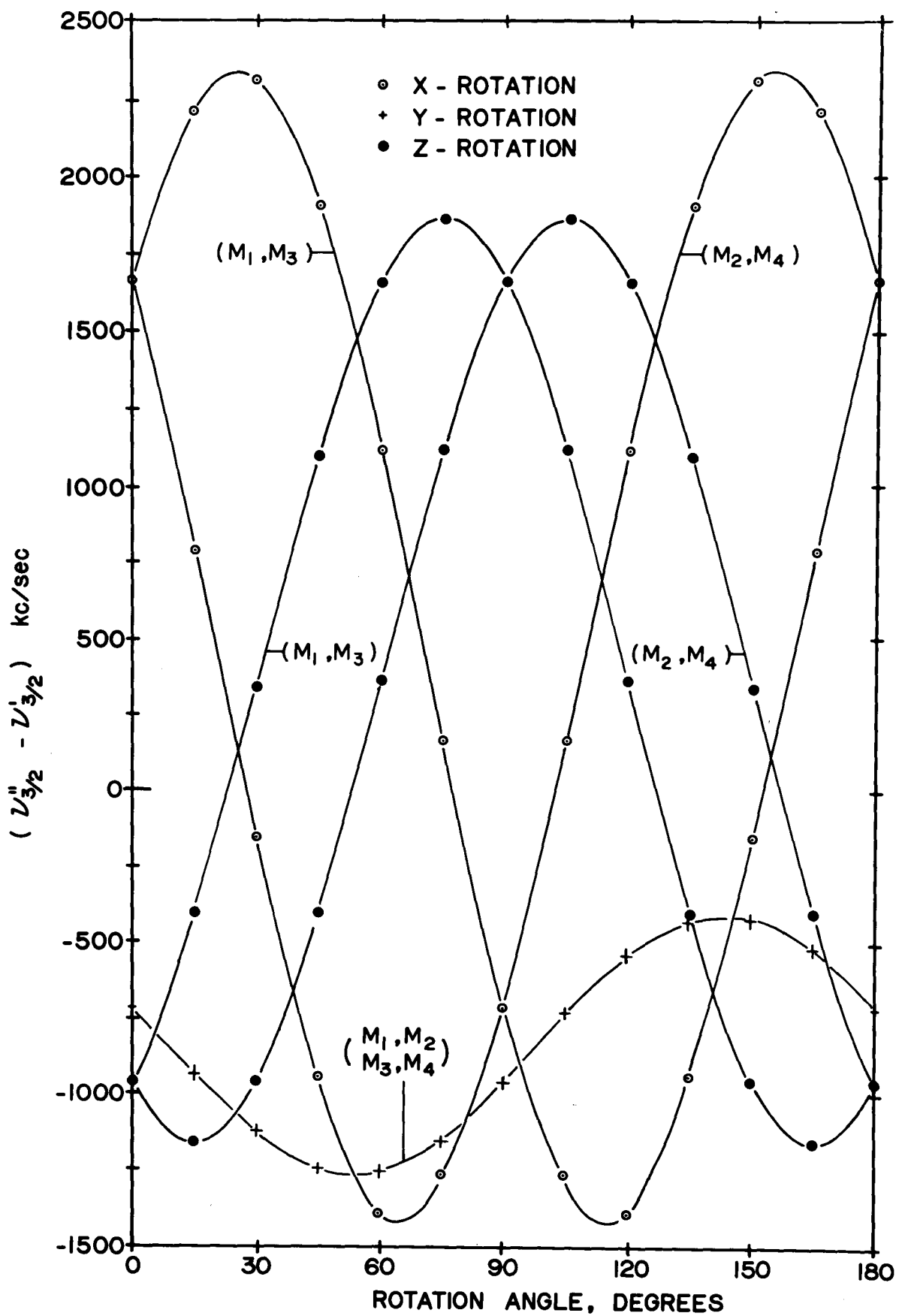


Figure 11

Angular dependence of the frequency difference between the B^{11} satellite lines arising at the L sites in tincalconite for rotations about the X,Y and Z axes.

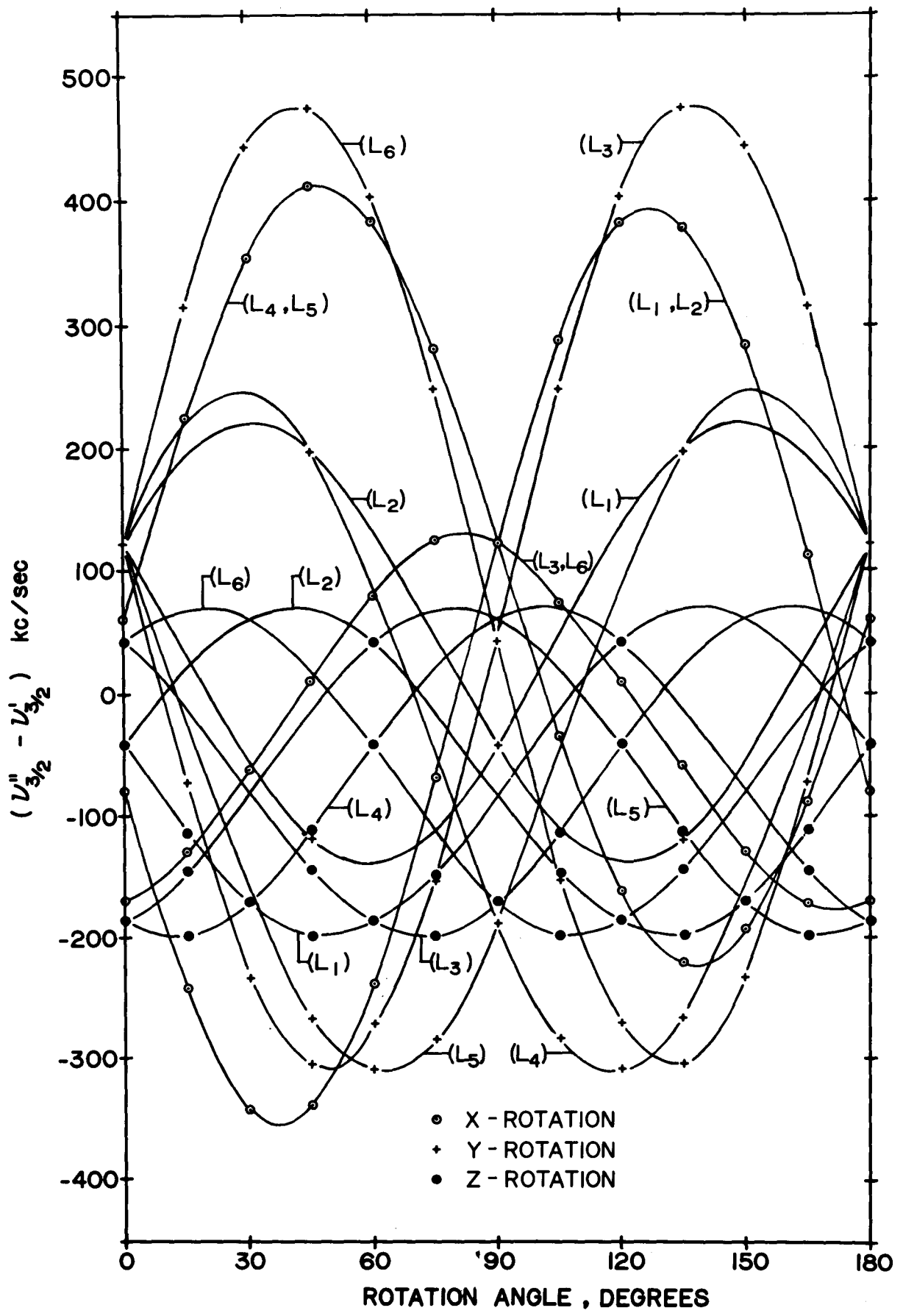


Figure 12

Angular dependence of the frequency difference between the B^{11} satellite lines arising at the M sites in tincalconite for rotations about the X,Y and Z axes.

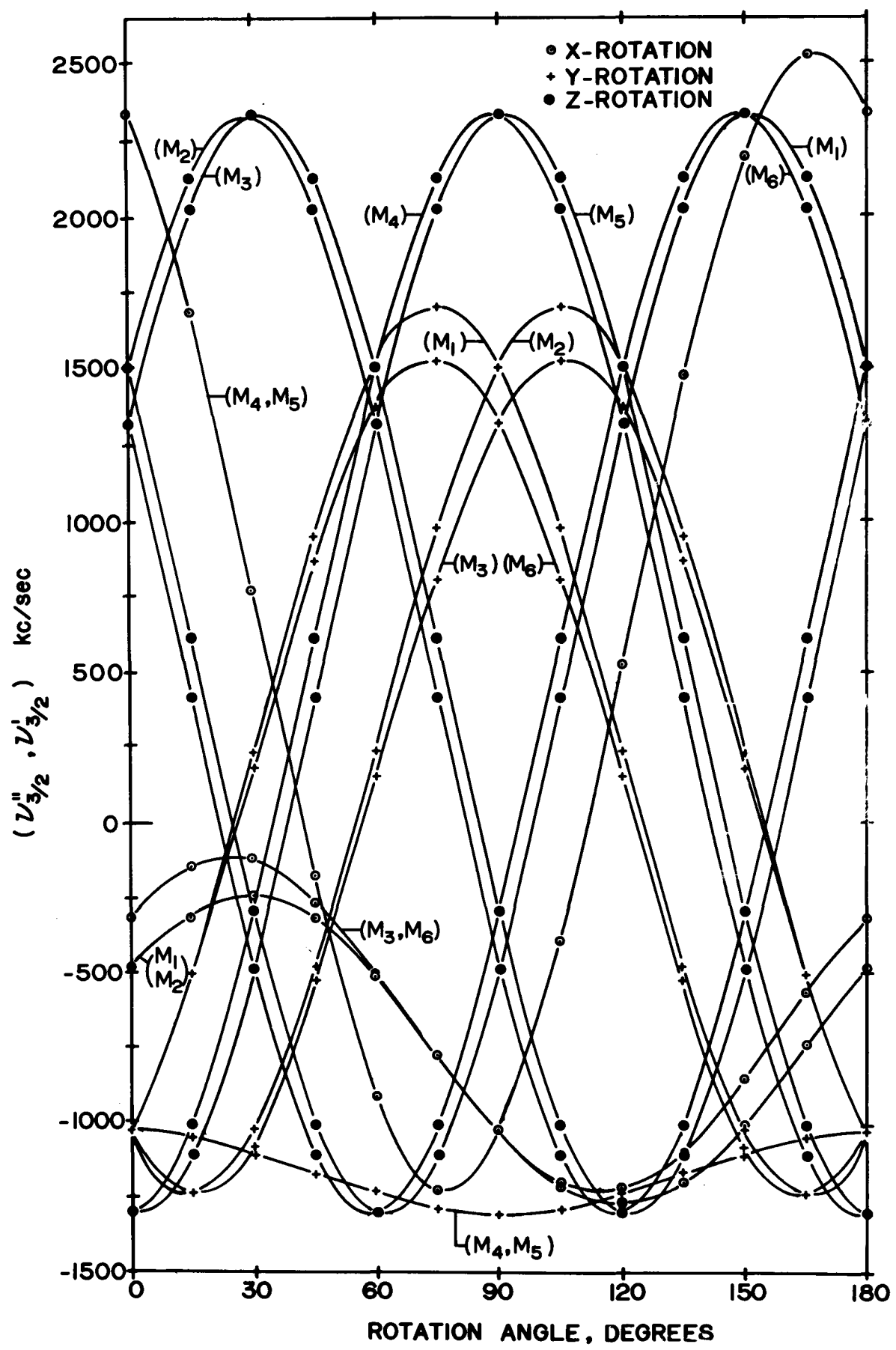


TABLE I.

Averaged Experimental Values of the Fourier Coefficients
(in kc/sec) of the Angular Variation of $\nu_{3/2}'' - \nu_{3/2}'$ and
 $\bar{\nu}_{3/2} - \nu_0$ for the B^{11} Satellite Lines Arising in Borax.

Where alternate signs are given, the upper sign refers to
the odd-numbered sites and the lower sign to the even
numbered sites.

Sites	Fourier Coefficients	Rotation		
		X	Y	Z
L_1, L_3	a	- 81.2	+ 50.8	+ 30.8
L_2, L_4	b	- 20.0	-110.4	+ 131.0
	c	± 118.5	+416.2	± 21.7
M_1, M_3	a	+ 484.0	-836.9	+ 354.8
M_2, M_4	b	+1188.2	+129.8	-1316.4
	c	±1424.6	-405.5	± 747.4
	n	+ 38.8	+ 24.3	+ 40.4
	p	+ 4.4	+ 13.5	- 18.1
	u	+ 5.8	+ 1.2	- 11.3
	r	± 5.6	- 21.2	± 11.2
	v	± 32.7	+ 1.2	± 18.8

TABLE II

Averaged Experimental Values of the Fourier Coefficients (in kc/sec) of $\nu''_{3/2} - \nu'_{3/2}$ and $\bar{\nu}_{3/2} - \nu_0$ for the B¹¹ Satellite Lines Arising in Tincalconite. Where alternative signs are given, the upper and lower signs refer to the first and second sites, respectively, at the top of the column.

Rotation	Fourier Coefficients	Boron Sites		
		L ₁ ,L ₂	L ₃ ,L ₆	L ₅ ,L ₄
X.	a	+ 21.4	- 25.2*	+ 94.9
	b	- 101.1	- 144.4*	- 30.9
	c	- 359.4	+ 39.7	+ 316.4
Y	a	+ 40.4	+ 85.1	- 32.8
	b	+ 83.6	+ 41.1	+ 156.0
	c	+ 158.5	+ 390.8	+ 232.6
Z	a	- 63.0	- 63.0	- 63.0
	b	+ 18.6	+ 107.0	- 125.6
	c	+ 134.3	+ 83.3	+ 51.1
X		M ₁ ,M ₂	M ₃ ,M ₆	M ₅ ,M ₄
	a	- 755.5	- 671.2	+ 652.5
	b	+ 269.4	+ 362.1	+1683.8
	c	+ 432.5	+ 417.4	- 831.9

TABLE II (continued)

Rotation	Fourier Coefficients	Boron Sites		
		M_1, M_2	M_3, M_6	M_5, M_4
Y	a	+ 236.4	+ 150.0	-1164.9
	b	-1268.0	-1179.1	+ 138.8
	c	\pm 720.2	\mp 728.8	\pm 2.5
Z	a	+ 512.3	+ 512.3	+ 512.3
	b	+ 996.1	+ 817.6	-1813.7
	c	\mp 1519.2	\pm 1622.2	\mp 103.0
X	n	+ 32.5	+ 35.3	+ 38.3
	p	+ 18.3	+ 21.5	- 0.2
	u	+ 2.5	+ 2.0	- 23.8
	r	+ 24.4	+ 23.9	- 0.3
	v	- 5.0	- 5.0	+ 30.0
Y	n	+ 48.6	+ 49.2	+ 6.2
	p	- 24.5	- 26.4	+ 8.2
	u	- 12.4	- 9.8	- 0.3
	r	\pm 12.7	\mp 12.2	0
	v	\pm 20.3	\mp 19.2	0
Z	n	+ 43.5	+ 43.5	+ 43.5
	p	+ 4.3	+ 3.9	- 8.3
	u	+ 14.7	+ 22.1	- 36.8
	r	\mp 7.0	\pm 7.3	\mp 0.2
	v	\pm 34.0	\mp 29.7	\mp 4.3

*These values were given half weight in the analysis.

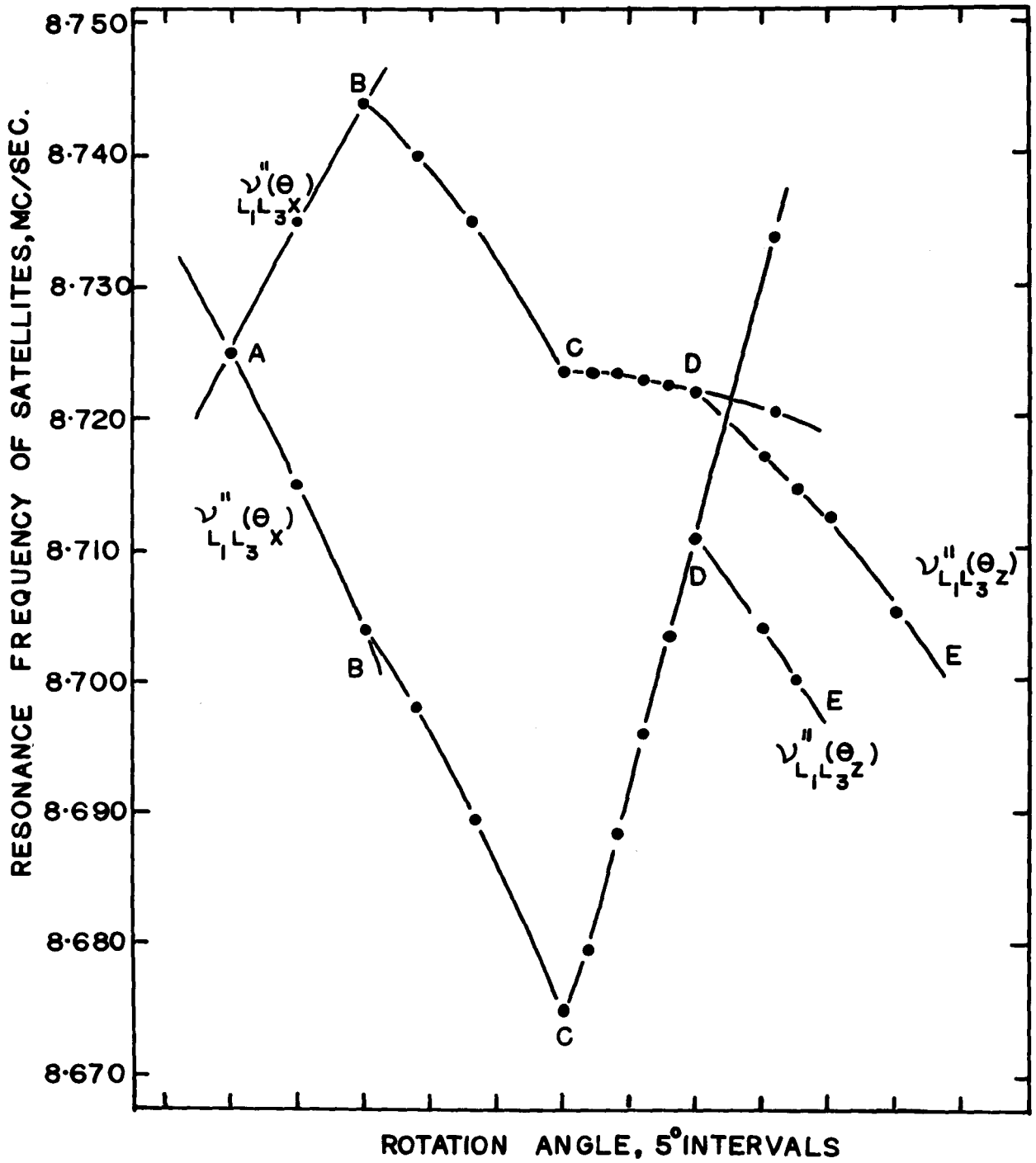
rotation axes was chosen parallel to a two-fold axis of symmetry, (see section II 8). The uncertainty was easily resolved for the M sites in borax and tincalconite as the coefficients of Table II give directly the correct combination of signs for the c-coefficients.

This method could not be used for the L sites, however, because the quadrupole interaction was so small that the coefficients were found to be zero within experimental error. Also with our choice of rotation axes in borax, Ψ_{XY} turned out to be small, so that the method usually used in these circumstances was not reliable (see section II. 8). Therefore a direct method of establishing the correct combination of signs was used. Starting with X along the normal rotation axis and Z also perpendicular to H_0 , the crystal was rotated until the Θ scale read 10° (ie $\Theta_x = 10^\circ$). By means of one of the goniometer arcs, the crystal was then rotated about the Z axis through an angle of 15° in a clockwise direction. Next, the crystal was rotated to return the Θ scale to zero so that the crystal was finally in an orientation equivalent to $\Theta_z = 105^\circ$. The satellite resonances were followed in detail during these maneuvers thus allowing a direct association of resonances observed in the three rotations. A graphic presentation of the procedure is shown in Fig. 13.

The symmetry of tincalconite permitted a still differ-

Figure 13

Angular dependence of satellite frequencies during the manoeuvres to find the correct combination of signs for the coefficients for the L sites in borax. The letters correspond to the following crystal orientations: A, $\theta_X = 0^\circ$; B, $\theta_X = 10^\circ$; C is derived from B by rotating the crystal through 15° counterclockwise about Z; D, $\theta_Z = 105^\circ$ being derived from C by returning the θ scale to 0° . D \rightarrow E is part of the usual Z rotation.



-ent method of obtaining the correct combination of signs of the L type sites. The threefold rotation axis generates three pairs of sites, the members of which are related by two-fold axes. The tensors at these three sets of sites must be identical in magnitude but, since they differ in orientation, they give c-coefficients which may have different magnitudes, as well as signs, for the different pairs. The correct choice for the combination of signs to associate with each site led to identical results within experimental error for the quadrupole coupling constant at each of the six sites, whereas the alternative choice would not give such internal agreement and was therefore rejected.

The a,b,c coefficients given in Tables I and II were used in calculating the components of the quadrupole coupling tensors in the X,Y,Z coordinate systems. The tensor components are shown in Table III. The tensors were diagonalised to yield the values of eQq/h and η listed in Table IV, and the direction cosines of the principal axes of the quadrupole coupling tensors which are given in Table V. The direction cosines are given only for one pair of L and one pair of M sites since the direction cosines of the additional pairs may be generated by operating on the tabulated values with the appropriate conversion matrices. For borax the matrix is

TABLE III

Quadrupole Coupling Tensors for the B¹¹ Sites in Borax and Tincalconite. Where alternate signs are given the upper and lower signs refer to the upper and lower sites respectively.

Site	Ψ_{XX}	Ψ_{YY}	Ψ_{ZZ}	Ψ_{XY}	Ψ_{YZ}	Ψ_{ZX}
Borax						
L ₁ ,L ₃ L ₂ ,L ₄	+ 161.8	- 101.0	- 60.8	± 21.7	± 118.5	-416.2
M ₁ ,M ₃ M ₂ ,M ₄	- 965.4	+1672.4	- 707.0	± 747.4	±1424.6	+405.5
Tincalconite						
L ₁ L ₂	- 43.5	- 80.8	+ 124.2	± 134.3	+ 359.4	±158.5
L ₃ L ₆	+ 45.3	- 170.1	+ 124.8	± 83.3	- 39.7	±390.8
L ₅ L ₄	- 189.1	+ 64.1	+ 125.0	± 51.1	- 316.4	±232.6
M ₁ M ₂	+1507.9	- 480.9	-1027.1	±1519.2	- 432.5	±720.2
M ₃ M ₆	+1333.8	- 304.8	-1029.0	±1622.2	- 417.4	±728.8
M ₅ M ₄	-1303.3	+2330.6	-1027.3	± 103.0	+ 831.9	± 2.5

TABLE IV

Quadrupole Coupling Constants and Asymmetry Parameters for B^{11} in Borax and Tincalconite Compared with Similar Values Reported for Kernite.

Crystal	L Sites		M Sites	
	eqQ/h (kc/sec)	η	eqQ/h (kc/sec)	η
Borax	487 \pm 1	0.714 \pm 0.003	2544 \pm 4	0.089 \pm 0.015
Tincalconite	478 \pm 1	0.473 \pm 0.005	2528 \pm 3	0.039 \pm 0.017
Kernite	645 \pm 3	0.54 \pm 0.01	2563 \pm 7	0.163 \pm 0.010
	588 \pm 3	0.60 \pm 0.02	2567 \pm 10	0.117 \pm 0.010

TABLE V

Direction Cosines of the Principal Axes x, y, z of the Quadrupole Coupling Tensors at B¹¹ Sites in Borax and Tincalconite. The direction cosines of the additional symmetry-related sites may be obtained by operating on these with the appropriate matrices. The tabulated standard errors were obtained by direct calculation except where noted.

Boron Sites	Reference Axes	Principal Axes					
		x		y		z	
Borax							
L ₁	b x c	±0.272	±0.017	∓0.560	±0.004	±0.782	±0.004
L ₂	b	∓0.941	±0.015	∓0.324	±0.004	±0.095	±0.002
	c	±0.200	±0.010	∓0.762	±0.006	∓0.616	±0.004
M ₁	b x c	±0.947	±0.012*	±0.219	±0.035*	∓0.235	±0.001
M ₂	b	±0.303	±0.008*	∓0.368	±0.007*	±0.879	±0.004
	c	±0.105	±0.030*	∓0.904	±0.015*	∓0.415	±0.003
Tincalconite							
L ₁	a ₁	∓0.928	±0.015	∓0.047	±0.003	∓0.317	±0.002
L ₂	c x a ₁	±0.184	±0.015	±0.806	±0.009	∓0.563	±0.001
	c	±0.325	±0.011	∓0.591	±0.009	∓0.739	±0.004
M ₁	a ₁	±0.340	±0.030 [#]	±0.390	±0.016 [#]	±0.855	±0.004
M ₂	c x a ₁	∓0.170	±0.053 [#]	∓0.868	±0.021 [#]	∓0.464	±0.003
	c	±0.924	±0.022 [#]	∓0.303	±0.064 [#]	∓0.229	±0.005

*Error estimated by comparison with the values obtained for tincalconite.

[#]Error estimated through comparison of the values obtained for the sets of sites related to the threefold axis.

$$\begin{pmatrix} +1 & 0 & 0 \\ 0 & -1 & 0 \\ 0 & 0 & +1 \end{pmatrix}$$

which corresponds to reflection of the sites in the mirror plane of point group 2/m. Bearing in mind that the unit cell of borax has a centre of symmetry, the direction cosines of the four other boron atoms in the unit cell are the same as those above. For tincalconite, the conversion matrix is

$$\begin{pmatrix} 0.5 & \mp 0.866 & 0 \\ \pm 0.866 & -0.5 & 0 \\ 0 & 0 & +1 \end{pmatrix}$$

corresponding to rotations through $\pm 120^\circ$ about the positive c axis. The direction cosines at the L_1, L_2 and M_1, M_2 sites for tincalconite are average values obtained by converting those for the other sites so that they relate to the same orientation and then averaging the three sets of results.

To avoid confusion during later discussions of the correlation between the orientation of the quadrupole coupling tensors and the interatomic directions, it should be noted that the direction cosines are given with reference to conventional crystallographic axes, so that in borax the two-fold axis is parallel to the b-axis, whereas in tincalconite it is parallel to the a-axis.

V. 2. Discussion of Results.

The n.m.r. study of B^{11} in tincalconite makes it possible to remove the uncertainty as to the space group of this crystal. The fact that all twelve boron sites in the unit cell were separately distinguished in the n.m.r. experiment indicates that the crystal cannot be centrosymmetric and therefore rules out $R\bar{3}$. Since the n.m.r. spectrum clearly indicates the presence of only two unique boron sites the space group cannot be $R3$ which, for the case of tincalconite, would allow four unique boron sites. Therefore, of the space groups permitted by the x-ray and etch figure evidence only $R32$ is possible on the basis of the number of observed sites and, furthermore, the symmetry properties of the B^{11} spectrum are entirely consistent with $R32$.

The n.m.r. results for borax should agree with the known symmetry and structure of the crystal and, indeed, were found to be consistent with the space group $C2/c$ both as to number of distinguishable sites and symmetry of the spectrum. It is of interest to compare the inferences regarding the boron-oxygen polyion drawn from the n.m.r. data with the known structure of the borax polyion because recent attempts (Pennington and Petch 1960, Bray et al 1961, Pennington and Petch 1962) have been made to infer from such data boron-oxygen coordinations and the types of polyions existing in

crystals whose structures remain unknown. As discussed in Section I.3 such inferences are drawn from consideration of the gross features of the quadrupole coupling tensors existing at the boron sites. It has been found that in several of the hydrated borates the B^{11} quadrupole coupling constants fall approximately within the ranges 50 - 100, 300 - 600 and 2500 - 2600 kc/sec for discrete BO_4 tetrahedra, BO_4 tetrahedra in closed ring polyions and BO_3 triangles, respectively. Further, for BO_3 triangles, the asymmetry parameter is about 0.1 or less and the z principal axis is nearly perpendicular to the plane of the triangular group. The values given in Table IV for the quadrupole coupling constants and asymmetry parameters immediately suggest that the M sites have triangular coordination and that the L sites have tetrahedral coordination and are linked in a closed-ring polyion. Also, the group of four sites (L_1 , L_2 , M_3 and M_4) has a two-fold rotation axis of symmetry as does the borax polyion. As a further check one may compare the known orientations of the BO_3 triangles in the polyion with the directions of the z principal axes at the M sites. The direction cosines, with regard to our X,Y,Z system of axes, of the normals to the two BO_3 planes in a given polyion, as calculated from the atomic parameters of the oxygens (Morimoto 1956) are $\bar{+}0.201$, $+0.893$ and $\bar{+}0.402$. These values are to be compared with $\bar{+}0.235$, $+0.879$ and

∓ 0.415 , the direction cosines of the z principal axes of the M sites in borax as given in Table V. They indicate that the angle between the normal to a given plane and the z principal axis at the boron site in the same plane is $2^{\circ}18'$ which is excellent agreement considering that only in an isolated triangle may one expect them to be exactly parallel. Thus the inferences drawn from the n.m.r. results regarding the nature of the borax polyion are in complete agreement with the known structure of the polyion.

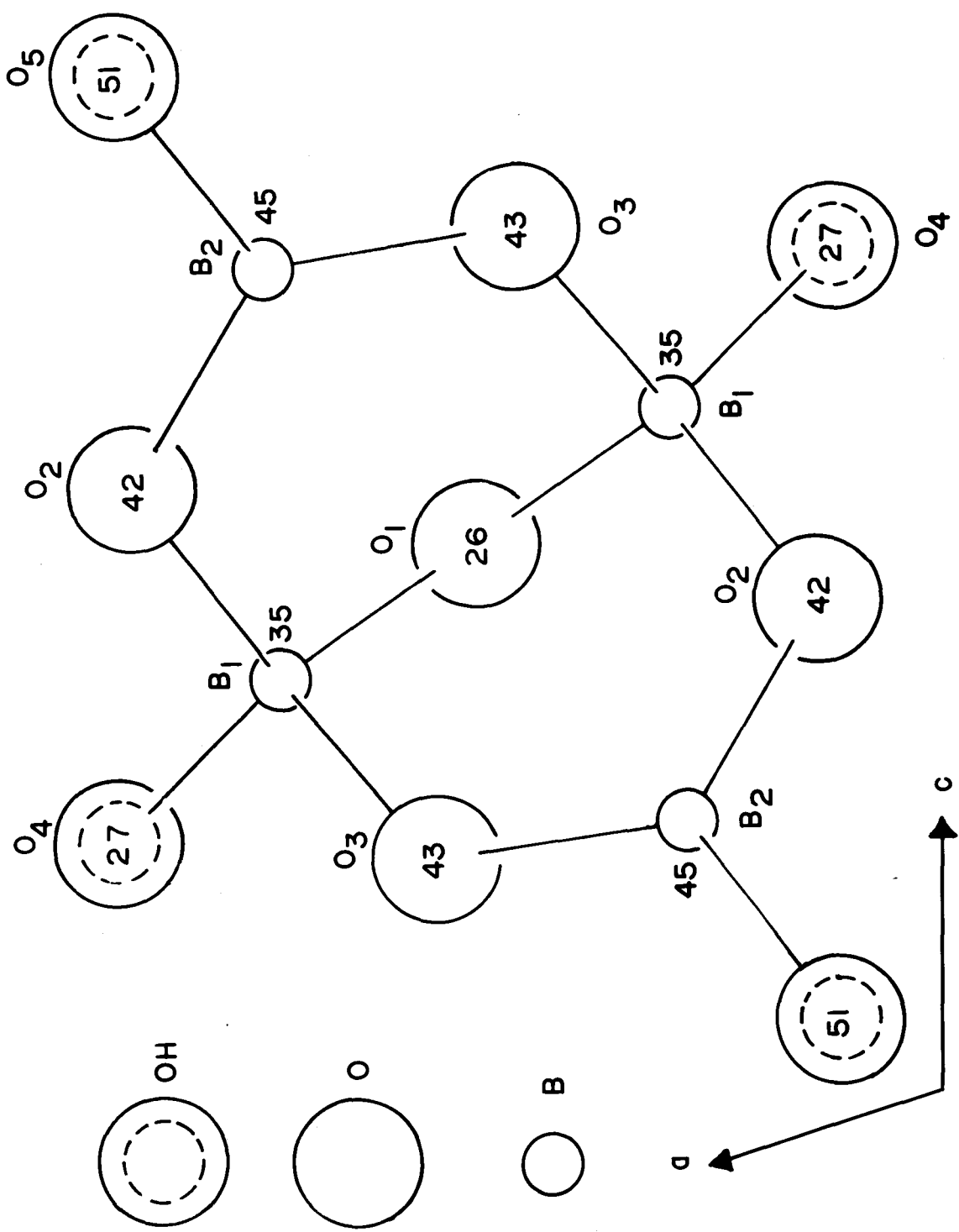
In the light of the above, let us test Christ's (1960) prediction that the same boron-oxygen polyion occurs in tincalconite as in borax. The n.m.r. results of Table IV indicate that in tincalconite, as in borax, there are only two unique sites in the unit cell and that the sites we have labelled M_i have triangular coordination and that the L_i sites have tetrahedral coordination and are linked in closed-ring polyions. The symmetry of the crystal allows the twelve boron sites to occur in three four-membered polyions with the polyions having a two-fold axis of symmetry, as in the borax polyion. As a check on the relative orientation of the triangles in the polyion, we may use the angle between the z principal axes at two sites related by the two-fold axis. In borax this angle is 123° . In tincalconite, the symmetry is such that we cannot tell unambiguously which two triangles are in a given

polyion so we are left with three possibilities, 118° , 112° and 3° ; if we accept 118° as the correct possibility then the agreement is satisfactory. In summary, the n.m.r. evidence as to the number of unique sites, the coordination of the sites, the symmetry of the polyion and, with some ambiguity, the relative orientation of the BO_3 triangles in the polyion all support the prediction that the same boron-oxygen polyion occurs in tincalconite as in borax.

Since the borax polyion is quite symmetrical and relatively weakly bonded to its neighbouring atoms, one would expect to find some correlation between the interatomic directions within the polyion and the orientation of the principal axes of the quadrupole coupling tensors at the tetrahedral sites in addition to that with the triangular sites. Such a correlation does exist. Referring to Fig. 14 the z principal axis at the tetrahedral L_1 site is within 5° of being parallel to the vector joining O_1 to O_4 (the direction cosines are $+0.782$, $+0.095$, -0.616 and $+0.761$, $+0.017$, -0.649 , respectively), the y principal axis in projection on the (010) plane is in the direction of the line joining O_3 to O_2 (the direction cosines are -0.636 , -0.070 , -0.768 and -0.560 , -0.324 , -0.762 , respectively) although it is tipped about 19° below the plane, and the x principal axis has its major component in the direction of the polyion's two-fold

Figure 14

A projection of the borax polyion on (010). The numbers give the height of each atom expressed as a percentage of the b-translation.



axis.

In tincalconite, if we associate the L_1 and L_2 sites with the M_1 and M_2 sites in a common polyion, the x principal axes at the tetrahedral sites have their major components along the polyion's two-fold axis as found in borax; the cosine of the angle between x and the two-fold axis is -0.928 for tincalconite and -0.941 for borax. Since the atomic parameters for tincalconite are not yet available we cannot make a direct comparison of the orientation of the y and z principal axes with the interatomic directions. However, we can get a workable impression of the orientation by using as a reference direction the projection, on the plane perpendicular to the two-fold axis, of the z principal axis at an M site. In borax, this projection is rotated only 9° from the direction of the long dimension (B_2-B_2 direction) of the polyion. In tincalconite, the projections on the (100) plane of the y and z principal axes at the L sites are rotated 11° and 111° , respectively, from the projection of the z axis at the M sites. It appears then that at the tetrahedral sites in tincalconite as in borax the y principal axis lies mainly in the O_2-O_3 direction with the z axis mainly in the O_1-O_4 direction.

For kernite, $Na_2B_4O_7 \cdot 4H_2O$ -- the third member of the borax family, Christ has predicted that the same polyions occur as in borax but that the polyions have polymerized to

form infinite chains. The B^{11} spectrum of kernite was studied some years ago by Waterman and Volkoff (1955). On examining their data (see Table IV), it is immediately evident that the polyion contains two tetrahedra and two triangles as in borax but lacks the two-fold symmetry of the borax polyion, although the two triangles differ only slightly and the two tetrahedra to a somewhat greater extent. If the borax-type polyions polymerize to form kernite there might be sufficient distortion of the polyions to cause the two-fold symmetry to be lost; however, the relative orientation of the two BO_3 triangles would be expected to remain the same. Waterman and Volkoff's results yield for the angle between the z principal axes at the sites in the BO_3 triangles in the kernite polyion a value of 121° , which is in good agreement with the value of 123° obtained by us for the equivalent angle in borax. Thus the n.m.r. results again strongly support Christ's prediction.

Borax would appear to be an excellent choice for a theoretical interpretation of the quadrupole coupling tensors at the various boron sites in the polyion. Its structure is well known and, since the compact polyion is only weakly bonded to the crystal framework, one would expect the tensors to be determined primarily by intramolecular effects. Das (1957) carried out such a calculation for kernite but, as

mentioned in Section I.3, it is now known that the structure on which his calculations were based is incorrect.

CHAPTER VI

N.M.R. STUDY OF THE Na^{23} SITES IN BORAX AND TINCALCONITE

VI. 1. Experimental Results.

For a given rotation, the Na^{23} resonances were studied immediately after the B^{11} results had been obtained to avoid errors introduced in remounting the crystals, and the rotation axes X,Y,Z again coincided with the crystallographic directions $\vec{b} \times \vec{c}$, \vec{b} and \vec{c} in borax and \vec{a}_1 , $\vec{a}_1 \times \vec{c}$ and \vec{c} in tincalconite. The rotation angles for the X,Y and Z rotations were measured from the positions in which the Y,Z and X axes, respectively, were parallel to the magnetic field direction. The sample coil was made of silver wire to avoid the Cu^{63} and Cu^{65} signals which would have obscured the Na^{23} satellites at certain crystal orientations. Magnetic fields of 7536 and 5645 gauss were used for the borax and tincalconite studies, respectively, and measurements were made at room temperature.

Since Na^{23} has a spin of $3/2$, each unique sodium site will give rise to a spectrum consisting of a single line, ν_c , and a pair of satellites, $\nu_{3/2}''$ and $\nu_{3/2}'$. In this work, the satellites were studied almost exclusively since they provided all the data needed for a complete evaluation of the quadrupole coupling tensors. In borax, the width of the satellites,

as defined by the extrema in the first derivative of the absorption peak, was about 5 kc/sec and did not vary appreciably with the crystal orientation. In tincalconite, on the other hand, the width of the satellites was considerably greater, about 15 kc/sec, and varied markedly with orientation in the X and Y rotation. We think that this effect is caused mainly by internal strains in the crystal.

The Na²³ spectrum in borax was observed to consist of a maximum of six resolved satellite resonance lines in three pairs centered about three partially resolved central lines. At all crystal orientations, the two satellite lines making up one of these pairs were approximately twice as intense as the other four satellite lines, indicating that each line actually consisted of two unresolved satellites. The two sites which gave rise to these intense lines appeared identical to the n.m.r. experiment so they were designated B_{1,2} sites. At special orientations, when the crystal two-fold (Y) axis was parallel or perpendicular to H₀, symmetry-related satellites of the two remaining pairs coalesced to produce two satellites in a single pair with intensities equal to those of the satellites arising from sites B_{1,2}. The two sites giving rise to these signals were related therefore by the two-fold axis and they were designated as A₁ and A₂. The behavior of the Na²³ satellites clearly

demonstrates that there are two unique sodium sites in borax.

Tincalconite gave a more complex Na^{23} spectrum with a maximum of five pairs of satellites. When the three fold (Z) axis was parallel to H_0 , all symmetry related satellites coincided to produce a reduced spectrum of three pairs of satellites with intensities in the ratio 3:2:1. Since this was the minimum number of lines observed for any orientation, there must be three unique sodium sites, which we will designate A, B and C, in the unit cell. The intensities suggest that the six sodium atoms which are known to occupy each unit cell must be distributed with three in A sites, two in B sites and one in the C site.

The three A sites in tincalconite, which we designate A_1 , A_2 and A_3 , are obviously related by the three fold axis for, as soon as the crystal was rotated to a non-special orientation, the members of the triply-intense pair of satellites split into three pairs. The members of this group are also inter-related by the system of three two-fold axes (space group R32) in the plane perpendicular to Z for, at $\theta_Z = 0^\circ, 60^\circ, \text{ and } 120^\circ$, satellite pairs from A_2 and A_3 , A_1 and A_2 , A_3 and A_1 , respectively, coincided. The two B sites appeared identical to the n.m.r. experiment for all crystal orientations so they were designated as the $B_{1,2}$ sites.

The Na^{23} spectra in borax and tincalconite were

recorded at 15° intervals from 0° to 360° for each of the rotations about the X, Y and Z axes. The frequencies (tabulated in Appendix II) of related lines were averaged over all symmetry equivalent orientations to give the $\nu''_{3/2} - \nu'_{3/2}$ data shown in Fig. 15 for borax and Fig. 16 for tincalconite. A Fourier analysis of these data gave the values listed in Table VI for the a, b and c coefficients of eq. 2.27, section II.6. For tincalconite, a few experimental observations of the splitting of the satellites belonging to the A sites were omitted from the Fourier analysis because the accuracy of these measurements was poor due to lack of resolution or excessive broadening of the signals. Such points, which occurred only in the X and Y rotations, have been indicated by small dots in Fig. 16.

As in the B^{11} investigations, the correct combination of signs for the c coefficients of Table VI could not be determined for the A sites from the $\nu''_{3/2} - \nu'_{3/2}$ data alone. As explained in Section II.8 the ambiguity arises because the X rotation axis in borax and the Y rotation axis in tincalconite were each parallel to a two-fold axis of symmetry. Although second order shifts in the frequencies of the satellites were observed in both crystals, they were too small to be used with confidence to resolve the ambiguity. These ambiguities were therefore resolved by the same techniques as

Figure 15

Angular dependence of the frequency difference between the Na^{23} satellite lines arising at the A_1, A_2 and $B_{1,2}$ sites in borax for rotations about the X, Y and Z axes.

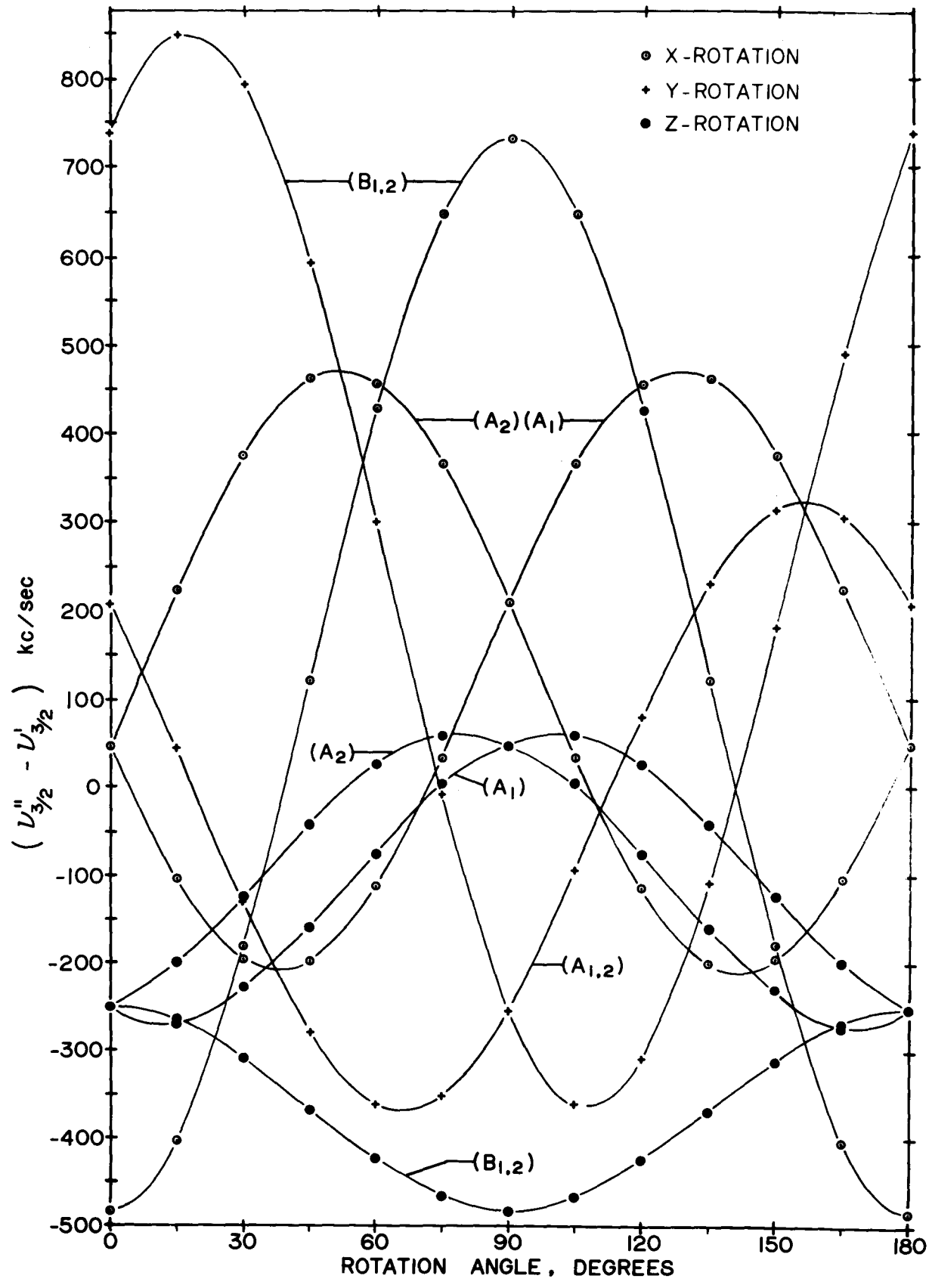


Figure 16

Angular dependence of the frequency differences between the Na^{23} satellite lines arising at the $A_1, A_2, A_3, B_{1,2}$ and C sites in tincalconite for rotations about the X, Y and Z axes.

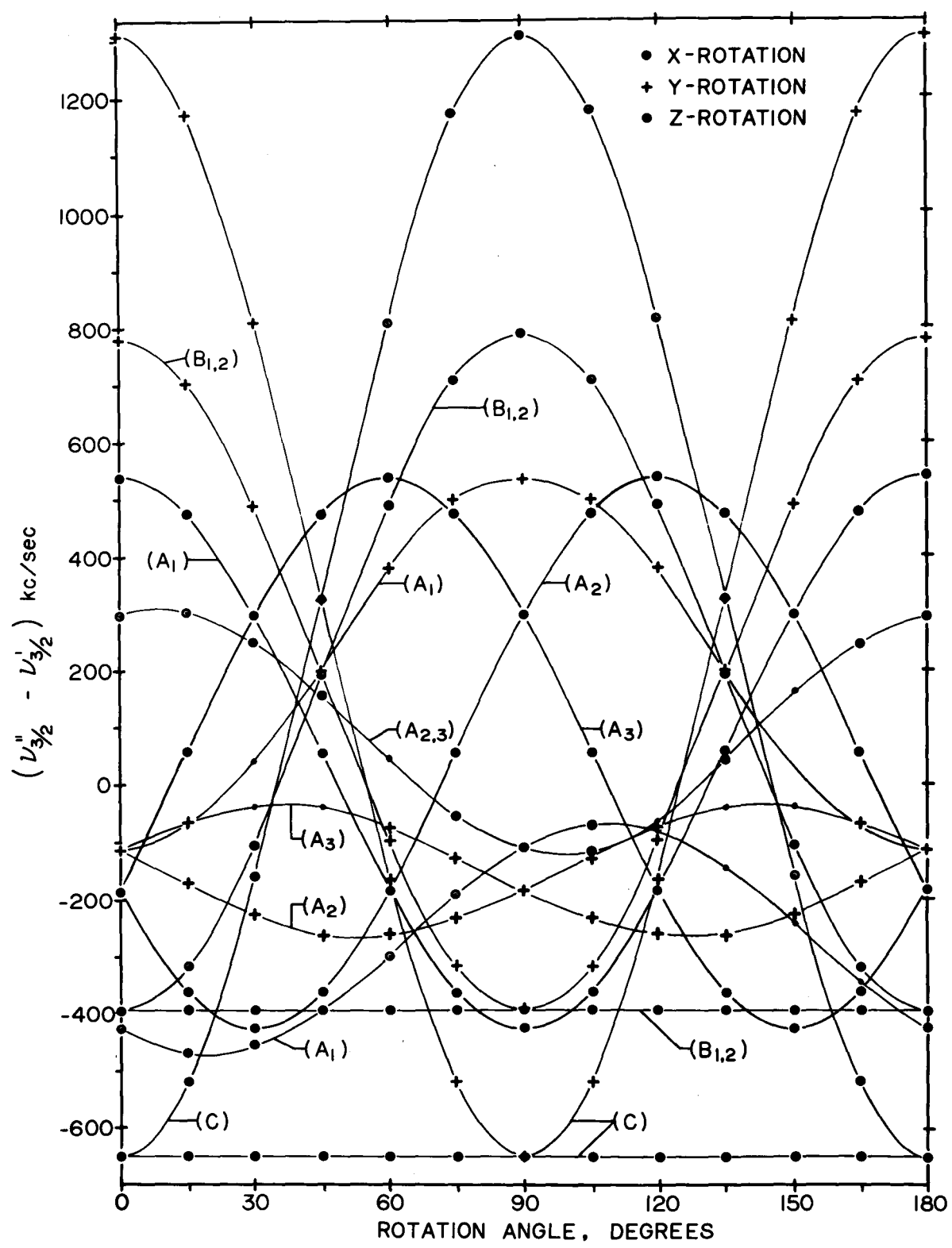


TABLE VI

Averaged Experimental Values of the Fourier Coefficients (in kc/sec) of the Angular Variation of $\nu_{3/2}'' - \nu_{3/2}'$ for Na^{23} Satellite Lines Arising in Borax and Tincalconite. Where alternative signs are given, the upper set refers to the upper site of the listed symmetry/^{related}pair.

Sites	Fourier Coefficients	X	Rotation Y	Z
Borax				
A ₁	a	+130.1	- 24.0	-120.0
A ₂	b	- 81.3	+230.9	-152.0
	c	+330.9	-256.8	+ 59.8
B _{1,2}	a	+122.5	+242.2	-369.4
	b	-607.9	+494.3	+116.4
	c	0	+352.9	0
Tincalconite				
A ₁	a	-270.0	+213.0	+ 55.9
	b	-158.6	-325.0	+482.7
	c	-123.1	0	0
A ₂	a	+ 94.7	-148.6	+ 55.9
A ₃	b	+206.0	+ 35.7	-241.3
	c	+ 56.6	+108.0	+418.0
B _{1,2}	a	+194.1	+195.0	-393.9
	b	-589.7	+588.3	0
	c	0	0	0

TABLE VI (continued)

Sites	Fourier Coefficients	Rotation		
		X	Y	Z
C	a	+327.8	+325.2	-649.0
	b	-978.0	+975.5	0
	c	0	0	0

described in Section V.1, for the tetrahedral boron sites. Thus, in borax, the signals were 'followed' directly through non-special orientations from the X rotation to the Z rotation leaving no doubt as to the correct association of lines, and, in tincalconite, the incorrect combinations of signs were eliminated because they would not give internal consistency among the tensors at the three A sites which must be identical in magnitude, within experimental error, and differ only in orientation.

The electric quadrupole coupling tensors in the X,Y,Z system were determined from the a,b,c coefficients of Table VI. Three values for each diagonal component are given by the three rotations and in the case of borax the three values were simply averaged. In tincalconite, a weighted average was obtained by weighing each value of a particular component according to an index of reliability based on the number of observations and the maximum separation of the satellites for the rotation from which the value was obtained, The off-diagonal elements could not be averaged, since only one value can be obtained for each. Table VII shows the averaged tensor components.

Except for the $B_{1,2}$ and C sites in tincalconite, the electric quadrupole coupling tensors were diagonalized in the usual way to yield the quadrupole coupling constants, eqQ/h ,

TABLE VII

Quadrupole Coupling Tensors for Na²³ Sites in Borax and
Tincalconite.

Site	Ψ_{XX}	Ψ_{YY}	Ψ_{ZZ}	Ψ_{XY}	Ψ_{YZ}	Ψ_{ZX}
Borax						
A _{1/2}	-256.3	+ 49.0	+ 207.4	⁺ 59.8	⁺ 330.9	+256.8
B _{1,2}	-250.1	-485.2	+ 735.2	0	0	-352.9
Tincalconite						
A ₁	+538.7	-426.9	- 111.7	0	+123.1	0
A _{2/3}	-185.6	+297.5	- 111.9	⁺ -418.0	- 56.7	[±] 108.0
B _{1,2}	-391.9	-393.1	+ 785.0	0	0	0
C	-649.0	-649.0	+1298.1	0	0	0

TABLE VIII

Quadrupole Coupling Constants, eqQ/h , and Asymmetry Parameters,

η , for Na^{23} Sites in Borax and Tincalconite.

Site	eqQ/h (Kc/sec)	η
Borax		
$A_{1,2}$	$+ 541 \begin{smallmatrix} + \\ -3 \end{smallmatrix}$	$0.449 \begin{smallmatrix} + \\ -0.015 \end{smallmatrix}$
$B_{1,2}$	$+ 849 \begin{smallmatrix} + \\ -4 \end{smallmatrix}$	$0.143 \begin{smallmatrix} + \\ -0.028 \end{smallmatrix}$
Tincalconite		
$A_{1,2,3}$	$+ 539 \begin{smallmatrix} + \\ -2 \end{smallmatrix}$	$0.741 \begin{smallmatrix} + \\ -0.005 \end{smallmatrix}$
$B_{1,2}$	$+ 785 \begin{smallmatrix} + \\ -2 \end{smallmatrix}$	0
C	$+1299 \begin{smallmatrix} + \\ -1 \end{smallmatrix}$	0

TABLE IX

Direction Cosines of the Principal Axes x,y,z of the Quadrupole Coupling Tensors at the Na²³ Sites in Borax and Tincalconite. The direction cosines of the additional symmetry-related sites may be obtained by operating with the appropriate matrices.

Site	Reference Axes	Principal Axes		
		x	y	z
Borax				
A ₁	b x c	$\bar{0}.481^{\pm}0.004$	$\bar{0}.826^{\pm}0.002$	$\bar{0}.292^{\pm}0.004$
A ₂	b	$^{\pm}0.788^{\pm}0.003$	$\bar{0}.262^{\pm}0.004$	$^{\pm}0.558^{\pm}0.004$
	c	$\bar{0}.384^{\pm}0.004$	$^{\pm}0.498^{\pm}0.004$	$^{\pm}0.777^{\pm}0.003$
B _{1,2}	b x c	$+0.952^{\pm}0.001$	0	$-0.306^{\pm}0.004$
	b	0	+1	0
	c	$+0.306^{\pm}0.004$	0	$+0.952^{\pm}0.001$
Tincalconite				
A ₁	a ₁	0	0	-1
	c x a ₁	$-0.324^{\pm}0.003$	$-0.946^{\pm}0.001$	0
	c	$-0.946^{\pm}0.001$	$+0.324^{\pm}0.003$	0
B _{1,2} and C	Tensors cylindrically symmetric, z principal axes parallel to c crystallographic axis.			

and asymmetry parameters, η , shown in Table VIII and the direction cosines shown in Table IX. For the symmetry-related group of three A sites in tincalconite, the values for eqQ/h and η given in Table VIII are averages of the values obtained for the three sites and the direction cosines given in Table IX for the A_1 site were obtained by operating on the tensors at the A_2 and A_3 sites with the threefold axis, so that they relate to the same orientation, and then averaging the three sets of results.

The $B_{1,2}$ and C sites in tincalconite present particularly simple problems. The lack of angular dependence of the satellite splittings for the Z rotation and the fact that for both the X and Y rotations the ratio of the extreme values of the splitting is 2:1 indicates that at both sites the tensor is cylindrically symmetric ($\eta = 0$) with the z principal axis along Z. The values of eqQ/h could have been obtained directly from the extreme values of the splitting but they were actually obtained by a complete analysis of all the experimental results for these sites.

VI. 2. Discussion of Results.

In his structure analysis of borax, Morimoto found that the eight sodium atoms in the multiple unit cell are located on special positions with four in each of the Wyckoff positions

a or e of space group C2/c. Because the unit cell is base-centered the number of sites observable by n.m.r. is halved and the complete Na²³ spectrum should consist of a superposition of the signals from two sites in a and two in e positions. Consideration of the space group C2/c reveals that the two sites in position a are related by the two-fold axis along the b-axis but no constraint is placed by symmetry on the orientation of the electric field gradient tensors at these sites. The four satellite signals from these two sites should thus be readily observed by n.m.r. as two pairs, and symmetry related members of these satellites should coincide to produce a single pair whenever the b(Y) axis is parallel or perpendicular to the applied magnetic field. The two sites in position e are located on the two-fold axis and are related by a center of symmetry. Their location on the two-fold axis demands that one of their principal axes be parallel to the b-axis and, because the two sites are related by a center of symmetry, they will give rise to a single pair of satellites, with the intensity of each line double that for a line from a single site in position a. The observed n.m.r. spectrum of Na²³ was consistent with this in every detail and analysis of the doubly-intense pair showed that the y-principal axis for these sites is parallel to the b-axis. The sites A₁ and A₂ are therefore identified with the Wyckoff a positions and the B_{1,2} sites with the Wyckoff e positions. Morimoto also

found that the octahedron formed by the oxygen atoms around a sodium atom in position a, his Na_I , is a regular one within the limits of error, but that the octahedron around a sodium atom in position e, his Na_{II} , is a little distorted. In support of this we note, Table VIII, that eqQ/h is rather smaller for the A sites than for the B sites. Thus our n.m.r. results are in complete agreement with Morimoto's proposed structure for borax.

For tincalconite, the number of observable sites and symmetry properties of the spectrum must be consistent with the space group R32 as deduced in the B^{11} n.m.r. study. Three unique sites occurring with intensities in the ratio of 3:2:1, as observed in this work, can be accounted for only if the six sodium atoms per unit cell are located on special positions with three atoms accommodated in Wyckoff positions e or d, two atoms in c, and one in position b or a of space group R32. Since these special positions have different point symmetries it is possible to check this conclusion by comparing the appearance of the spectra at special orientations of the crystal and the orientations of the tensors with the demands made by the symmetry properties. Three sodium atoms in e or d positions would give rise to three observable pairs of satellites except at special orientations: when the three fold axis is parallel to H_0 all pairs of satellites should

coincide to produce one pair of triple intensity, and when one of the two-fold axes is parallel to H_0 two satellite pairs should coincide to give one pair of double intensity with one pair of unit intensity. Further, the tensors at these sites must have one principal axis parallel to one of the two-fold axes. Consideration of the $\nu''_{3/2} - \nu'_{3/2}$ data in Fig 16 and the direction cosines in Table IX shows that each of these conditions is met by the group of sites labelled A_1 , A_2 and A_3 . The two sites in special positions c should always appear identical in the n.m.r. experiment and the quadrupole coupling tensor at these sites should have $\eta = 0$ and its z principal axis parallel to the three fold axis. These conditions are met by the sites $B_{1,2}$. Finally, the tensor at the site in position a or b should have $\eta = 0$ and its z principal axis parallel to the three fold axis as found for our C site. Thus, the symmetry requirements for the above distribution of sodium atoms are borne out in detail.

It is instructive to compare the single crystal n.m.r.. results with those obtained with powder samples. As indicated in Section I.3, Dharmatti et al (1962) inferred from their study of powdered borax that the sodium atoms occupy only one unique site in disagreement with the known crystal structure and they set an upper limit of 750 kc/sec for the quadrupole coupling constant. The single crystal work shows quite clearly

that there are two unique sodium sites with quadrupole coupling constants, see Table VIII, that bracket the upper limit set by Dharmatti et al. Also, in tincalconite, the powder work gave only two unique sites where there are in fact three. Again, the upper limit, given as 630 kc/sec, turns out to be close to the average value of the quadrupole coupling constants at the A and B sites, Table VIII. The quadrupole coupling constant of 1360 ± 50 kc/sec, obtained in the powder work for the remaining site in tincalconite, is in agreement with the single crystal value of 1299 ± 1 kc/sec (site C, Table VIII). This comparison shows that the results obtained with powder data must be interpreted with great caution when there is the possibility of overlap of signals from sites which do not differ greatly in environment.

Comparison of the quadrupole coupling constants for Na^{23} in tincalconite with those obtained for borax, whose structure is known, might give some suggestion as to the environment of the sodium atoms in tincalconite. The quadrupole coupling constants at the A sites are relatively small and nearly equal (541 kc/sec in borax and 539 kc/sec in tincalconite) which strongly suggests that a sodium atom in an A site in tincalconite also has six oxygen nearest-neighbours forming a nearly regular oxygen octahedron. The B sites in tincalconite have a quadrupole coupling constant (785 kc/sec)

which is somewhat larger than that at the A sites but close in value to that at the B site in borax (849 kc/sec) which probability indicates a slightly distorted octahedral arrangement of oxygen atoms for these sites, as also found in borax. Incidentally, the quadrupole coupling constants for Na^{23} at the A and B sites in tincalconite and borax fall within the range of 330 to 860 kc/sec (Pound 1950, Gutowsky and Williams 1957 Itoh et al 1954) observed in several other crystals for sodium atoms with coordination groups of six oxygen atoms in slightly distorted octahedra. The large value of eqQ/h (1299 kc/sec) associated with the C site in tincalconite clearly indicates a much less regular environment though it is still within the range (Weiss 1960, Petch and Pennington 1962) found for severely distorted oxygen octahedra. In assessing the above comparisons, we draw attention to the fact that in borax the ratio of sodium atoms to water molecules is ideal for octahedral arrangements, whereas, in tincalconite, it is possible that one or more oxygen atoms from the $\text{B}_4\text{O}_7(\text{OH})_2^{--}$ polyions may form part of the oxygen environment of at least one sodium site.

Attempts to correlate the direction cosines of the principal axes with the environments of the sodium sites in borax have met with limited success. However, there is some evidence that sodium neighbours exert a strong influence on

the orientation of the quadrupole coupling tensors.

CHAPTER VII

N.M.R. STUDIES OF FERROELECTRIC LITHIUM HYDRAZINIUM SULPHATE

VII. 1. Experimental Results.

A. Li^7 Study.

a. Spectrum at Room Temperature.

At room temperature, the Li^7 resonance was observed to be split by the quadrupole interaction into a spectrum of five lines, a central line plus two pairs of satellites. The separation between the satellites displayed the orientation dependence of eq. 2.27 although the total separation was always small. Symmetry-related satellite lines coalesced to produce a simple three-line spectrum whenever the X and Y axes were either parallel or perpendicular to H_0 indicating that the four lithium atoms in the unit cell occupy chemically-equivalent sites. The quadrupole coupling tensors at two of these sites differ in orientation so that they are distinguished by their resonance signals.

For each of the rotations about the X, Y and Z axes, the Li^7 spectra was recorded at 15° intervals from 0° to 360° . The rotation angles for the X, Y and Z rotations were measured from the positions at which the Y, Z and X axes, respectively, were parallel to the magnetic field. The frequencies of

corresponding lines at equivalent orientations were averaged and the results are shown in Fig. 17. The $\nu''_{3/2} - \nu'_{3/2}$ data obtained from these curves was analysed to yield the a,b,c coefficients listed in Table X. For the X rotation, only the data for $\theta_X = 0^\circ$ and 90° were used due to large overlap of the satellites at other angles. In accordance with Section II.6, the values of a,b and c^{were} used to calculate the components of the quadrupole coupling tensors in the X,Y,Z coordinate system and then the tensors were diagonalized. The values for the quadrupole coupling constant and asymmetry parameter listed in Table XI are the averages for the two sites which can be distinguished in the n.m.r. experiment. The orientation of the principal axes for the tensor at one of the sites, considered the progenitor of the others, is also given in Table XI; the orientations of the other tensors may be obtained from this by carrying out the appropriate symmetry transformations.

b. Indication of Phase Change.

The changes accompanying a ferroelectric transition, although normally quite detectable by n.m.r. methods, may be very small. In a search for an unknown transition it is of great help to be able to orient the crystal in such a way that the transition will manifest itself by a distinct change in the type of spectrum rather than by slight frequency shifts of some or all the lines present. This is often possible because the

Figure 17

Angular dependence of the frequency separation of the Li^7 satellite lines from the central resonance in lithium hydrazinium sulphate at room temperature. The rotation axes X,Y,Z were parallel to the a,b,c crystallographic axes, respectively, and the rotation angles for the X,Y and Z rotations were measured from the positions in which the Y,Z and X axes, respectively, were parallel to the magnetic field direction.

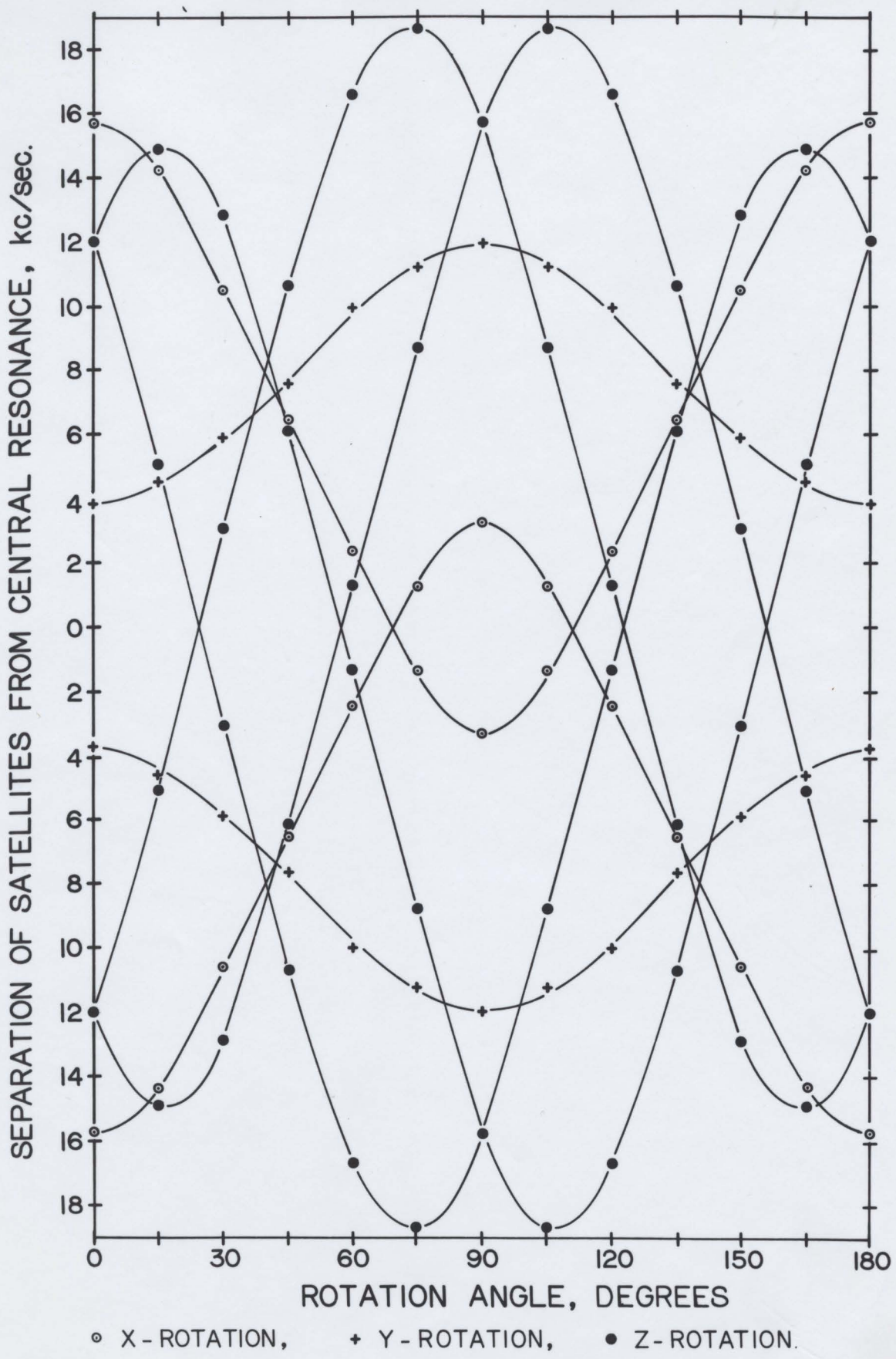


TABLE X

Averaged Experimental Values for the a,b,c Coefficients of the Angular Variation of $\nu''_{3/2} - \nu'_{3/2}$ for the Li^7 Resonance Lines Arising in Lithium Hydrazinium Sulphate. Alternative signs, where given, refer to symmetry-related sites.

	Rotation	Coefficients (kc/sec)		
		a	b	c
Room Temperature	X	+12.5	+19.1	0
	Y	-15.72	+ 7.88	0
	Z	+ 3.98	-27.57	± 17.93
+205°C	X	+ 9.07	+16.63	0
	Y	-12.12	+ 4.04	0
	Z	+ 4.70	-21.20	0

TABLE XI

Quadrupole Coupling Tensors for Li^7 in the Low- and High-Temperature Forms of Lithium Hydrazinium Sulphate.

eqQ/h (kc/sec)	3	Orientation of Principal Axes			
		x	y	z	
Low-temperature (+ 23°C) form					
36.8 ± 0.3	0.59	± 0.03	Parallel to c	Rotated 16°31' ±15'* clock- wise from a	Rotated 16°31' ±15' clock- wise from b
High-temperature (+ 205°C) form					
25.8 ± 0.1	0.33	±0.01	Parallel to c	Parallel to a	Parallel to b

*Error estimated by comparison of phase angle predicted from Fourier Coefficient with that obtained directly from experiment by observing the intensity of the Li^7 resonance as a function of θ_z in the region of $\theta_z = 31^\circ$.

high-temperature form of the crystal always has a higher symmetry than the low-temperature form. Then, if the orientation is chosen properly, certain lines will coalesce to form a reduced spectrum as the crystal transforms.

For these studies the LiH₂S crystal was oriented with the Z axis perpendicular to H₀ and $\theta_Z = 75^\circ$. This orientation produced the clearest separation of the five Li⁷ lines as can be seen from Fig. 17. At -70°C the spectrum was practically identical to that obtained at room temperature, although the separation of the lines was slightly greater. As the crystal was heated, the separation between the two satellites on the same side of the central line decreased gradually at first but, in the region of $+70^\circ\text{C}$, the separation started to decrease at an accelerating rate, as is shown in Fig. 18. At $+164^\circ\text{C}$ the separation had definitely reached zero and the crystal existed entirely in the high temperature phase. The appearance of the spectrum at selected temperatures is shown in Fig. 19. No further changes in the spectrum were detected as the crystal temperature was increased to $+205^\circ\text{C}$, although the signals became asymmetric. This asymmetry is noticeable in the central signal of the 164 C-spectrum of Fig. 19, but it became much more pronounced at higher temperatures. The above effects were completely reversible and even after several temperature cycles through the phase transition there were no

Figure 18

The open circles give the variation with temperature of the frequency separation between two Li^7 satellites which occur on the same side of the central line and coincide in the high temperature polymorph of lithium hydrazinium sulphate. These data were recorded at the orientation $\theta_Z = 75^\circ$. The solid circles give the variation with temperature of the second moment of the proton resonance in powdered lithium hydrazinium sulphate

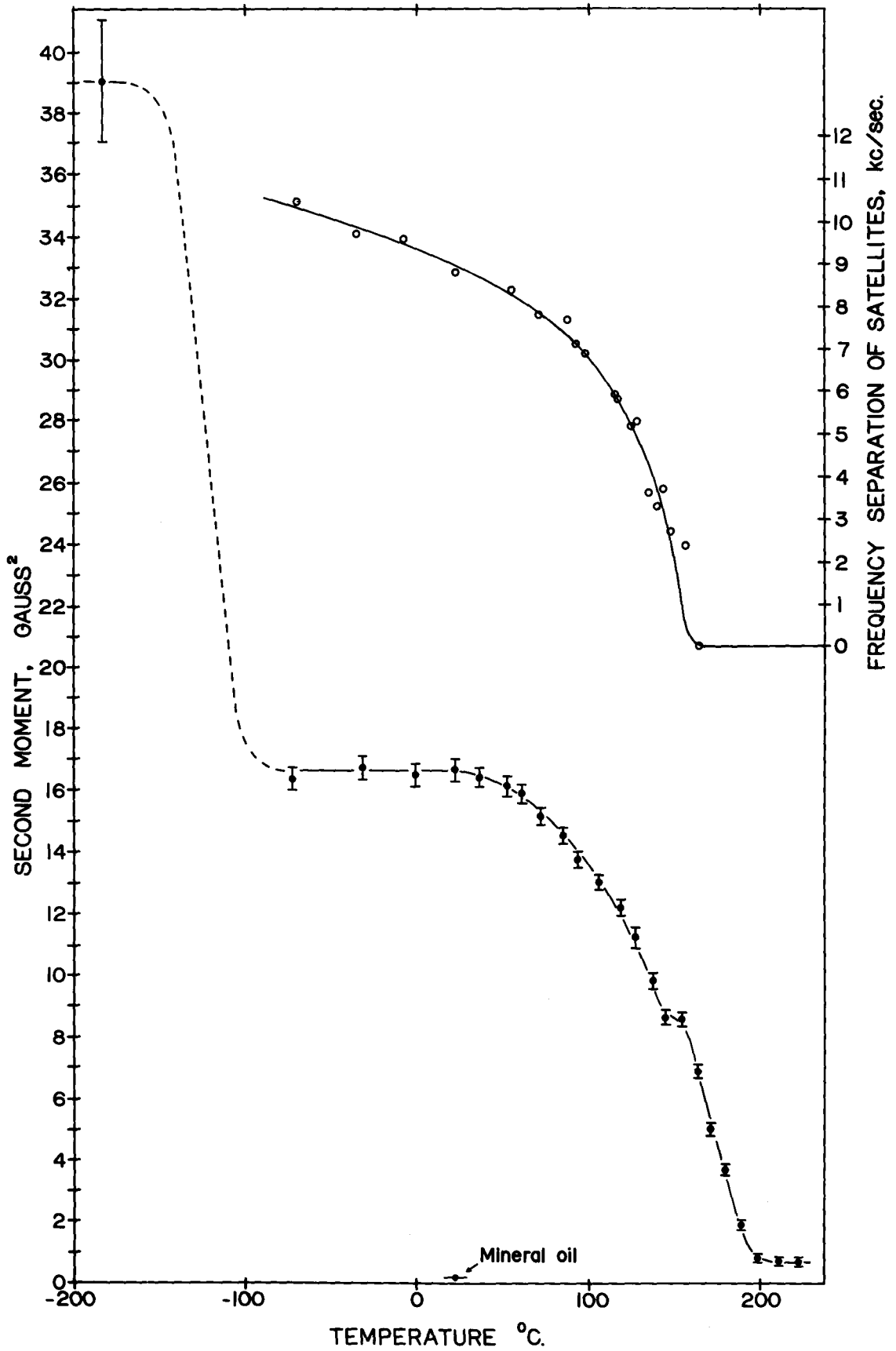
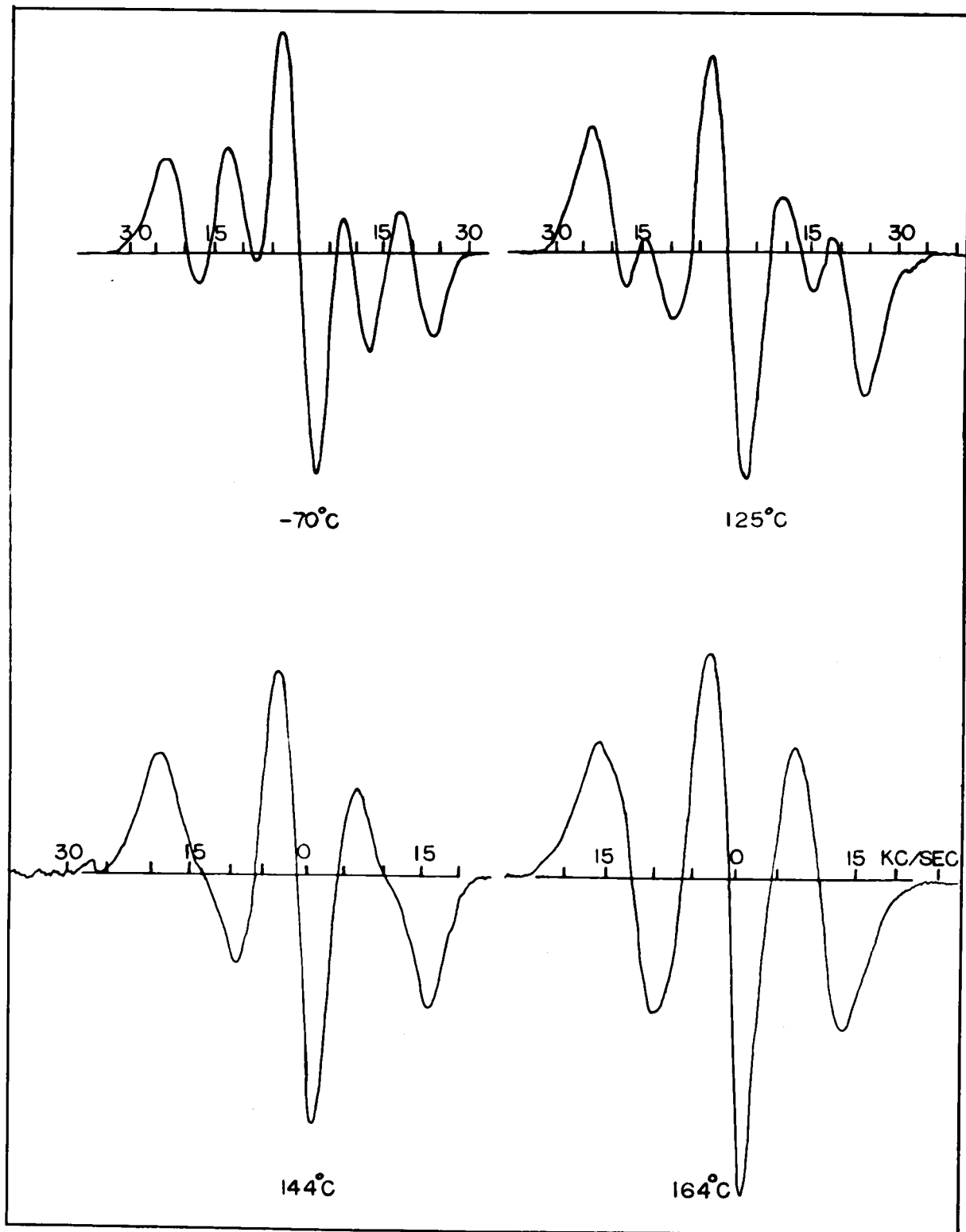


Figure 19

Tracings of the recorded derivatives of the Li^7 n.m.r. spectrum obtained at various temperatures. The single crystal of lithium hydrazinium sulphate was oriented with the Z(c) axis perpendicular to H_0 and $\theta_Z = 75^\circ$



observable changes in the room temperature spectrum.

c. Spectrum at +205°C

At +205°C, the Li^7 spectrum consisted of a maximum of only three lines, a central line plus one pair of satellites, regardless of crystal orientation. This indicates that in the high temperature phase the lithium atoms in the unit cell occupy sites which are not only chemically-equivalent but also physically-equivalent. That is, the electric quadrupole coupling tensors at the Li^7 sites are identical in magnitude and in orientation.

The shifts of the satellites from the central signal at 205°C are shown in Fig. 20. Preliminary examination of the spectra revealed that for each rotation the c-coefficient of eq. 2.27 was zero. The remaining coefficients were determined therefore, by simply using the splitting at $\theta_i = 0^\circ$ and 90° rather than carrying out complete rotations. This is in effect a direct measurement of the components of the quadrupole coupling tensor in the direction of its principal axes. The a and b coefficients are given in Table X with the complete description of the quadrupole coupling tensor following in Table XI.

B. Proton Resonance Study.

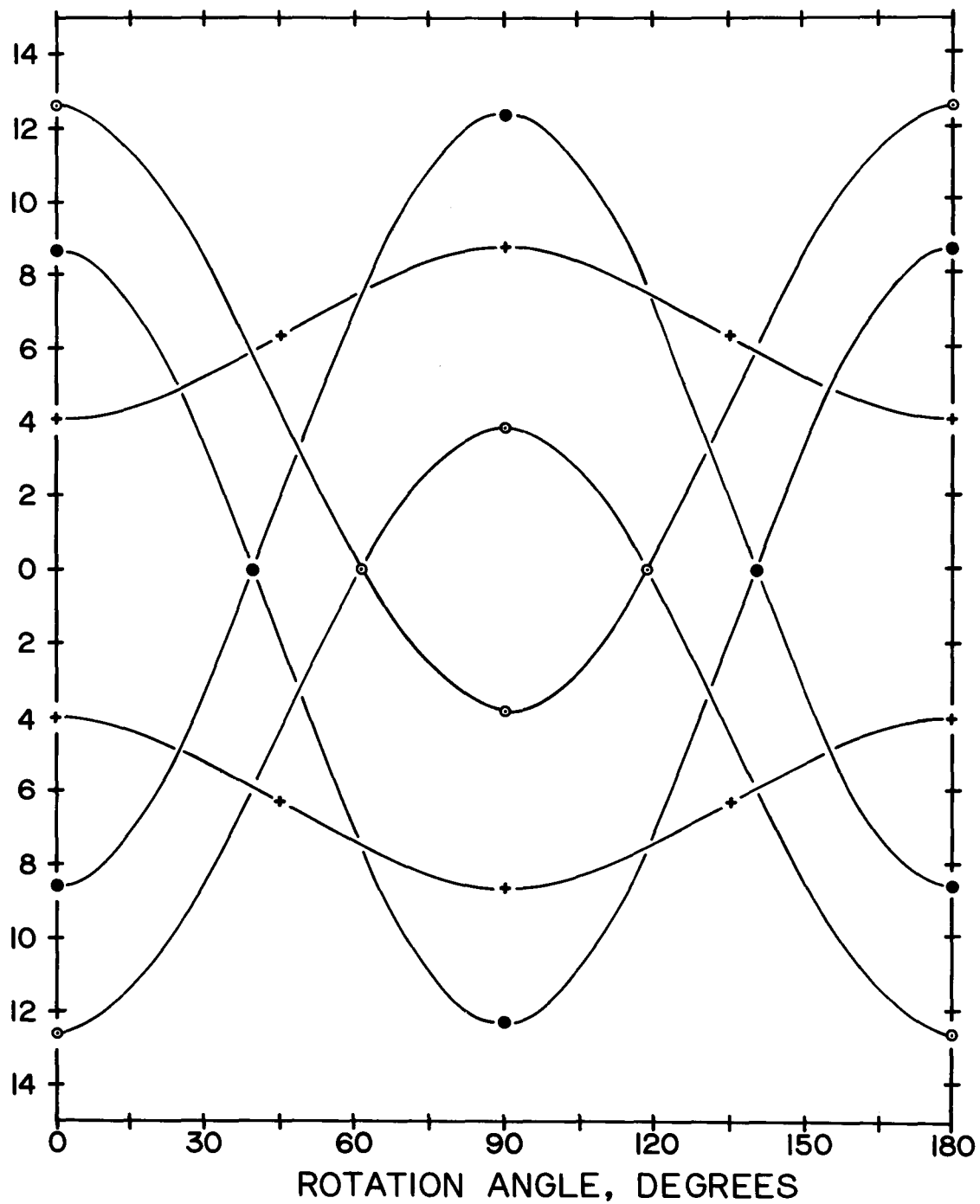
a. Second Moment of the Proton Signal in Powdered LiHzS

If a reorientation of some or all of the protons is

Figure 20

Angular dependence of the frequency separation of the Li^7 satellite signals from the central resonance in lithium hydrazinium sulphate at $+205^\circ\text{C}$. The rotation axes X,Y,Z were parallel to the a,b,c crystallographic axes, respectively, and the rotation angles for the X,Y,Z rotations were measured from the positions in which the Y,Z,X axes, respectively, were parallel to the magnetic field direction.

SEPARATION OF SATELLITES FROM CENTRAL RESONANCE, kc/sec.



○ X - ROTATION, + Y - ROTATION, ● Z - ROTATION.

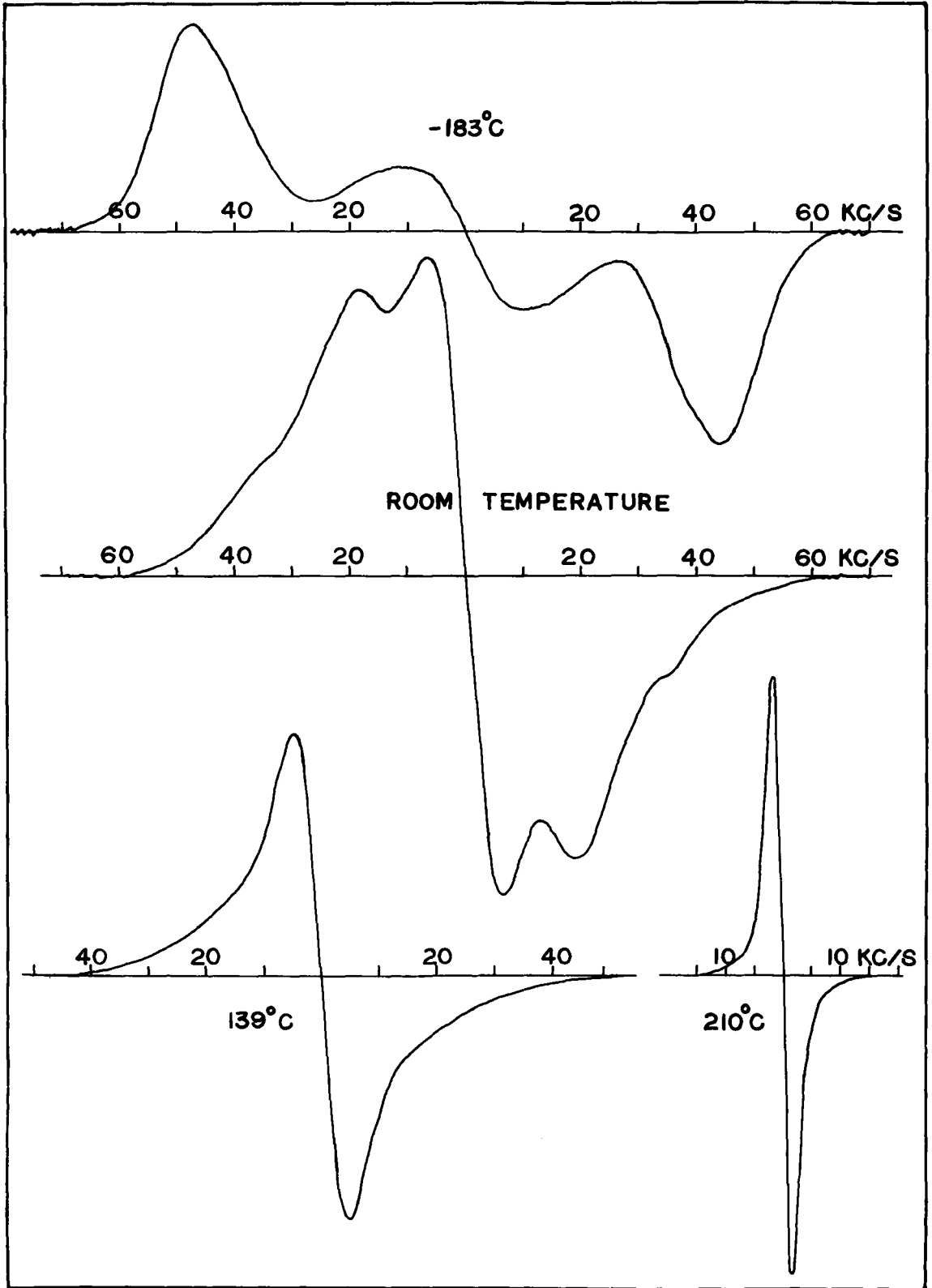
involved in the phase transition, one would expect a rapid narrowing of the proton signal in the same temperature range as the Li^7 signal was affected. A powdered sample was used for this proton investigation because the crystal structure was unknown at the time and the large number of interproton vectors was expected to produce a very complex signal from a single crystal which would have been very difficult to interpret. The second moment* of the proton signal, plotted as a function of temperature in Fig. 18, does indeed undergo a striking decrease with increasing temperature in the region of the phase transition revealed by the Li^7 signals. Traces of actual recordings of the proton resonance signal obtained at various temperatures are shown in Fig. 21.

Excellent reproducibility of the features of the second moment curve was found in three runs through the complete temperature range. Thus the projections of the final

* For the definition of the second moment of a broadened n.m.r. signal, see Section II. 12. The second moments were evaluated by measuring the height of the derivative signal at regular frequency intervals, and then treating the problem as an example of numerical integration. By using a cosine function as a hypothetical signal shape the procedure was estimated to be accurate to within 1%.

Figure 21

Derivatives of the proton resonance in powdered lithium hydrazinium sulphate at various temperatures. The curves have been arbitrarily scaled to have approximately the same extreme vertical values.



almost linear drop of each second moment curve on to the temperature axis cut it within the narrow temperature interval $194^{\circ} \pm 1^{\circ}\text{C}$. Also the slight arrest in the curve at about 150°C appears to be significant since the data from two of the runs showed such an arrest and the third run with much higher modulation amplitude exhibited a knee or abrupt change in the rate of change of slope at the same temperature, although it did not show an actual arrest.

The magnitude of the second moment at various temperatures raises further questions and, because of the way it led to further work, one will be discussed here. The value $16.7 \pm 0.5 \text{ gauss}^2$ observed at room temperature is much too small for a rigid N_2H_5^+ group. Two alternatives suggest themselves: either the group is not rigid but all or part of it is already undergoing some form of reorientation at room temperature, or the structure does not involve the hydrazinium ion but might conceivably be $\text{LiH}(\text{N}_2\text{H}_4)\text{SO}_4$. Fortunately, one does not need to depend upon small differences in the line shapes or values of the second moment produced by models based upon these two alternatives to distinguish between them. If the hydrazinium ion is already undergoing reorientation at room temperature, then one would expect a rapid broadening of the proton signal as the crystal is cooled to some lower temperature at which reorientation ceases. It was found that the second moment

remained virtually constant at the room temperature value down to -70°C . At the temperature of liquid air, a much broader signal was observed, and is compared in Fig 21 with that obtained at room temperature. The second moment was $39 \pm 2 \text{ gauss}^2$, which is consistent with that obtained in other hydrazinium salts (Deeley, Lewis and Richards, 1954). This broadening of the proton signal in LiHzS at temperatures approaching that of liquid air has also been noted by Burns (1962) and Blinc, Schara and Poberaj (1963). Unfortunately, the limitations of our apparatus did not permit observations in the temperature range -180°C to -70°C in which the transition takes place.

b. Proton Resonance in a LiHzS Single Crystal

A study of the proton spectrum in a single crystal is generally valuable when only a few interproton vectors are involved but it may also be valuable in a more complicated case where it is possible to choose special crystal orientations at which the complex spectrum is simplified in some respect. Luckily the structure and symmetry of LiHzS is such that detailed information about the structure of the hydrazinium ion can be obtained from a single crystal study.

It was inferred from the second moment study (see the discussion section of this Chapter) in powdered LiHzS that at room temperature the protons in the $-\text{NH}_2$ group are effectively

rigid but that the triangular array of protons in the $-\text{NH}_3^+$ group is rotating about the N-N axis. The protons in a rigid $-\text{NH}_2$ group will give rise to the familiar Pake doublet. It has been shown in Section II.11 that an equilateral triangle of protons rotating about the normal of the triangle gives rise to a pair of lines, each with probability $\frac{1}{4}$, flanking a central line, which has probability $\frac{1}{2}$. The pair of lines has the same angular dependence and splitting as that for a Pake doublet with the interproton distance equal to the side of the equilateral triangle and the rotation angle defined as the angle between the normal to the triangle and the magnetic field. The complete spectrum will be a superposition of these five lines plus equivalent lines from the symmetry-related hydrazinium ions.

The problem is to choose special crystal orientations which give spectra in which lines from selected groups of protons are resolved from the remaining complex of overlapping lines. This situation is most likely to occur at those orientations for which the separations of the various doublets are at their maxima. A further advantage of measuring the maximum separations is that the interproton distances can then be obtained directly from the individual measurements. The important directions that must be considered in choosing these special orientations are the interproton directions for the

$-\text{NH}_2$ group, which can only be inferred from the x-ray analysis and the normal to the proton triangle in the $-\text{NH}_3^+$ group which would be expected to lie along the N-N direction.

According to the x-ray structure analysis the N-N direction lies within 1° of the (001) plane and makes an angle of 34° with the X(a) axis. Therefore, if the triangle is rotating about the N-N axis, one would expect to find maximum separation of its doublet at $\theta_Z = 34^\circ$ at which angle H_0 should coincide with the normal to the proton triangle. At this orientation the signals from the two $-\text{NH}_3^+$ groups related by the screw axis should be indistinguishable because the two N-N directions are practically colinear. There will be little interference from the signals from the two $-\text{NH}_3^+$ groups related to the first set by glide planes, because the separation of the doublets from these groups will be small due to the fact that their N-N directions make an angle of 60° with H_0 . Likewise, the separations between the doublets from the various $-\text{NH}_2$ groups will be fairly small at this orientation because all the expected proton-proton directions are inclined well away from H_0 . Therefore, at $\theta_Z = 34^\circ$ we expect to observe that the members of the doublet arising at a rotating $-\text{NH}_3$ group are wholly or partially separated from the main complex proton resonance signal. The ratio of the integrated intensity of the doublets to the total intensity would be expected to

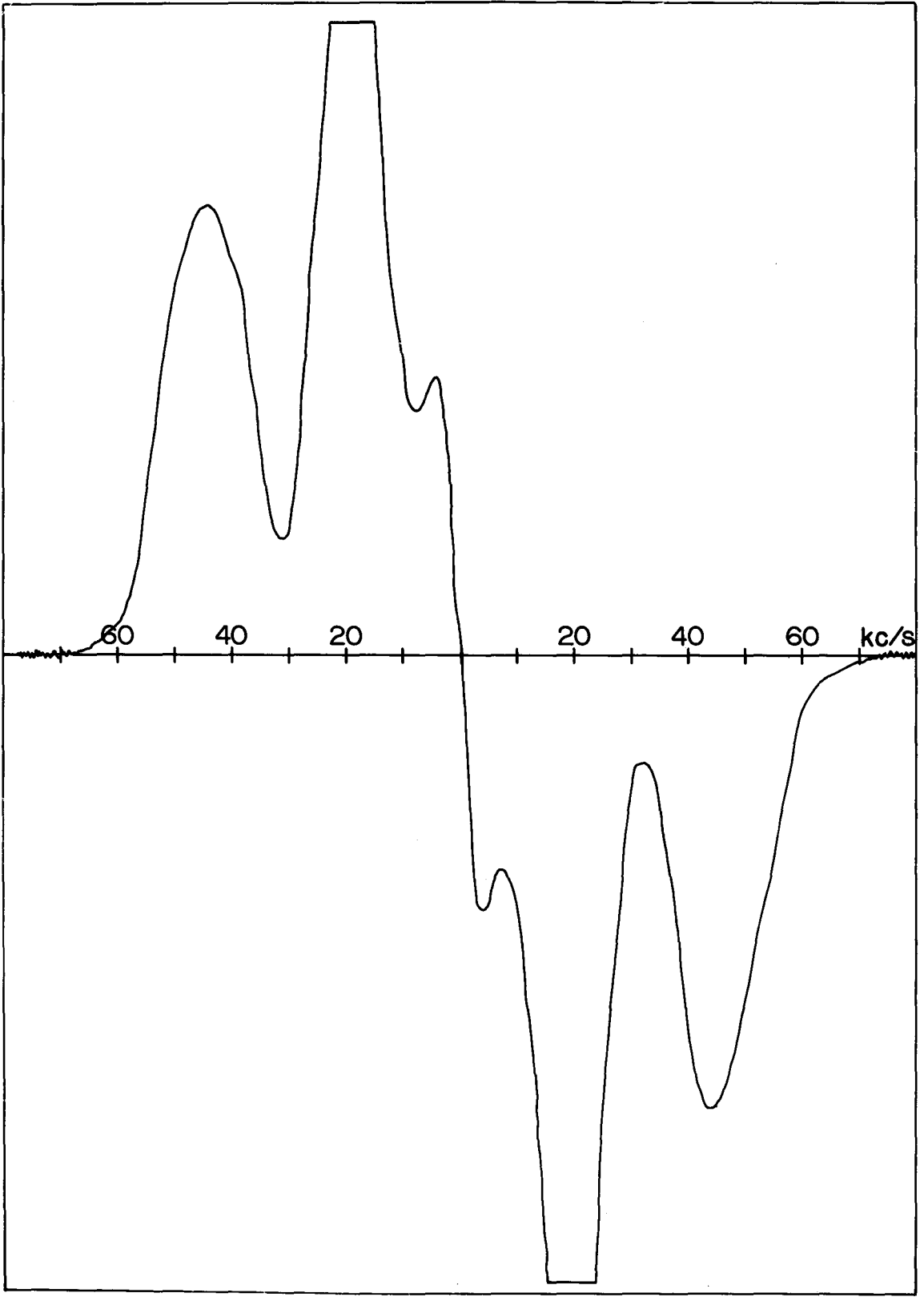
be 0.15 based on the appropriate probabilities and number of protons involved.

In the Z rotation of the single crystal, two lines did appear on the wings of the main proton resonance, as shown in Fig. 22, with their maximum separation occurring at $\theta_Z = 35^{\circ} \pm 3^{\circ}$. It was difficult to make accurate measurements of the separation and intensities of these lines because they were not completely resolved even at this orientation. The recorded derivative signal was integrated to obtain the complete absorption curve from which the members of the doublet pair were isolated by subtracting the tail of the complete central signal, whose shape at its extremities was estimated from signals obtained at other crystal orientations which gave better resolutions. The ratio of the integrated intensity of the doublet members to the total integrated intensity was found to be 0.18 ± 0.02 . The maximum value obtained for the separation between these doublets was 81.5 ± 3 kc/sec which, if we attribute these signals to the rotating $-\text{NH}_3^+$ group, gives a value of $1.64 \pm 0.02 \text{ \AA}$ for the side of the equilateral triangle of protons.

For the special orientation chosen to reveal the signals from the $-\text{NH}_2$ group, the crystal was aligned with the rotation axis in the XY plane making an angle of 35° with the X axis. Rotation about this axis, which is parallel to the

Figure 22

Derivative of the proton resonance absorption line in a single crystal of LiH_2S at the orientation $\theta_z = 35^\circ$. The two peaks at the extremities of the signal are believed to be due to the rotating $-\text{NH}_3^+$ group.



N-N axes of half the hydrazinium ions, should bring the -NH_2 groups of these hydrazinium ions very nearly into a position for which the interproton directions are parallel to H_0 so that the separation of the Pake doublet will be at its maximum while at the same time the interproton vectors of the other -NH_2 groups and the normals to the rotating -NH_3^+ groups are all inclined at substantial angles to H_0 so that the separations of their doublets would be considerably less than their maxima. One would expect therefore, that the doublet from the -NH_2 group would stand out fairly clearly at the extremities of the proton signal and that the ratio of the integrated intensity of the doublets to the total integrated intensity should be 0.10.

As shown in Fig 23, the expected doublet did appear at the extremities of the main proton resonance. Once the doublet had been located, the rotation angle and arc settings were adjusted to locate the orientation for maximum separation. A plot of the separation between the members of the doublet versus the angle for a counterclockwise rotation is given in Fig. 24. The same method as described previously was used to separate the members of the doublet from the total resonance but the accuracy was somewhat better because these signals were more nearly resolved.

The intensity ratio was found to be 0.096 ± 0.008 in

Figure 23

Derivative of the proton resonance absorption line in a single crystal of LiHzS oriented with the $N_1 - N_2$ axis perpendicular to H_0 and rotated to give the maximum separation of the Pake doublet whose members appear at the extremities of the signal. This doublet is believed to be due to the protons in the $-NH_2$ group.

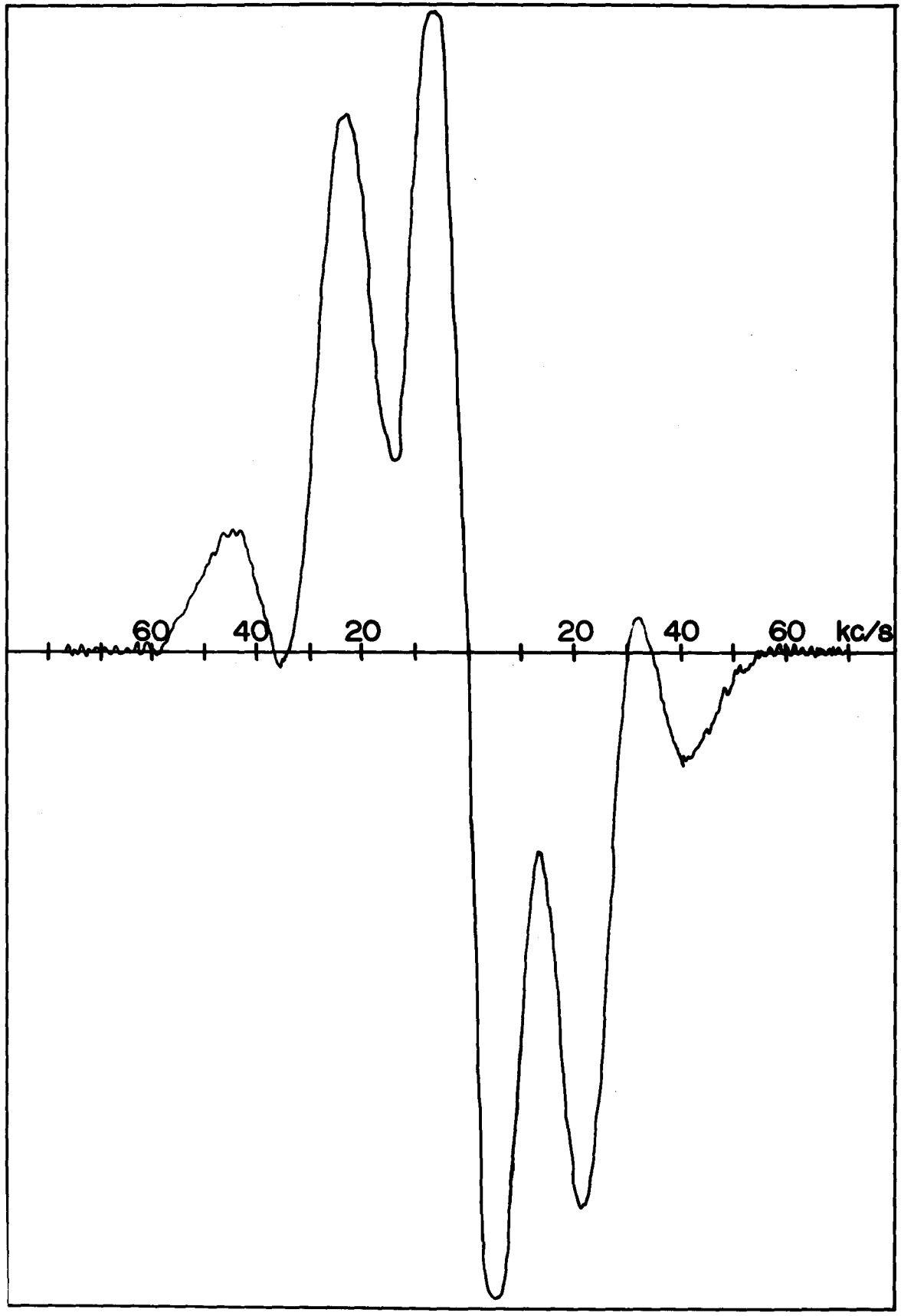
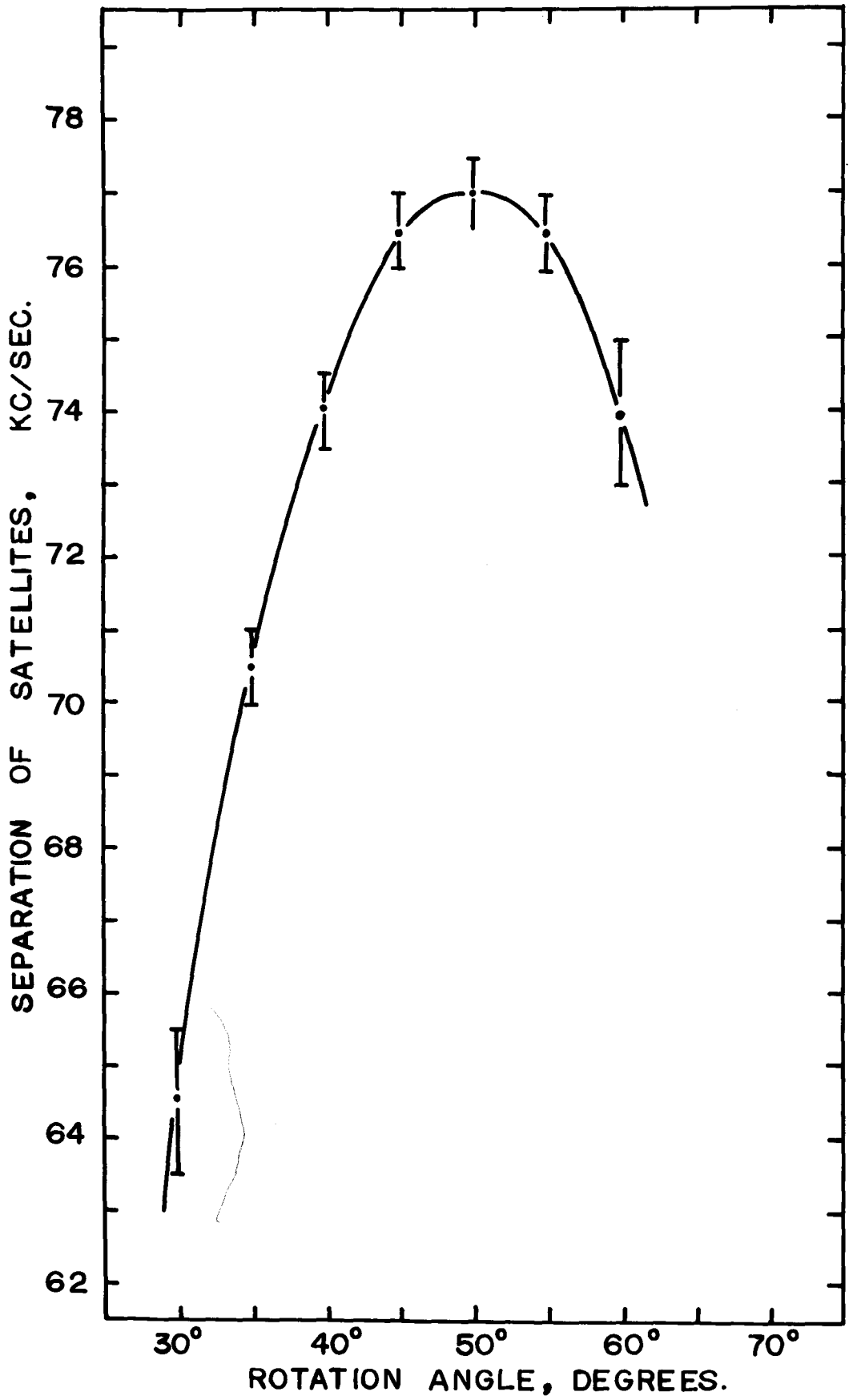


Figure 24

Separation versus angle of rotation of the members of the doublet seen at the extremities of the signal shown in Fig.23. The axis of rotation was parallel to the N_1-N_2 axis of the hydrazinium ion and the angle of rotation was measured from the position in which the c crystallographic axis was parallel to H_o .



excellent agreement with the value expected for the signals from a $-\text{NH}_2$ group. The maximum separation of 77.0 ± 1.5 kc/sec occurred at a rotation angle of $49^\circ 40' \pm 1^\circ 30'$. From this we find that the interproton vector has a magnitude of 1.67 ± 0.01 Å and an orientation given by the direction cosines 0.44 ± 0.02 , 0.62 ± 0.02 and 0.65 ± 0.02 , relative to the crystallographic axes a, b and c.

VII. 2. Discussion of Results.

The experimental values of 39 ± 2 gauss² obtained for the second moment of the proton resonance signal at -183°C is very likely characteristic of the rigid structure, although our apparatus did not permit examination of the signal at still lower temperatures to see if there was any further broadening. This quantity can serve as a useful check on the existence of the hydrazinium ion by comparing it with the calculated value for a model ion. An isolated $\text{NH}_2-\text{NH}_3^+$ ion in which the N-H distance of the $-\text{NH}_3^+$ group is 1.01 Å (see later), the N-H distance of the NH_2 group is 1.03 Å (see later), and the N-N distance is 1.46 Å (x-ray analysis) and all bond angles are tetrahedral would produce a second moment of 30.6 gauss². To this we must add interionic and lattice broadening, which we calculate amounts to 9.6 gauss², giving a total calculated second moment of 40.2 gauss². The second moment is not

significantly different for the staggered and eclipsed configurations of the -NH_2 and -NH_3^+ groups. A similar calculation with the assumption that the structure is not based on a hydrazinium ion but that the structural formula should be written as $\text{LiH}(\text{N}_2\text{H}_4)\text{SO}_4$ yields a second moment of only 24 gauss². Table XII shows in more detail the individual component values contributing to these totals. Other experimental values for solids containing the hydrazinium ion are 37.4 and 38.5 gauss² obtained by Pratt and Richards (1953) for hydrazinium oxalate and hydrazinium sulphate, respectively. This excellent agreement of experimental value with the calculated value and other experimental values obtained with materials containing the hydrazinium ion, confirms the view that the nitrogen and hydrogen atoms exist in the forms of hydrazinium ions in LiH_2S .

The lower value of the second moment at room temperature, 16.7 ± 0.5 gauss², clearly indicates that the hydrazinium ion is undergoing some reorientation. It would seem that the molecular reorientation most likely to occur in the hydrazinium ion involves rotation of the -NH_3^+ group about the $\text{N}_1\text{-N}_2$ axis. The x-ray structure shows that the -NH_3^+ group is surrounded by five oxygen atoms with N-O distances short enough to represent hydrogen bonds, so that there are several permitted orientations for the -NH_3^+ group and it is likely

TABLE XII

Individual Contributions to the Second Moment of the Proton
Magnetic Resonance Signal from Powdered LiHzS Calculated

Using eq. 2.24.

(a) Rigid Lattice with Asymmetric Unit Existing as

$\text{Li}^+(\text{NH}_2\text{-NH}_3)^+ \text{SO}_4^{--}$; Eclipsed Configuration.*

Proton interactions within NH_3^+ and NH_2 groups	28.54	gauss ²
Interproton broadening within $(\text{NH}_2\text{-NH}_3)^+$ groups	4.33	
Interproton broadening in same chain;		
between NH_3^+ groups	0.23	
between NH_2 groups	3.01	
between NH_2 and NH_3^+ groups (not intraionic)	1.01	
Interchain broadening	0.79	
Broadening due to nitrogen nuclei	2.09	
Broadening due to lithium nuclei	0.25	
Total	40.25	gauss ²

(b) Rigid Lattice with Asymmetric Unit Existing as

$\text{Li}^+(\text{NH}_2\text{-NH}_2) \text{HSO}_4^-$; Eclipsed Configuration

Proton interactions within NH_2 groups	13.08	gauss ²
Interproton broadening within $(\text{NH}_2\text{-NH}_2)$ groups	3.63	
Interproton broadening in same chain		
between hydrogen bonded NH_2 groups	3.01	
between other NH_2 groups	~ 1.23	
Interchain broadening	~ 0.79	

TABLE XII (continued)

Broadening due to lithium nuclei	0.20
Broadening due to nitrogen nuclei	1.66
	<hr style="width: 100%; border: 0.5px solid black;"/> 24 gauss ²
(c) Reorienting $-\text{NH}_3^+$ Group with Asymmetric Unit Existing as $\text{Li}^+(\text{NH}_2-\text{NH}_3)^+\text{SO}_4^{--}$.	
Proton interactions within NH_2^+ and NH_2 groups	12.03 gauss ²
Interproton broadening within $(\text{NH}_2-\text{NH}_3)^+$ groups**	~1.00
Interproton broadening in same chain,	
between NH_3^+ groups	~0.0
between NH_2 groups	3.01
between NH_3^+ and NH_2 groups	~0.20
Broadening due to nitrogen nuclei	0.92
Broadening due to lithium nuclei	~0.06
	<hr style="width: 100%; border: 0.5px solid black;"/> 17 gauss ²
(d) Reorienting $(\text{NH}_2-\text{NH}_3)^+$ Group with Asymmetric Unit Existing as $\text{Li}^+(\text{NH}_2-\text{NH}_3)^+\text{SO}_4^{--}$	
Proton interactions within NH_3^+ and NH_2 groups	7.13 gauss ²
Broadening from nitrogen nuclei	0.51
	<hr style="width: 100%; border: 0.5px solid black;"/> 8 gauss ²

* The eclipsed and staggered configurations give the same second moments within accuracy of the calculation.

** Estimated by using the $F(\gamma_{ij})$ function of Section II.12 with $\gamma_{ij} = 30^\circ$ and an average value of r^{-6} .

that the heights of the potential barriers between these various orientations are small. Several pieces of experimental evidence suggest that such a motion of the $-\text{NH}_3^+$ group occurs. First, the doublet from the $-\text{NH}_2$ group, observed when the N_1-N_2 axis was perpendicular to the magnetic field, clearly established that the $-\text{NH}_2$ group is not undergoing reorientation at room temperature nor is the $\text{NH}_2-\text{NH}_3^+$ ion as a whole. The only possibility left is an independent reorientation of the $-\text{NH}_3^+$ group. Second, the calculated value (see Table XII) for the second moment of the proton signal, based on the $\text{NH}_2-\text{NH}_3^+$ ion with dimensions used in the preceding paragraph, a rotating $-\text{NH}_3^+$ group and a rigid $-\text{NH}_2$ group, gives 17 gauss², in good agreement with the experimental value of 16.7 ± 0.5 gauss². Third, a doublet which gave its maximum separation when the N_1-N_2 axis was parallel to the magnetic field was found as predicted. It seems very unlikely that this doublet has been incorrectly ascribed to the $-\text{NH}_3^+$ group, for its intensity was reasonably consistent with the calculated intensity for a rotating triangle, but too great for a doublet from a $-\text{NH}_2$ group, and there seems to be no structural possibility for the maximum separation of a doublet associated with a $-\text{NH}_2$ group to occur at such an orientation. Fourthly, the motion begins in the same temperature range, around -130°C , as Deeley, Lewis and Richards

(1954) found for the onset of rotation of the $-\text{NH}_3^+$ group in a number of hydrazine salts. The conclusion seems inescapable that the $-\text{NH}_3^+$ group is rotating about the N-N axis of the hydrazinium ion in LiHzS at room temperature.

The nitrogen atom in the $-\text{NH}_3^+$ group of the hydrazinium ion forms four bonds so that one expects the bond angles to be tetrahedral. The situation is not so clear for the $-\text{NH}_2$ group but again one might expect tetrahedral bond angles because the nitrogen atom forms three σ bonds and uses its lone pair electrons to accept a hydrogen bond from a neighbouring hydrazinium ion. No strictly comparable examples have yet been studied by neutron diffraction but it has been shown that the H-N-H angles are tetrahedral within experimental error in crystalline deuterioammonia (Reed and Harris, 1961) and sulphamic acid (Sass, 1960). Assuming that the bonds are indeed tetrahedral and that the N-H distances within a particular type of $-\text{NH}_x$ group are equal, we calculate from the proton-proton distances obtained by n.m.r. that the N-H distances are $1.01 \pm 0.01 \text{ \AA}$ and $1.03 \pm 0.01 \text{ \AA}$ in the $-\text{NH}_3^+$ and $-\text{NH}_2$ groups, respectively, of LiHzS . These values are compared in Table XIII with the N-H distances in crystalline deuterioammonia, sulphamic acid and gaseous ammonia.

We can now establish a fairly complete picture of the disposition of the atoms in the $-\text{NH}_2$ group of a hydrazinium

TABLE XIII

N-H Distances in $\text{Li}(\text{N}_2\text{H}_5)\text{SO}_4$ Compared with Values Obtained by Neutron Diffraction (N.D.) and Infrared Measurements (I.R.) for the N-H Distances in NH_3^+ Groups

Substance	N-H Distance(\AA)	H-N-H Angle	Method	Reference
$\text{Li}(\text{N}_2\text{H}_5)\text{SO}_4$				
- NH_3^+ group	1.01 ± 0.01	assumed 109.5°	N.M.R.	
- NH_2 group	1.03 ± 0.01			
Sulphamic Acid	1.024 ± 0.03	107.6°	N.D.	Sass (1960)
$\text{NH}_3^+ \cdot \text{SO}_4^-$	(average)	(average)		
Crystalline Deuteroammonia	1.005 ± 0.023	$110.4^\circ \pm 2.0^\circ$	N.D.	Reed and Harris (1961)
Gaseous Ammonia	1.014	106.8°	I.R.	Herzberg (1945)

ion in LiHzS. A hydrogen atom linking adjacent hydrazinium ions through a bond $N_I-H\dots N_I$ will be referred to as H_I and a hydrogen atom linking a hydrazinium ion to the framework through a bond $N_I-H\dots O_4$ will be referred to as H_{II} . Combining the value of 1.03 Å for the N-H distances with the orientation obtained for the interproton vector, we calculate that H_I is slightly displaced from the line joining two N_I atoms, with the N_I-H_I direction making an angle of $4.5^\circ \pm 2.5^\circ$ with the N_I-N_I direction. The $N_I-H_{II}\dots O_4$ hydrogen bond is much more bent with the N_I-H_{II} direction making an angle of either $29^\circ \pm 2.5^\circ$ or $38^\circ \pm 2.5^\circ$ with the N_I-O_4 direction. The ambiguity in the value of this angle arises because the n.m.r. experiment cannot determine the sense of the interproton vector. One would expect the smaller angle to lead to the lowest energy condition, so only this angle has been used in the derivation of the direction cosines of the H_I-H_{II} , N_I-H_I , N_I-H_{II} , N_I-N_I , and N_I-O_4 directions which are given in Table XIV. This arrangement of atoms is shown graphically in Fig. 25.

A possible mechanism for the ferroelectric behavior of LiHzS is now apparent. If the hydrogen bonds linking adjacent hydrazinium ions are ordered, there are two possible configurations of the chain, which are illustrated with the $N_I-H_I\dots N_I$ bonds pointing in the negative c direction in Fig.

TABLE XIV

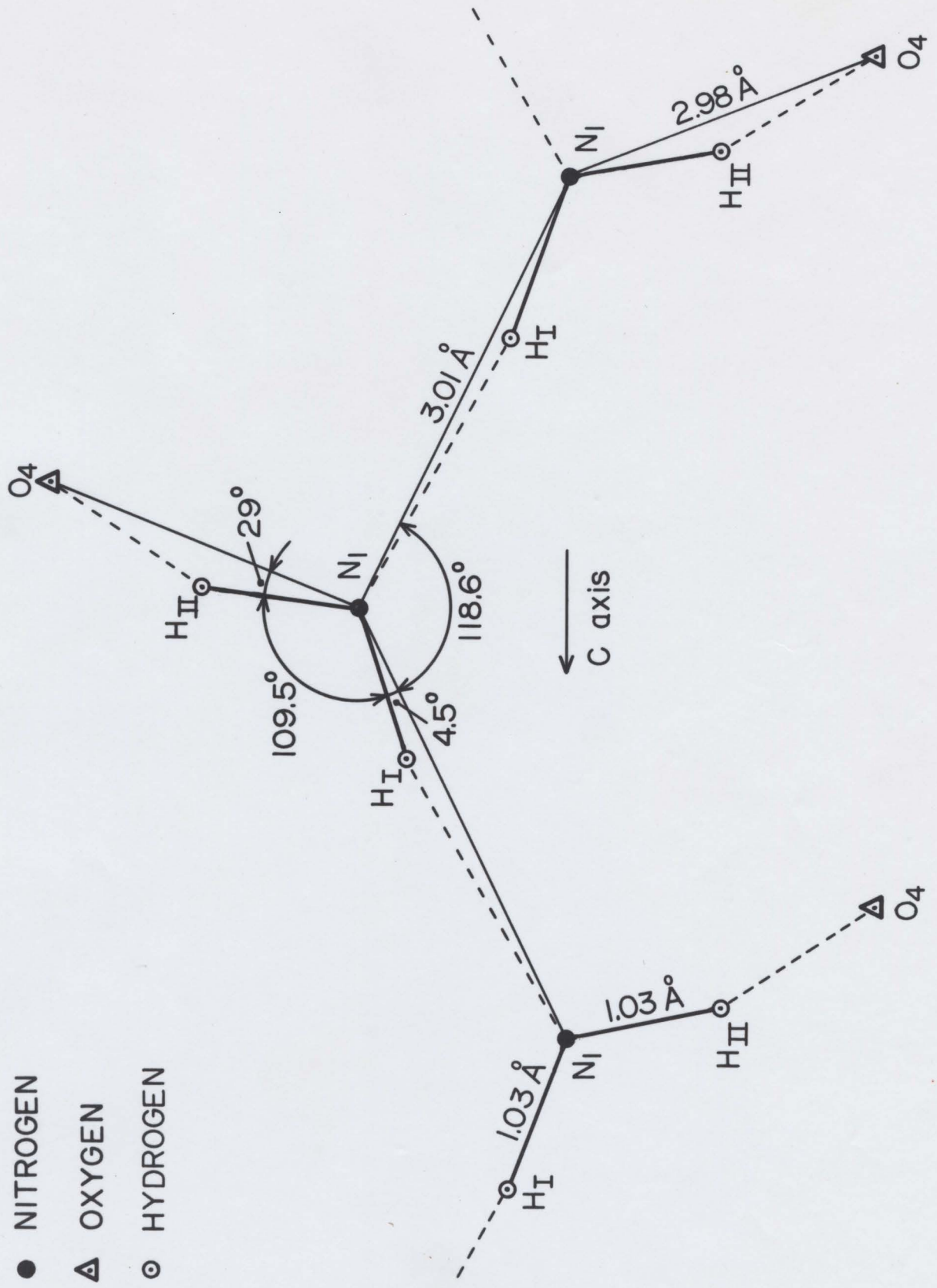
Direction Cosines of the Interatomic Directions in the $-\text{NH}_2$ Group of the Hydrazinium Ion. To facilitate comparison with the structural work, the $-\text{NH}_2$ group and its neighbours referred to here are those obtained directly from the atomic coordinates listed by Brown (1963).

Interatomic Directions	Crystallographic Reference Axes		
	a	b	c
$\text{H}_I - \text{H}_{II}^*$	+0.44 \pm 0.02	-0.63 \pm 0.02	+0.65 \pm 0.02
$\text{N}_1 - \text{H}_I$	+0.46 \pm 0.04	-0.07 \pm 0.04	+0.89 \pm 0.01
$\text{N}_1 - \text{N}_1$	+0.489 \pm 0.008	-0.145 \pm 0.006	+0.860 \pm 0.015
$\text{N}_1 - \text{H}_{II}$	-0.26 \pm 0.02	+0.95 \pm 0.01	-0.17 \pm 0.04
$\text{N}_1 - \text{O}_4$	+0.239 \pm 0.007	+0.935 \pm 0.014	-0.261 \pm 0.009

* The interproton vector referred to here is related to that given in the text by the point group mirror plane perpendicular to the b axis.

Figure 25

Hydrogen bond configuration around N_1 projected on a plane perpendicular to the N_1-N_2 direction.



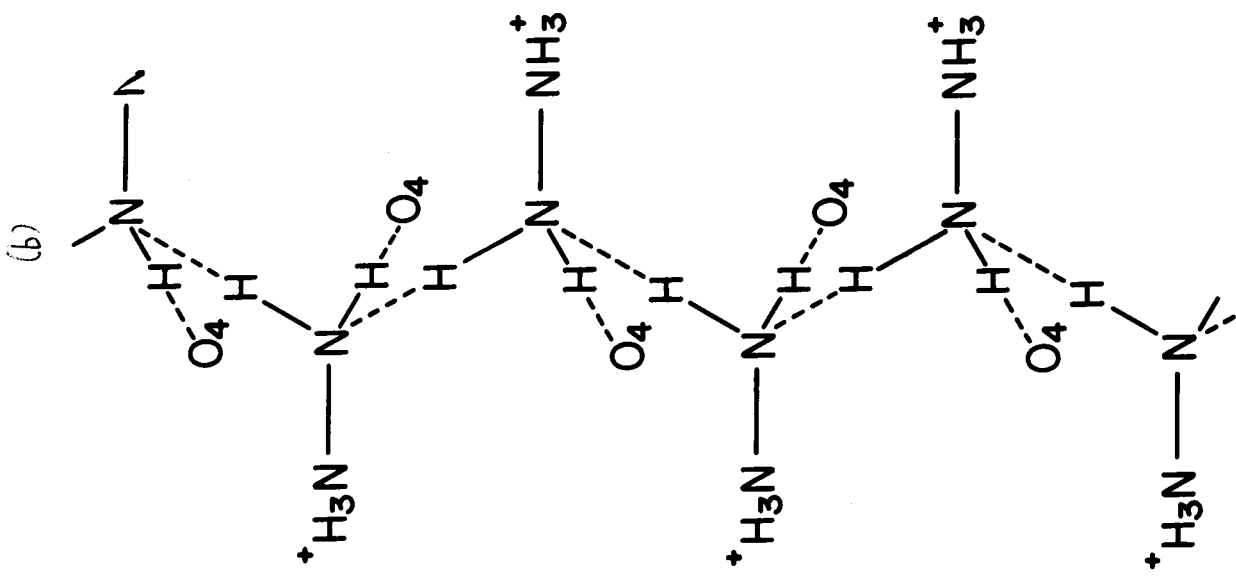
26a and in the positive c direction in Fig. 26b. Since a N-H group is polar, a spontaneous polarization may arise parallel to the c axis, the ferroelectric direction in LiHzS, and the two alternative configurations of bonds permit it to be reversible in accordance with the definition of a ferroelectric material. Of course the direction of polarization in one chain must be communicated to the others to obtain an overall polarization of the crystal. Presumably this is done through the $N_1-H_{II} \dots O_4$ bond via the framework. The reversal of a $N_1-H_I \dots N_1$ bond along the chain would require an alteration of 20° in the direction of its associated N_1-H_{II} group assuming that the $H_I-N_1-H_{II}$ angle remains tetrahedral. The effect of this shift in the direction of N_1-H_{II} might be to cause a slight tilting of the lithium-oxygen tetrahedra to bring the O_4 oxygen atoms into position where the hydrogen bonds would be more effective, but, in any case, it must switch the framework from a righthanded to a lefthanded system, which transmits the information regarding the sense of polarization from one hydrazinium ion to another. The framework is non-centrosymmetric and may also contribute to the overall spontaneous polarization of the crystal.

The phase transition revealed by the Li^7 signal is clearly accompanied, and probably triggered, by an additional reorientation of the hydrogen atoms. Rotation of the $-NH_2$

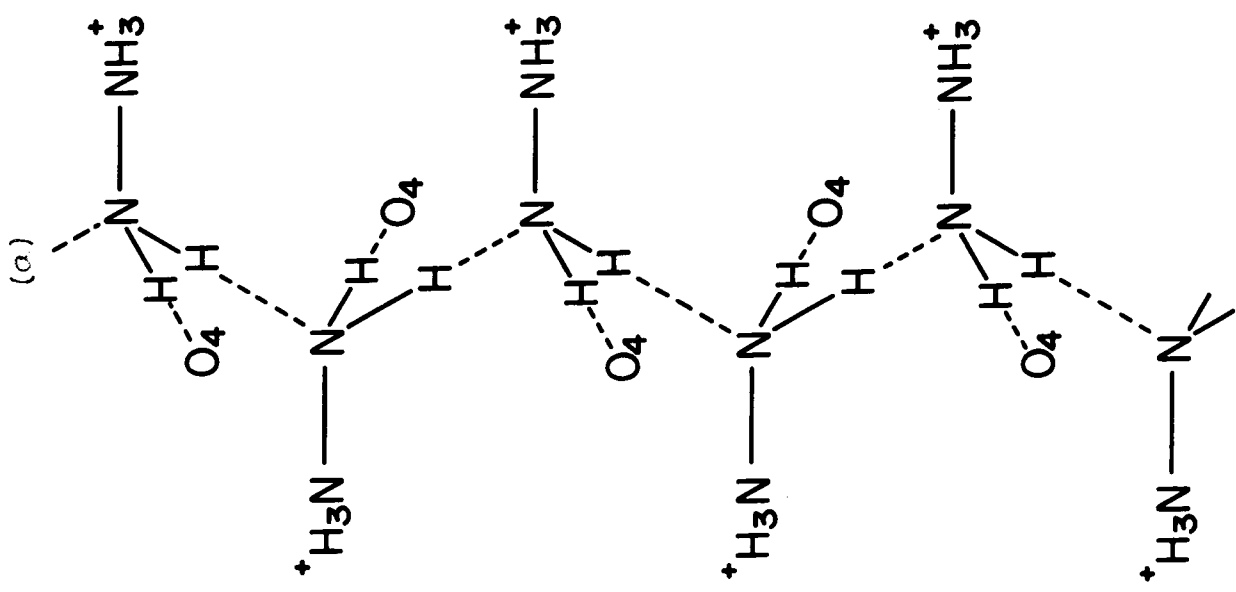
Figure 26

The two alternative configurations of hydrogen bonds linking the hydrazinium ions:

- (a) N-H...N directed in the negative c direction
- (b) N-H...N directed in the positive c direction.



C



group about the N_1-N_2 axis of the hydrazinium ion immediately suggests itself as the most likely motion. We calculate (see Table XII) that such a rotation should lead to a decrease in the second moment of close to 8 gauss^2 but experiment shows that the second moment drops to the very low value $0.74 \pm 0.14 \text{ gauss}^2$ at 210°C . However, the arrest in the curve at about 8.8 gauss^2 suggests that there are in fact two motions involved. It is significant that the decrease to 8.8 gauss^2 occurs over the same temperature range as the change in the Li^7 spectrum and that the break in the second moment curve occurs at $+150^\circ\text{C}$ just a few degrees below the temperature at which there are no further structural changes that are sufficiently drastic to affect the Li^7 spectrum. The nearness of the value observed for the second moment at the break, 8.8 gauss^2 , to the value calculated for a hydrazinium ion with both the $-\text{NH}_3^+$ and $-\text{NH}_2$ groups rotating, 8 gauss^2 , strongly suggests that the onset of rotation of the $-\text{NH}_2$ group is associated with this transition. Such a rotation would lead to disordering of the N-H dipoles and hence to a loss of ferroelectricity, if our model is correct. Due to the high conductivity of the crystal, it has not proved possible to observe a dielectric hysteresis loop above $+80^\circ\text{C}$ so that this prediction has not been checked. Such a rotation of the $-\text{NH}_2$ group would affect the framework through the change in status

of the hydrogen bond to the O_4 oxygen atom and would, therefore, be likely to produce a small change, such as observed in the Li^7 spectrum.

The question still remains as to what kind of motion brings about the further reduction of the proton second moment above $150^\circ C$ to the very low value of 0.74 ± 0.14 gauss². This additional motion apparently has little effect on the structure as a whole for no change in the Li^7 spectrum was observed in this temperature range. Rotation of the hydrazinium ion as a unit about other axes would produce quite a small value of the second moment, perhaps about 1.5 gauss², but it would seem to require translational motion to bring about the high degree of averaging of the local fields indicated by the small second moment at high temperatures. It is possible that the hydrazinium ions themselves diffuse about, but a more likely explanation is that the protons diffuse along the c axis by transfer from one hydrazinium ion to the next. Such a motion would have almost no structural effect but might be sufficient to produce the slight asymmetry observed in the Li^7 signals at high temperatures. This also immediately suggests that these mobile protons are responsible for the high conductivity observed by Pepinsky et al (1958) . Our electrical conductivity measurements have shown that even at room temperature the conductivity along

the c axis is appreciable, being some 250 times greater than along the a or b axes and electrolysis has verified that the charge carriers are protons. The activation energy of the conduction process was found to be about 10 kcal/mole.

The Li^7 signals were used primarily to detect and to follow the progress of the phase transition as it affected the framework of the structure. However, it is worth noting that the room temperature value of the quadrupole coupling constant, 36.8 ± 0.3 kc/sec, falls at the lower end of the range of values, from 35 kc/sec for $\text{LiH}_3(\text{SiO}_3)_2$ (Anderson 1961) to 110 kc/sec for LiOH (Hon and Bray 1958), previously observed for Li^7 . This low value is consistent with a comparatively symmetrical environment for the lithium atoms. Burns (1962) who has observed the Li^7 signals in powdered LiHzS noted that eqQ/h decreases as the temperature is increased although he did not follow the change as high as the phase transition. The value of 25.8 ± 0.1 kc/sec found in the high temperature form of LiHzS is the smallest observed for Li^7 and it probably indicates a reduction in the distortion of the oxygen tetrahedron surrounding the lithium atom observed by Brown (1963). The rotation of the electric field gradient tensor at the lithium sites to an orientation such that all principal axes coincide with the crystallographic axes is without doubt due to the constraints imposed by the higher

symmetry in the high-temperature form. The interpretation of this rotation in terms of atomic displacements must await a structure determination of the high-temperature polymorph.

CHAPTER VIII

SUMMARY OF RESULTS

- A. N.M.R. Studies of Single Crystals of Borax and Tincalconite.
1. Complete descriptions of the quadrupole coupling tensors at the B^{11} and Na^{23} sites have been obtained. (see Tables III, IV, V, VII, VIII, IX.)
 2. The picture of the boron-oxygen polyion in borax, derived from the n.m.r. results for the B^{11} sites, is in complete agreement with the x-ray diffraction work of Morimoto (1956).
 3. The space group of tincalconite, whose structure is unknown, has been determined to be R32.
 4. The n.m.r. results for the B^{11} sites in tincalconite, show that the borax type polyion exists in tincalconite, in agreement with Christ's (1960) prediction. The three polyions per unit cell are each situated on a crystallographic two-fold axis, and their orientations have been specified.
 5. Our interpretation of the n.m.r. results of Waterman and Volkoff (1955) for the B^{11} sites in kernite, whose structure is unknown, shows that the borax type polyion also exists in kernite, again agreeing with Christ's prediction.

The polyion no longer possesses two-fold symmetry, which is in keeping with the further prediction by Christ that polymerisation of the polyions has occurred.

6. The n.m.r. data for the Na^{23} sites in borax are entirely consistent with Morimoto's (1956) proposed structure. Thus it has been verified that the two unique sodium atoms occupy special positions in the unit cell, and, judging from the size of the quadrupole coupling constants (see Table VIII) it has been inferred that the surrounding octahedra of oxygen atoms are quite regular for one sodium site and slightly distorted for the other.
7. The n.m.r. data for the Na^{23} sites in tincalconite have shown that there are three unique sodium atoms in the unit cell, and that all occupy special positions. It has been inferred by comparing the quadrupole coupling constants with those of borax, that the environments of two atoms are very similar to those in borax, but the third has a much less regular environment.
8. Regarding the proposed number of unique sites in borax and tincalconite, our single crystal data for the Na^{23} sites are in direct disagreement with the conclusions of Dharmatti et al (1962), who used powdered samples. This emphasises that n.m.r. data from powdered samples must be interpreted with much caution for substances with struc-

tures as complex as the tetraborates.

B. N.M.R. Studies of Ferroelectric Lithium Hydrazinium Sulphate.

1. A previously undetected second order phase transition has been discovered in lithium hydrazinium sulphate. It begins at about 50°C and is complete by 164°C.
2. The quadrupole coupling tensors have been evaluated in the ferroelectric phase at room temperature and in the high temperature phase at 205°C. (see Table XI).
3. The second moments of the proton resonance signal from powdered lithium hydrazinium sulphate have been obtained between -183°C and 225°C (see Fig 18). These indicate that the nitrogen and hydrogen atoms exist in the structure as the hydrazinium ion, $\text{NH}_2 - \text{NH}_3^+$. At -183°C the structure is virtually rigid. Between -183°C and room temperature the $-\text{NH}_3^+$ group begins to reorient about the N-N axis. Above room temperature the $-\text{NH}_2$ groups also begin to rotate about the N-N axis, and in doing so, trigger the second order phase transition. Further narrowing of the proton resonance signal is attributed to proton transfer along the c-axis.
4. Supporting evidence for much of the above is found in the single crystal proton magnetic resonance work. These

results have also enabled the lengths of the p-p vectors (see Table XIII) in the $-\text{NH}_2$ and $-\text{NH}_3^+$ groups to be determined, have confirmed that the $-\text{NH}_3^+$ group reorients about the N-N axis, and have enabled the hydrogens in the $-\text{NH}_2$ groups to be located (see Table XIV, Fig.25).

5. On the basis of the above evidence, proposed mechanisms for the ferroelectric switching and phase transition to the high temperature polymorph have been described in detail.

APPENDIX I

EXPERIMENTALLY MEASURED VALUES OF THE B^{11} SATELLITE RESONANCE

FREQUENCIES IN MC/SEC FOR THE X ROTATION OF BORAX.

0°	15°	30°	45°	60°	75°	90°	105°	120°	135°	150°	165°
	9.805		9.665	9.351					9.674		8.815
	9.150	9.844	9.173	9.302	9.315		9.314	9.315	9.173	9.854	9.157
9.560	8.753	8.815	8.775	8.764	8.826	9.069	8.829	9.293	8.778	8.815	8.755
8.726	8.695	8.772	8.697	8.697	8.740	8.710	8.738	8.766	8.693	8.776	8.698
8.626	8.655	8.675	8.695	8.663	8.620	8.650	8.617	8.590	8.666	8.677	8.655
7.893	8.596	8.585	8.579	8.593	8.665	8.366	8.656	8.195	8.576	8.579	8.596
	8.345	7.539	8.234	8.189	8.055		8.058	8.005	8.234	7.529	8.349
	7.589		7.769	8.005					7.759		7.580

EXPERIMENTALLY MEASURED VALUES OF THE B^{11} SATELLITE RESONANCE

FREQUENCIES IN MC/SEC FOR THE X ROTATION OF BORAX.

180°	195°	210°	225°	240°	255°	270°	285°	300°	315°	330°	345°
	9.807		9.661	9.351				9.345	9.678		9.815
	9.146	9.845	9.176	9.310	9.312		9.317	9.314	9.170	9.855	9.145
9.559	8.755	8.819	8.775	8.762	8.825	9.069	8.839	8.766	8.779	8.810	8.755
8.726	8.695	8.772	8.693	8.696	8.743	8.709	8.743	8.693	8.696	8.775	8.696
8.627	8.655	8.580	8.660	8.662	8.660	8.629	8.655	8.664	8.658	8.675	8.655
7.892	8.596	8.676	8.578	8.591	8.617	8.367	8.617	8.588	8.740	8.577	8.595
	8.355	7.540	8.228	8.181	8.055		8.053	8.175	8.240	7.526	8.350
	7.586		7.773	8.003				8.005	7.751		7.577

EXPERIMENTALLY MEASURED VALUES OF THE B^{11} SATELLITE RESONANCE

FREQUENCIES IN MC/SEC FOR THE Y ROTATION OF BORAX.

0°	15°	30°	45°	60°	75°	90°	105°	120°	135°	150°	165°
9.073	9.174	9.255	9.302	9.302	9.255	9.171	9.073	8.988	8.938	8.937	8.987
8.653	8.762	8.858	8.908	8.909	8.854	8.757	8.711	8.805	8.861	8.860	8.803
8.705	8.595	8.498	8.443	8.445	8.502	8.601	8.646	8.547	8.505	8.541	8.553
8.361	8.237	8.130	8.058	8.045	8.105	8.206	8.332	8.441	8.494	8.495	8.465
180°	195°	210°	225°	240°	255°	270°	285°	300°	315°	330°	345°
9.073	9.173	9.255	9.303	9.301	9.253	9.169	9.071	8.986	8.938	8.938	8.988
8.654	8.764	8.859	8.912	8.910	8.855	8.757	8.713	8.807	8.860	8.858	8.802
8.707	8.594	8.498	8.443	8.446	8.503	8.603	8.645	8.444	8.506	8.515	8.554
8.360	8.240	8.129	8.058	8.050	8.107	8.210	8.335	8.547	8.493	8.496	8.465

EXPERIMENTALLY MEASURED VALUES OF THE B¹¹ SATELLITE RESONANCE

FREQUENCIES IN MC/SEC FOR THE Z ROTATION OF BORAX

0°	15°	30°	45°	60°	75°	90°	100°	120°	135°	150°	165°
	9.257	9.165	9.292		9.654		9.658			9.167	9.260
	8.025	8.912	8.915	9.557	9.301		9.298	9.561	9.294	8.917	8.927
9.173	8.760	8.741	8.920	8.926	8.727	9.564	8.725	8.930	8.916	8.740	8.760
8.762	8.749	8.719	8.708	8.707	8.714	8.731	8.718	8.706	8.707	8.720	8.749
8.601	8.615	8.643	8.655	8.652	8.642	8.631	8.643	8.651	8.656	8.645	8.615
8.212	8.605	8.626	8.527	8.559	8.637	7.891	8.634	8.559	8.527	8.625	8.603
	8.518	8.575	8.524	7.904	8.183		8.180	7.898	8.193	8.572	8.516
	8.098	8.218	8.195		7.786		7.784			8.216	8.098

EXPERIMENTALLY MEASURED VALUES OF THE B¹¹ SATELLITE RESONANCE

FREQUENCIES IN MC/SEC FOR THE Z ROTATION OF BORAX.

180°	195°	210°	225°	240°	255°	270°	285°	300°	315°	330°	345°
	9.257	9.165	9.296		9.659		9.656			9.169	9.257
	8.924	8.920	8.917	9.563	9.298		9.299	9.558	9.290	8.913	8.932
9.173	8.760	8.740	8.916	8.925	8.725	9.563	8.714	8.925	8.920	8.741	8.760
8.761	8.724	8.720	8.707	8.706	8.718	8.730	8.727	8.706	8.708	8.719	8.749
8.601	8.615	8.645	8.656	8.651	8.643	8.631	8.642	8.652	8.655	8.643	8.615
8.212	8.603	8.625	8.527	8.558	8.635	7.894	8.637	8.561	8.524	8.624	8.605
	8.518	8.569	8.524	7.895	8.184		8.185	7.901	8.196	8.574	8.513
	8.098	8.217	8.188		7.930		7.785			8.215	8.098

EXPERIMENTALLY MEASURED VALUES OF THE RESONANCE FREQUENCIES FROM
TETRAHEDRALLY BONDED B¹¹ FOR THE X ROTATION IN TINCALCONITE, IN MC/SEC.

0°	15°	30°	45°	60°	75°	90°	105°	120°	135°	150°	165°
7.783	7.825	7.880	7.907	7.895	7.843		7.849		7.895	7.844	7.787
7.744	7.813	7.870	7.907	7.822	7.767		7.738	7.897	7.811	7.801	7.761
7.735	7.765	7.730	7.869	7.741	7.738	7.765	7.723	7.786	7.670	7.765	7.749
7.673	7.637	7.667	7.531	7.663	7.669	7.645	7.674	7.622	7.727	7.635	7.660
7.665	7.593	7.528	7.497	7.583	7.641		7.665	7.512	7.589	7.607	7.650
7.613	7.583	7.523	7.494	7.512	7.562		7.560		7.515	7.559	7.615
180°	195°	210°	225°	240°	255°	270°	285°	300°	315°	330°	345°
7.785	7.824	7.880	7.907	7.895	7.844		7.850		7.892	7.848	7.790
7.742	7.813	7.871	7.907	7.822	7.766		7.740	7.893	7.815	7.796	7.762
7.735	7.767	7.732	7.870	7.743	7.740	7.765	7.726	7.783	7.672	7.772	7.750
7.673	7.637	7.669	7.533	7.662	7.670	7.645	7.673	7.622	7.729	7.642	7.660
7.665	7.595	7.526	7.496	7.582	7.642		7.666	7.512	7.593	7.603	7.652
7.615	7.637	7.527	7.494	7.509	7.563		7.561		7.512	7.565	7.618

EXPERIMENTALLY MEASURED VALUES OF THE RESONANCE FREQUENCIES FROM
 TETRAHEDRALLY BONDED B¹¹ FOR THE Y ROTATION OF TINCALCONITE, IN MC/SEC

0°	15°	30°	45°	60°	75°	90°	105°	120°	135°	150°	165°
			7.941						7.941		
			7.856	7.907				7.906	7.856		
		7.927	7.839	7.862	7.845		7.848	7.859	7.836	7.927	
	7.809	7.822	7.808	7.841	7.829		7.827	7.839	7.803	7.822	
7.769	7.863	7.784	7.764	7.660	7.777	7.796	7.779	7.655	7.762	7.783	7.808
7.645	7.604	7.630	7.647	7.743	7.626	7.609	7.626	7.741	7.645	7.629	7.603
	7.547	7.589	7.607	7.567	7.579		7.582	7.568	7.605	7.588	
		7.483	7.571	7.547	7.562		7.562	7.549	7.573	7.484	
			7.551	7.503				7.500	7.552		
			7.466						7.465		

EXPERIMENTALLY MEASURED VALUES OF THE RESONANCE FREQUENCIES FROM
TETRAHEDRALLY BONDED B¹¹ FOR THE Y ROTATION IN TINCALCONITE, IN MC/SEC

180°	195°	210°	225°	240°	255°	270°	285°	300°	315°	330°	345°
			7.939						7.939		
			7.855	7.907				7.906	7.855		
		7.927	7.840	7.860	7.844		7.846	7.860	7.837	7.927	
	7.836	7.823	7.804	7.840	7.835		7.829	7.840	7.808	7.820	
7.769	7.809	7.785	7.760	7.663	7.774	7.797	7.778	7.653	7.764	7.784	7.808
7.646	7.602	7.628	7.643	7.745	7.626	7.610	7.626	7.740	7.644	7.626	7.604
	7.545	7.588	7.605	7.569	7.580		7.583	7.569	7.608	7.588	
		7.481	7.569	7.548	7.562		7.563	7.545	7.574	7.483	
			7.550	7.502					7.554		
			7.467						7.466		

EXPERIMENTALLY MEASURED VALUES OF THE RESONANCE FREQUENCIES FROM
TETRAHEDRALLY BONDED B¹¹ FOR THE Z ROTATION OF TINCALCONITE, IN MC/SEC

0°	15°	30°	45°	60°	75°	90°	105°	120°	135°	150°	165°
7.300	7.807		7.803	7.800	7.805		7.805	7.802	7.802		7.805
7.733	7.765	7.796	7.762	7.728	7.762	7.795	7.763	7.728	7.764	7.794	7.768
7.689	7.652	7.625	7.648	7.684	7.650	7.626	7.648	7.685	7.645	7.623	7.653
7.612	7.607		7.608	7.612	7.611		7.609	7.612	7.612		7.609
180°	195°	210°	225°	240°	255°	270°	285°	300°	315°	330°	345°
7.803	7.810			7.806			7.803		7.801	7.733	7.805
7.730	7.768	7.800	7.811	7.727	7.768	7.796	7.763	7.805	7.764	7.791	7.767
7.687	7.653	7.622	7.614	7.684	7.655	7.626	7.646	7.617	7.645	7.619	7.651
7.615	7.610			7.618			7.606		7.612	7.689	7.608

EXPERIMENTALLY MEASURED VALUES OF THE RESONANCE FREQUENCIES FROM
 TRIGONALLY BONDED B¹¹ FOR THE X ROTATION OF TINCALCONITE, IN MC/SEC.

0°	15°	30°	45°	60°	75°	90°	105°	120°	135°	150°	165°
8.889	8.599	8.159	7.920	8.179				8.334	8.303	8.834	8.969
8.000	7.916	7.877	7.883	8.010	8.315		8.303	8.309	8.256	8.222	8.113
7.918	7.836	7.832	7.858	8.000	8.123	8.232	7.950	8.047	8.503	8.156	8.034
7.605	7.690	7.705	7.685	7.510	7.348	7.203	7.560	7.512	7.166	7.307	7.466
7.515	7.608	7.388	7.623	7.495	7.088		7.103	7.095	7.113	7.226	7.374
6.548	6.912	7.632	7.596	7.271				7.069	7.025	6.620	6.438

EXPERIMENTALLY MEASURED VALUES OF THE RESONANCE FREQUENCIES FROM
 TRIGONALLY BONDED B¹¹ FOR THE Y ROTATION OF TINCALCONITE, IN MC/SEC.

0°	15°	30°	45°	60°	75°	90°	105°	120°	135°	150°	165°
		8.262	8.292	8.508	8.603		8.610	8.513	8.294	8.262	
		8.262	8.255	8.450	8.515		8.537	8.476	8.256	8.262	
	8.317	8.227	8.217	8.319	8.345	8.515	8.347	8.326	8.214	8.227	8.317
	8.239	7.890	8.035	7.906	8.265	8.435	8.265	7.906	8.034	7.889	8.243
8.230	8.003	7.862	7.989	7.837	8.183	8.355	8.183	7.833	7.989	7.868	8.003
7.205	7.497	7.675	7.510	7.724	7.370	7.105	7.382	7.724	7.511	7.675	7.496
	7.196	7.655	7.464	7.658	7.289	7.050	7.288	7.660	7.464	7.655	7.193
	7.088	7.207	7.343	7.093	7.063	7.011	7.059	7.086	7.340	7.206	7.087
		7.175	7.305	7.072	7.015		6.987	7.068	7.303	7.175	
		7.171	7.133	7.020	6.912		6.910	7.014	7.123	7.167	

EXPERIMENTALLY MEASURED VALUES OF THE RESONANCE FREQUENCIES FROM
 TRIGONALLY BONDED B¹¹ FOR THE Y ROTATION OF TINCALCONITE, IN MC/SEC

180°	195°	210°	225°	240°	255°	270°	285°	300°	315°	330°	345°
		8.262	8.294	8.508	8.605		8.610	8.513	8.295	8.262	
		8.262	8.256	8.450	8.516		8.537	8.458	8.260	8.262	
	8.317	8.229	8.217	8.322	8.346	8.514	8.348	8.324	8.213	8.230	8.317
	8.240	7.890	8.038	7.906	8.269	8.439	8.262	7.906	8.039	7.888	8.242
8.231	8.000	7.866	8.256	7.835	8.183	8.355	8.179	7.835	7.989	7.865	8.005
7.206	7.496	7.675	7.509	7.724	7.370	7.108	7.382	8.086	7.515	7.675	7.496
	7.195	7.655	7.466	7.643	7.290	7.050	7.294	7.724	7.468	7.655	7.193
	7.087	7.207	7.345	7.093	7.062	7.013	7.060	7.663	7.346	7.205	7.087
		7.175	7.308	7.073	7.015		6.987	7.064	7.305	7.175	
		7.170	7.131	7.020	6.910		6.908	7.014	7.127	7.168	

EXPERIMENTALLY MEASURED VALUES OF THE RESONANCE FREQUENCIES FROM
 TRIGONALLY BONDED B¹¹ FOR THE Z ROTATION OF TINCALCONITE, IN MC/SEC

0°	15°	30°	45°	60°	75°	90°	105°	120°	135°	150°	165°
	8.803		8.803		8.803		8.803		8.804		8.808
	8.756		8.757		8.756		8.757		8.759		8.760
	8.273		8.272		8.278		8.279		8.277		8.280
8.521	8.227	8.891	8.233	8.518	8.235	8.891	8.231	8.517	8.232	8.892	8.236
8.437	8.094	8.000	8.091	8.436	8.098	8.003	8.093	8.437	8.093	8.003	8.091
8.355	7.997	7.917	7.992	8.355	7.993	7.925	7.990	8.357	7.989	7.924	7.987
7.113	7.584	7.620	7.582	7.107	7.579	7.626	7.583	7.117	7.578	7.624	7.585
7.052	7.480	7.518	7.479	7.052	7.478	7.523	7.476	7.053	7.476	7.522	7.483
7.015	7.227	6.557	7.228	7.016	7.223	6.555	7.225	7.014	7.229	6.554	7.224
	7.165		7.165		7.160		7.163		7.168		7.168
	6.722		6.725		6.726		6.724		6.728		6.724
	6.671		6.675		6.674		6.670		6.683		6.672

EXPERIMENTALLY MEASURED VALUES OF THE RESONANCE FREQUENCIES FROM
 TRIGONALLY BONDED B¹¹ FOR THE Z ROTATION OF TINCALCONITE, IN MC/SEC

180°	195°	210°	225°	240°	255°	270°	285°	300°	315°	330°	345°
	8.805		8.805		8.806		8.806		8.812		8.808
	8.760		8.758		8.762		8.758		8.767		8.758
	8.278		8.283		8.277		8.282		8.282		8.281
8.520	8.233	8.890	8.233	8.523	8.233	8.891	8.237	8.522	8.235	8.894	8.232
8.440	8.095	8.003	8.094	8.444	8.093	8.003	8.096	8.443	8.094	8.006	8.093
8.358	7.990	7.923	7.997	8.359	7.990	7.925	7.997	8.362	7.992	7.928	7.988
7.115	7.585	7.623	7.588	7.116	7.587	7.627	7.583	7.115	7.588	7.625	7.580
7.054	7.482	7.523	7.485	7.056	7.486	7.523	7.478	7.057	7.484	7.523	7.480
7.019	7.230	6.555	7.225	7.017	7.232	6.555	7.226	7.019	7.234	6.557	7.222
	7.169		7.167		7.169		7.168		7.171		7.168
	6.729		6.733		6.732		6.726		6.730		6.726
	6.676		6.675		6.675		6.677		6.676		6.677

APPENDIX II

RESONANCE FREQUENCIES IN MC/SEC FOR THE X-ROTATION OF BORAX

0°	15°	30°	45°	60°	75°	90°	105°	120°	135°	150°	165°
8.467	8.439	8.390	8.389	8.262	8.170	8.860	8.168	8.259	8.257	8.302	8.287
8.575	8.490	8.405	8.441	8.284	8.309	8.127	8.308	8.285	8.389	8.679	8.692
8.246	8.542	8.486	8.483	8.433	8.479		8.674	8.434	8.437	8.390	8.542
8.732	8.694	8.587	8.490	8.483	8.487		8.818	8.481	8.558	8.405	8.603
	8.289	8.305	8.558	8.489	8.503		8.475	8.487	8.588	8.586	8.378
	8.380	8.678	8.592	8.550	8.680		8.485	8.546	8.720		8.437
	8.601		8.260		8.819		8.509	8.709			
			8.720					8.718			
180°	195°	210°	225°	240°	255°	270°	285°	300°	315°	330°	345°
8.467	8.287	8.301	8.718	8.545	8.506	8.594	8.507	8.545	8.587	8.584	8.602
8.488	8.689	8.388	8.589	8.429	8.472	8.383	8.473	8.433	8.556	8.405	8.539
8.490	8.377	8.402	8.557	8.706	8.814	8.853	8.306	8.717	8.435	8.389	8.433
8.512	8.436	8.584	8.436	8.278	8.672	8.123	8.673	8.707	8.388	8.679	8.374
8.245	8.540	8.674	8.388	8.258	8.306	8.487	8.815	8.281	8.720	8.299	8.687
8.729	8.600		8.258	8.715	8.167	8.388	8.167	8.257	8.258		8.286
						8.598					

EXPERIMENTALLY MEASURED VALUES OF THE Na²³ RESONANCE

FREQUENCIES IN MC/SEC. FOR THE Y-ROTATION OF BORAX

0°	15°	30°	45°	60°	75°	90°	105°	120°	135°	150°	165°
8.592	8.908	8.882	8.190	8.304	8.308	8.358	8.442	8.642	8.545	8.330	8.245
8.386	8.059	8.081	8.788	8.341	8.662	8.360	8.536	8.331	8.605	8.644	8.736
8.119	8.465	8.553	8.347	8.644	8.482	8.613	8.305	8.449	8.372	8.482	8.640
8.855	8.482	8.424	8.627	8.666	8.485		8.665	8.488	8.435	8.584	8.335
8.119	8.509	8.482			8.491			8.529		8.402	
180°	195°	210°	225°	240°	255°	270°	285°	300°	315°	330°	345°
8.119	8.061	8.425	8.193	8.304	8.662	8.613	8.442	8.332	8.373	8.332	8.245
8.855	8.909	8.553	8.786	8.344	8.309	8.359	8.535	8.461	8.439	8.647	8.337
8.591	8.466	8.884	8.627	8.642	8.497		8.667	8.448	8.545	8.586	8.642
8.383	8.484	8.089	8.347	8.667			8.305	8.487	8.105	8.402	8.739
	8.512							8.530			

RESONANCE FREQUENCIES IN MC/SEC FOR THE Z-ROTATION OF BORAX

0°	15°	30°	45°	60°	75°	90°	105°	120°	135°	150°	165°
8.481	8.347	8.327	8.462	8.442	8.456	8.235	8.245	8.442	8.295	8.545	8.348
8.354	8.380	8.366	8.477	8.478	8.482	8.458	8.304	8.470	8.400	8.595	8.382
8.608	8.481	8.420	8.481	8.482	8.509	8.505	8.480	8.482	8.465	8.639	8.582
	8.513	8.481	8.506	8.499	8.714	8.722	8.482	8.498	8.479	8.325	8.612
	8.583	8.513	8.560	8.519	8.245		8.512	8.520	8.482	8.365	8.618
	8.613	8.546	8.297	8.267			8.715	8.266	8.503	8.423	
	8.616	8.593	8.400	8.693				8.694	8.561		
		8.638	8.665						8.667		
180°	195°	210°	225°	240°	255°	270°	285°	300°	315°	330°	345°
8.481	8.348	8.325	8.296	8.442	8.244	8.236	8.244	8.694	8.397	8.324	8.613
8.355	8.381	8.365	8.400	8.471	8.455	8.459	8.453	8.440	8.296	8.364	8.616
8.607	8.583	8.420	8.463	8.481	8.482	8.483	8.482	8.469	8.462	8.422	8.584
	8.613	8.481	8.505	8.495	8.510	8.479	8.512	8.482	8.482	8.544	8.380
	8.615	8.456	8.561	8.519	8.713	8.505	8.713	8.519	8.505	8.595	8.349
		8.594	8.666	8.265		8.722		8.265	8.813	8.638	
		8.637		8.693					8.562		
									8.665		

EXPERIMENTALLY MEASURED VALUES OF THE Na²³ SATELLITE RESONANCE

FREQUENCIES IN MC/SEC. FOR THE X ROTATION OF TINCALCONITE

0°	15°	30°	45°	60°	75°	90°	105°	120°	135°	150°	165°
6.676					6.947						
6.560	6.619			6.775	6.707	7.007	6.948				
6.551	6.588	5.580	6.549	6.603	6.419	6.746	6.708	6.780	6.545		6.482
6.506	6.508	6.481	6.432	6.507	6.383	6.409	6.412	6.605	6.378		6.615
6.208	6.206	6.235	6.275	6.205	6.329	6.289	6.294	6.110	6.334		6.238
6.156	6.116	6.123	6.215	6.115	6.259	6.963	6.006	6.963	6.216		6.098
6.137	6.606			5.968	6.004	5.701	5.773				
6.029					5.774						

EXPERIMENTALLY MEASURED VALUES OF THE Na²³ SATELLITE RESONANCE

FREQUENCIES IN MC/SEC. FOR THE X ROTATION OF TINCALCONITE

180°	195°	210°	225°	240°	255°	270°	285°	300°	315°	330°	345°
6.677					6.949						
6.564	6.619			6.772	6.703	7.005	6.945				
6.551	6.586	6.580	6.544	6.603	6.447	6.744	6.709	6.779	6.544		6.621
6.506	6.507	6.479	6.429	6.489	6.379	6.409	6.412	6.605	6.378		6.480
6.209	6.209	6.233	6.215	6.202	6.324	6.298	6.297	6.114	6.334		6.235
6.154	6.115	6.125	6.277	6.112	6.256	5.961	6.002	5.965	6.217		6.101
6.131	6.060			5.960	6.001	5.699	5.770				
6.029					5.772						

EXPERIMENTALLY MEASURED VALUES OF THE Na²³ SATELLITE RESONANCE

FREQUENCIES IN MC/SEC. FOR THE Y ROTATION OF TINCALCONITE

0°	15°	30°	45°	60°	75°	90°	105°	120°	135°	150°	165°
					6.618		6.617				
	6.943				6.604	6.678	6.603				6.942
7.005	6.704	6.779		6.544	6.512	6.621	6.511	6.543		6.779	6.707
6.743	6.442	6.603	6.492	6.490	6.478	6.548	6.468	6.478	6.538	6.602	6.440
6.410	6.387	6.467	6.460	6.455	6.415	6.450	6.418	6.458	6.461	6.466	6.386
6.298	6.324	6.243	6.255	6.290	6.299	6.265	6.299	6.290	6.256	6.242	6.320
5.960	6.270	6.108	6.221	6.220	6.237	6.158	6.245	6.223	6.220	6.112	6.268
5.698	6.004	6.967		6.160	6.195	6.081	6.196	6.163		5.968	6.000
	5.775				6.098	6.029	6.099				5.772
					6.096		6.099				

EXPERIMENTALLY MEASURED VALUES OF THE Na²³ SATELLITE RESONANCE

FREQUENCIES IN MC/sec FOR THE Y ROTATION OF TINCALCONITE

180°	195°	210°	225°	240°	255°	270°	285°	300°	315°	330°	345°
					6.617		6.619				
	6.942				6.601	6.675	6.602				6.943
7.004	6.705	6.777		6.545	6.511	6.621	6.515	6.546	6.542	6.778	6.707
6.744	6.440	6.601	6.540	6.454	6.480	6.545	6.470	6.484	6.470	6.602	6.440
6.409	6.385	6.468	6.458	6.230	6.424	6.452	6.422	6.455	6.461	6.465	6.386
6.297	6.322	6.240	6.259	6.492	6.291	6.266	6.292	6.290	6.258	6.245	6.322
5.960	6.266	6.115	6.217	6.290	6.237	6.154	6.246	6.231	6.215	6.113	6.269
5.699	6.002	5.968		6.163	6.196	6.085	6.195	6.162		5.965	6.001
	5.777				6.101	6.026	6.100				5.772
							6.099				

EXPERIMENTALLY MEASURED VALUES OF THE Na²³ SATELLITE RESONANCE

FREQUENCIES IN MC/SEC FOR THE Z ROTATION OF TINCALCONITE

0°	15°	30°	45°	60°	75°	90°	105°	120°	135°	150°	165°
	6.681		6.679		6.679		6.681		6.681		6.684
6.625	6.590	6.680	6.594	6.680	6.593	6.680	6.595	6.681	6.593	6.681	6.593
6.552	6.545	6.564	6.591	6.626	6.550	6.570	6.550	6.624	6.550	6.570	6.550
6.455	6.541	6.557	6.545	6.553	6.546	6.556	6.545	6.554	6.543	6.556	6.540
6.270	6.394	6.510	6.392	6.456	6.395	6.511	6.393	6.456	6.393	6.511	6.389
6.159	6.336	6.213	6.337	6.270	6.339	6.214	6.340	6.269	6.334	6.215	6.335
6.085	6.174	6.160	6.173	6.158	6.171	6.141	6.170	6.161	6.172	6.160	6.170
6.033	6.160	6.142	6.160	6.086	6.162	6.033	6.162	6.085	6.163	6.143	6.158
6.683	6.120	6.034	6.122	6.270	6.120	6.160	6.120	6.033	6.119	6.035	6.116
	6.033		6.030		6.033		6.030		6.030		6.030

EXPERIMENTALLY MEASURED VALUES OF THE Na²³ SATELLITE RESONANCE

FREQUENCIES IN MC/ SEC FOR THE Z ROTATION OF TINCALCONITE

180°	195°	210°	225°	240°	255°	270°	285°	300°	315°	330°	345°
	6.680		6.680				6.682		6.682		6.681
6.683	6.593	6.681	6.595	6.682	6.679	6.683	6.595	6.682	6.595	6.680	6.595
6.626	6.551	6.569	6.550	6.625	6.593	6.569	6.548	6.626	6.547	6.572	6.550
6.553	6.544	6.556	6.545	6.552	6.544	6.553	6.542	6.552	6.545	6.557	6.543
6.454	6.394	6.510	6.391	6.455	6.394	6.509	6.390	6.454	6.397	6.512	6.391
6.266	6.335	6.213	6.338	6.270	6.338	6.213	6.337	6.270	6.335	6.215	6.337
6.162	6.170	6.162	6.172	6.162	6.169	6.161	6.174	6.159	6.174	6.160	6.172
6.087	6.161	6.142	6.161	6.086	6.123	6.142	6.161	6.087	6.163	6.141	6.162
6.033	6.119	6.033	6.119	6.032	6.033	6.031	6.120	6.030	6.123	6.033	6.121
	6.032		6.033				6.031		6.033		6.033

REFERENCES

- Anderson, D.H., 1961, Bull. Am. Phys. Soc., 6, 363.
- Andrew, E.R. and Bersohn, R., 1950, J. Chem. Phys., 18, 159.
- Bersohn, R., 1952, J. Chem. Phys., 20, 1505.
- Blinic, R., Schara, M., and Poberaj, S., 1963, J. Phys. Chem. Solids, 24, 559.
- Bloch, F., Hansen, W.W., and Packard, M.E., 1946, Phys. Rev., 69, 127.
- Bloembergen, N., Purcell, E.M., and Pound, R.V., 1948, Phys. Rev., 73, 679.
- Bray, P.J., Edwards, J.O., O'Keefe, J.G., Ross, V.F., and Tatzuzaki, I., 1961, J. Chem. Phys., 35, 435.
- Brown, I.D., 1963, Acta Cryst., to be published.
- Burns, G., 1962, Phys. Rev., 127, 1193.
- Christ, C.L., 1960, Am. Mineralogist, 45, 334.
- Dale, J., 1961, J. Chem. Soc., 191, 922.
- Das, T.P., 1957, J. Chem. Phys., 27, 1.
- Datars, R.D., 1956, M.Sc.Thesis, McMaster University, Hamilton, Ontario.
- Deeley, C.M., Lewis, P., and Richards, R.E., 1954, Trans. Faraday Soc., 50, 556.
- Dharmatti, S.S., Iyer, S.A., and Vijayaraghavan, R., 1962, J. Phys. Soc. Japan, 17, 1736.
- Edwards, J.O. and Ross, J., 1960, J. Inorg.Nucl. Chem., 15, 329.
- Gorter, C.J., 1936, Physica, 3, 995.
- Gorter, C.J. and Broer, L.F.T., 1942, Physica, 9, 591.

- Gutowsky, H.S., Kistiakowsky, G.B., Pake G.E., and Purcell, E.M., 1949, J. Chem. Phys., 17, 972.
- Gutowsky, H.S. and Pake, G.E., 1950, J. Chem. Phys. 18, 162.
- Gutowsky, H.S., Pake, G.E., and Bersohn, R., 1954, J. Chem. Phys. 22, 643.
- Gutowsky, H.S. and Williams, G.A., 1957, Phys. Rev., 105, 464.
- Holuj, F., 1956, M.Sc. Thesis, Mc Master University, Hamilton Ontario.
- Holuj, F. and Petch, 1960, Can. J. Phys., 38, 515.
- Hon, J.F. and Bray, P.J., 1958, Phys. Rev., 110, 624.
- Herzberg, G., 1945, 'Infra-red and Raman Spectra of Polyatomic Molecules', van Nostrand Co., New York.
- Itoh, J., Kusaka, R., and Yamagata, Y., 1954, J. Phys. Soc. Japan, 9, 289.
- Lasarew, B.G. and Schubnikow, L.W., 1937, Phys. Z. Sowjet, 11, 445.
- Maricic, S., Veksli, Z., and Pintar, M., 1962, J. Phy. Ch. Solids, 23, 743.
- Minder, W., 1935, Zeits. Krist., 92, 301.
- Morimoto, N., 1956, Mineral J. (Japan), 2, 1.
- Pabst, A. and Sawyer, D.L., 1948, Am. Mineralogist, 33, 472.
- Pake, G.E. 1948, J. Chem. Phys., 16, 327.
- Pake, G.E. and Gutowsky, H.S., 1950, J. Chem. Phys., 18, 162.
- Palache, C., Berman, H., and Frondel, C., 1951, Dana's System of Mineralogy, 7th ed., Vol. 2 (John Wiley and Sons, Inc., New York,).
- Pennington, K.S. and Petch, H.E., 1960, J. Chem. Phys., 33, 329.
- Pennington, K.S. and Petch, H.E., 1962, J. Chem. Phys., 36, 2151.

- Pepinsky, R., Vedam, K., Okaya, Y., and Hoshino, S., 1958, Phys. Rev., 111, 1467.
- Petch, H.E. and Pennington, K.S., 1962, J. Chem. Phys., 36, 1216.
- Portoles, L., (1945), Euclides 5, 599; Estud. Geol. 5, 3, 1947; Estud. Geol. 7, 21, 1948.
- Pound, R.V., 1950, Phys. Rev., 79, 685.
- Pratt, L. and Richards, R.E., 1953, Trans. Faraday Soc., 49, 744.
- Purcell, E.M., Torrey, H.C., and Pound, R.V., 1946, Phys. Rev., 69, 37.
- Rabi, I.I., Millman, S., Kusch, P., and Zacharias, J.R., 1939, Phys. Rev., 55, 526.
- Reed, J.W. and Harris, P.M., 1961, J. Chem. Phys., 35, 1730.
- Ross, V. and Edwards, J.O., 1959, Am. Mineralogist, 44, 875.
- Sass, R., 1960, Acta Cryst. 13, 320.
- Schuster, N.A., 1951, Rev. Sci. Inst., 22, 254.
- Stem, O. and Gerlach, W., 1921, Z. Phys., 7, 249.
- Van Velck, J.H., 1948, Phys. Rev., 74, 1168.
- Volkoff, G.M., 1953, Can. J. Phys., 31, 820.
- Volkoff, G.M., Petch, H.E., and Smellie, D.W.L., 1952, Can. J. Phys., 30, 270.
- Waterman, H.H. and Volkoff, G.M., 1955, Can. J. Phys., 33, 156.
- Weiss, A. Naturforsch, Z., 1960, 15a, 536.
- Whittaker, E. and Robinson, G., 1948, The Calculus of Observations, Blackie and Sons, London.